A METHODOLOGY FOR THE SYNTHESIS OF ROBUST FEEDBACK SYSTEMS

by
David Albert Milich
S.B., Massachusetts Institute of Technology, 1982
M.S., Stanford University, 1984

Submitted to the
DEPARTMENT OF MECHANICAL ENGINEERING
in partial fulfillment of the requirements for the degree of

DOCTOR OF PHILOSOPHY

at the

MASSACHUSETTS INSTITUTE OF TECHNOLOGY

February 1988

Signature of Author _____
Department of Mechanical Engineering
February 1988

Certified by _____
Michael Athans
Thesis Co-Supervisor

Certified by _____
Lena Valavani
Thesis Co-Supervisor

Certified by _____
J. Karl Hedrick
Chairman, Doctoral Committee

Accepted by _____
Ain A. Sonin
Chairman, Department Graduate Committee

A METHODOLOGY FOR THE SYNTHESIS OF ROBUST FEEDBACK SYSTEMS

by

David Albert Milich

Submitted to the Department of Mechanical Engineering on February 17, 1988 in partial fulfillment of the requirements for the degree of Doctor of Philosophy.

ABSTRACT

A new methodology is developed for the synthesis of linear, time-invariant (LTI) controllers for multivariable LTI systems. The resulting closed-loop system is nominally stable and exhibits a known level of performance. In addition, robustness of the feedback system is guaranteed. That is, stability *and* performance are retained in the presence of *multiple* unstructured uncertainty blocks located at various points in the feedback loop.

The design technique is referred to as the Causality Recovery Methodology (CRM). The CRM relies on the Youla parameterization of all stabilizing compensators to ensure nominally stability of the feedback system. A frequency-domain inequality in terms of the structured singular value μ defines the robustness specification. The optimal compensator, with respect to the μ condition, is shown to be noncausal in general. The aim of the CRM is to find a stable, causal transfer function matrix that approximates the robustness characteristics of the optimal solution.

The CRM, via a series of infinite-dimensional convex programs, produces a closed-loop system whose performance-robustness is at least as good as that of any initial design. The algorithm is approximated by a finite-dimensional process for the purposes of implementation. Two numerical examples confirm the potential viability of the CRM concept; however, the robustness improvement comes at the expense of increased computational burden and compensator complexity.

Thesis Co-Supervisor: Dr. Michael Athans
Title: Professor of Systems Science and Engineering

Thesis Co-Supervisor: Dr. Lena Valavani
Title: Boeing Assistant Professor of Aeronautics and Astronautics

ACKNOWLEDGEMENTS

I am extremely grateful to my thesis co-supervisors, Professors Michael Athans and Lena Valavani, for their invaluable guidance, support, and technical assistance throughout the course of this research. The successful conclusion of this work is due in large measure to Professor Athans' insight and instincts. Professor Valavani kept me going through the ups and downs of research. In addition, their friendship has become an important part of my education.

The remaining members of my thesis committee deserve recognition as well. Professor Gunter Stein was extremely helpful in keeping the research on the right track. Professor Sanjoy Mitter's comments and suggestions were always welcome. I thank Professor J. Karl Hedrick for serving as committee chairman.

I would also like to express appreciation to my fellow students at the Laboratory for Information and Decision Systems. I value their friendship, as well as their technical advice. They made life at M.I.T. a more pleasant experience. Over the years, I have had the priviledge of knowing and learning from Dan Grunberg, Rick LaMaire, Petros Kapasouris, Wilma Quinn, Tony Rodriguez, Jeff Shamma, Jim Walton, Jason Papastavrou, Patrick Hosein, Louise Alterman, and Javed and Asif Pothiawala. I am grateful to Fifa Monserrate and Lisa Babine for their assistance and cheerful conversation. Thanks go to Bill Hanway for providing a great deal of computer support.

Most importantly, I would like to thank my family for their steadfast support and love throughout my long academic career. They make all the hard work worthwhile.

This research was conducted at the M.I.T. Laboratory for Information and Decision Systems with support provided by the NASA Ames and Langley Research Centers under grant NASA/NAG-2-297, the Office of Naval Research under contract ONR/N00014-82-K-0582 (NR 606-003), the National Science Foundation under grant NSF/ECS-8210960, and the AFOSR-Eglin A.F.B. under grant F08635-87-K-0031.

TABLE OF CONTENTS

LIST OF FIGURES

LIST OF TABLES

CHAPTER 5. DESIGN EXAMPLES

NOTATION AND DEFINITIONS

$\mathbf{R}$	field of real numbers
$\mathbf{R}_+$	non-negative real numbers
$\mathbf{R}^n$	space of ordered n-tuples of real numbers
$\mathbf{C}$	field of complex numbers
$\mathbf{C}^{mxp}$	space of complex matrices of dimension m x p
A^{-1}	inverse of matrix A
$A^\dagger$	pseudo-inverse of matrix A
$A^\perp$	orthogonal complement of matrix A
A^T	transpose of matrix A
A^*	complex conjugate transpose of matrix A
$A > 0$	matrix A is positive definite
$A \geq 0$	matrix A is positive semi-definite
$\lambda_i(A)$	the i^{th} eigenvalue of matrix A
$\overline{\lambda}(A)$	the largest (i.e. maximum modulus) eigenvalue of matrix A
$\sigma_i(A)$	the i^{th} singular value of matrix A
$\overline{\sigma}(A)$	the maximum singular value of matrix A
$\rho(A)$	the spectral radius of matrix A, equals $\lvert \overline{\lambda}(A) \rvert$
$\mu(A)$	the structured singular value of matrix A
$Tr(A)$	the trace of matrix A
$\lVert A \rVert_F$	the Frobenius norm of matrix A, equals $[\ Tr\ (A^*A)\ ]^{1/2}$
$G^*(s)$	$:= G^T(-s)$
$j\omega$	point on imaginary axis ($\omega \in \mathbf{R}$)
$j\mathbf{R}$	the imaginary axis

L_2 Hilbert space of matrix-valued functions which are square integrable on **jR** in the sense of the inner product on **jR**

$$\langle F, G \rangle = \frac{1}{2\pi} \int_{-\infty}^{\infty} \mathrm{Tr}\left[F(j\omega)^* G(j\omega) \right] d\omega \qquad \text{if } F, G \in L_2(\mathbf{jR})$$

BL_2 set of bounded L_2 functions, defined as

$$BL_2 = \left\{ v \;\middle|\; \| v \|_2^2 = \int_{-\infty}^{\infty} \| v(t) \|^2 dt < 1 \right\}$$

H_2 the functions in L_2 that are analytic in the open right half plane and satisfying

$$\sup_{\sigma>0} \int_{-\infty}^{\infty} \mathrm{Tr}\left[G(\sigma+j\omega)^* G(\sigma+j\omega) \right] d\omega < \infty$$

$H_2^\perp$ the orthogonal complement of H_2 in L_2

Π the orthogonal projection from L_2 to $H_2^\perp$

L_∞ Banach space of matrix-valued functions which are (essentially) bounded on **jR**

RL_∞ rational functions in L_∞ with real coefficients

$RL_\infty(n)$ rational functions in L_∞ with real coefficients and McMillan degree $\leq n$

H_∞ functions in L_∞ with bounded analytic continuation to right half plane

RH_∞ rational functions in H_∞ with real coefficients

$RH_\infty(n)$ rational functions in H_∞ with real coefficients and McMillan degree $\leq n$

$\|G\|_2$ L_2 / H_2 norm

$$= \frac{1}{2\pi} \int_{-\infty}^{\infty} \mathrm{Tr}\left[G(j\omega)^* G(j\omega) \right] d\omega \quad \text{if} \quad G \in L_2(\mathbf{jR}) \text{ or } H_2(\mathbf{jR})$$

$\|G\|_\infty$ L_∞ / H_∞ norm

$$= \operatorname{ess\,sup}_{\omega \in \mathbf{R}} \bar{\sigma}\left[G(j\omega) \right] \quad \text{if } G \in L_\infty(\mathbf{jR}) \text{ or } H_\infty(\mathbf{jR})$$

$\| G \|$ the operator norm of G

Γ_G Hankel operator generated by $G \in L_\infty$

$[A,B,C,D]$ $:= D + C (sI - A)^{-1} B$, transfer function notation

$F_l(H,R)$ the *lower* linear fractional transformation, equals the closed-loop transfer function from u_1 to y_1 in Figure 1,

$= H_{11} + H_{12} R (I - H_{22} R)^{-1} H_{21}$

$F_u(H,R)$ the *upper* linear fractional transformation, equals the closed-loop transfer function from u_2 to y_2 in Figure 2,

$= H_{22} + H_{21} R (I - H_{11} R)^{-1} H_{12}$

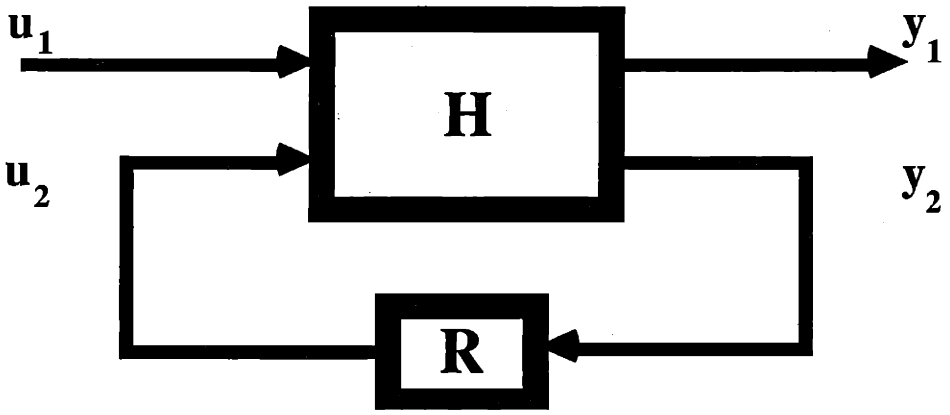

Figure 1 Block diagram for the lower linear fractional transformation.

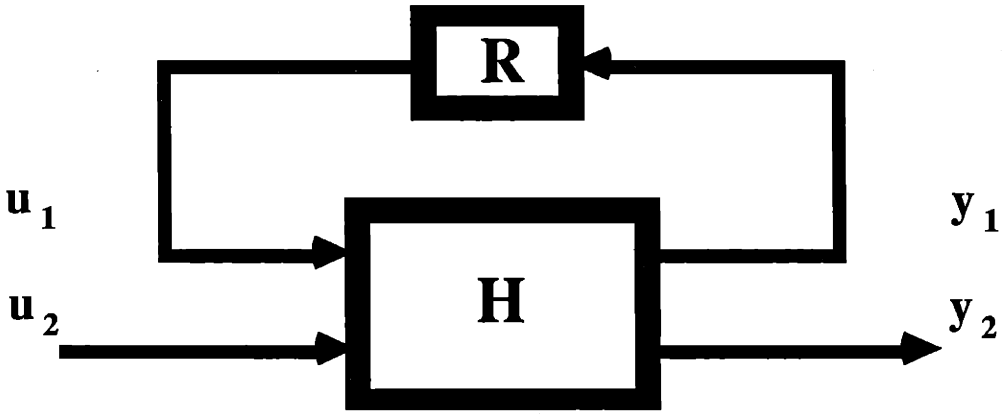

Figure 2 Block diagram for the upper linear fractional transformation.

Definition 1 A time signal f(t) is *left-sided stable* if and only if

$$\lim_{t \to -\infty} f(t) = 0.$$

Definition 2 A time signal f(t) is *right-sided stable* if and only if

$$\lim_{t \to \infty} f(t) = 0.$$

Definition 3 A time signal f(t) is *causal* if and only if

$$f(t) = 0 \quad \text{for } t < 0.$$

Definition 4 A time signal f(t) is *anti-causal* if and only if

$$f(t) = 0 \quad \text{for } t > 0.$$

Definition 5 A time signal f(t) is *noncausal* if and only if

$$f(t) \neq 0 \quad \text{for some } t < 0.$$

Remark The terms *stable* and *causal* will be used frequently throughout this thesis. We see from the above definitions that these are fundamentally time-domain concepts. For a frequency-domain interpretation, let F(s) be a rational transfer function matrix in RL_∞. In general, the poles and zeros of F(s) will lie over the entire complex plane. However since F(s) is rational and has no poles on the imaginary axis, it must be analytic in some strip containing the imaginary axis. Let f(t) denote the inverse bilateral Laplace transform of F(s) with this strip being the region of convergence. Then f(t) is stable (left and right-sided), but noncausal in general. In this thesis, a noncausal rational transfer function is analytic in a strip containing the imaginary axis (i.e. it may have poles in the left and right half planes).

CHAPTER 1. INTRODUCTION

1.1 Overview

1.1.1 Motivation

Any mathematical description of a physical phenomenon is an abstraction (i.e. simplification) of the process. The result is an inherent discrepancy between a mathematical formulation and the plant being modeled. Therefore, a complete description of a physical system consists not only of some nominal mathematical model, but also *must* include an accompanying description of the modeling uncertainty.

The purpose of a feedback system is to improve the dynamic performance of a physical plant in the presence of uncertainty. That is, the performance of the closed-loop system should be insensitive to changes in the process or the environment. A common approach to the design of a feedback system requires that the plant be described in formal mathematical terms. The modeling procedure produces a "simple" description of the plant dynamics (i.e. the nominal plant model), as well as a characterization of the uncertainty associated with the nominal model. In addition to the nominal model and the uncertainty description, the desired feedback system performance is specified. The ultimate objective of any feedback system is to achieve the desired performance (e.g. command-following, disturbance-rejection) when operating in a closed-loop with the actual, physical plant. This requires the nominal mathematical system to be robust; that is, perform satisfactorily in the presence of uncertainty.

The process of design consists of two distinct steps: analysis and synthesis. Analysis allows one to quantitatively assess the performance of a system in terms of some mathematical tools. Synthesis is the creation of a system with desired performance

characteristics expressed in terms of the analysis framework. This thesis is concerned with the problem of feedback system design in the presence of modeling uncertainty and the main contributions are in the area of synthesis.

Maintaining stability in the presence of uncertainty has long been recognized as the crucial requirement for the closed-loop system [1,2]. Classical designers developed the concepts of gain and phase margin to quantify stability-robustness measures. In the modern control era, criteria for maintaining closed-loop stability in the presence of a single, unstructured (i.e. norm bounded) modeling uncertainty have been formulated in terms of a singular value frequency-domain inequality on the closed-loop transfer function [3].

It is only recently that the issue of multiple modeling uncertainties appearing at different locations in the feedback loop and the related requirement of performance-robustness have been addressed [4]. Multiple unstructured uncertainty blocks, parameter uncertainty, and performance specifications give rise to so-called structured uncertainty. A new analysis framework based on the structured singular value, μ, has been proposed by Doyle to assess the stability and performance robustness of linear, time-invariant (LTI) feedback systems in the presence of structured uncertainty [5].

While the analysis aspect of LTI feedback design is well-established, the definitive robust synthesis methodology has yet to be developed. The problem of designing a feedback system that exhibits closed-loop stability *and* performance in the face of modeling uncertainty, so-called "μ-synthesis", is nonconvex. The synthesis approach proposed by Doyle in [6] is an iterative scheme, referred to as DK iteration, that involves a sequence of scaled H_∞-based feedback design problems. Unfortunately, convergence to the global solution is not guaranteed due to the inherent nonconvexity of the problem. Since local solutions may result, it is worthwhile to explore other fundamentally different approaches to μ-synthesis that may result in feedback systems with improved robustness properties; this provided a motivation for the thesis.

There was another motivating force behind the search for a system that exhibits robust performance in the presence of structured uncertainty: the adaptive control problem. In fact, it provided the original impetus to this research. An adaptive system deals with uncertainty via on-line plant identification and compensator parameter adjustment. A very active search for a robust adaptive control methodology was begun following the discovery of fundamental instability mechanisms in the primary adaptive algorithms due to the presence of unmodeled dynamics [7]. A trend has developed and many researchers believe that a robust adaptive control system must consist of a robust system identification algorithm [8] coupled with a robust control design method [9-13]. Compensator redesign takes place infrequently compared to the system sample period and only when more accurate information about the system can be provided by the identification algorithm. The design of a fixed-parameter robust compensator is at the heart of this adaptive control philosophy; such a synthesis methodology is only currently emerging.

Over the years a great deal of attention has been paid to the development of specific adaptive algorithms; however, very little consideration has been given to an issue at the heart of the adaptive control problem: *what are the performance benefits of adaptive control?* In theory, an adaptive control system will ultimately provide better performance with respect to a fixed-parameter compensator because more information about the physical plant is incorporated into the design process (on-line). Robust adaptive control systems, in practice, rely upon gain-scheduling for gross adaptation, some combination of external persistently exciting signals (to ensure good identification), slow sampling (to provide stability robustness with respect to unmodeled high-frequency dynamics [14]), and extensive real-time computation (to provide safety nets that turn off the adaptation when it exhibits instability [15]). These robustifying measures degrade command-following and disturbance-rejection performance and tend to neutralize the anticipated benefits of an adaptive compensator.

In light of these circumstances it is prudent that the decision to use adaptive control, in a real engineering application, be based upon a quantitative assessment of the costs and benefits of an adaptive system. A fixed-parameter feedback system designed for robust performance may serve as a benchmark to which an adaptive control system is compared.

It is clear that a new robust design methodology will be a welcome addition to the set of design paradigms available to the control engineer. In the sequel we develop such a methodology.

1.1.2 Contributions of the Thesis

The primary contribution of this thesis is the development and presentation of a new methodology for the synthesis of robust feedback systems. The design technique is referred to as the Causality Recovery Methodology (CRM), and it may be applied to any finite-dimensional, linear, and time-invariant system. Given a plant model, a description of the modeling uncertainty, and performance specifications, the CRM will design a compensator that yields a closed-loop system with the following guarantees:

(1) nominal closed-loop stability

(2) stability-robustness with respect to some modeling uncertainty

(3) nominal performance

(4) performance-robustness with respect to some specification

The concept of robustness margin is introduced to quantify the notion of stability and performance robustness. The CRM is guaranteed to produce a compensator and closed-loop system with a robustness margin greater than or equal to that of a given, fixed feedback loop. The CRM accomplishes the improvement by augmenting the existing compensator. The implication is that the CRM is likely to improve the performance-robustness of a compensator

designed by another synthesis method.

The CRM initially lifts the natural and physically necessary restriction of compensator causality. This permits a simpler view of the feedback problem. The stability and performance robustness requirements may be examined on a frequency point by frequency point basis. A feasible set of noncausal compensators, in the space of complex matrices, satisfying the robustness condition is constructed at each frequency. Causality of the compensator is then recovered via an optimization problem that minimizes the Hankel norm (i.e. the measure of noncausality) over the feasible set.

From a theoretical point of view the CRM is characterized by iterating two sets of *convex static, infinite-dimensional optimization* problems. The practical algorithm that has been constructed obviously limits the set of frequency points over which the noncausal compensator is derived, and uses a high-order, finite-dimensional compensator in the Hankel norm minimization. Unfortunately, when these finite-dimensional approximations are used the convexity of the underlying mathematical optimization problems is lost, and consequently only local convergence can be guaranteed.

From an applied viewpoint, the CRM is characterized by extensive (off-line) computational requirements. However, the programming effort is modest. In addition, part of the design algorithm is parallelizable, so that super-computer implementation should bring the design time down to a reasonable level.

The development of a complete methodology for the design of robust feedback systems (i.e. the exact global solution to the μ-synthesis problem and its extensions to real parameter uncertainty sets) will ultimately produce control systems with optimal performance in the presence of uncertainty. The CRM represents a small step toward achieving this goal.

1.1.3 A Historical Note

When the CRM was developed in early summer 1987, the solution of the μ-synthesis problem using DK iteration [6, 16] was viewed as relatively cumbersome, due to the computational complexity of solving the underlying H_∞ synthesis problem [17-20]. In fact, published numerical studies [21] did not even solve the full-blown H_∞ synthesis problem because of the computational burden.

However, a very recent advance by Doyle and Glover (as yet unpublished) was communicated to the author in October 1987 by G. Stein [22]. Doyle and Glover have succeeded in showing how to *efficiently* solve H_∞ synthesis problems through the solution of two (nonstandard) Riccati equations. We summarize, for the sake of completeness, these results in Section 4.2.1. This advance greatly improves the efficiency of the DK iteration for solving the μ-synthesis problem.

1.1.4 Organization of the Thesis

The thesis is organized into 6 chapters. In the remainder of this chapter, the FDLTI feedback design problem in the presence of uncertainty is defined. In addition, previous results are outlined and the CRM is formally introduced. Chapter 2 contains the basic mathematical background and concepts required by the Causality Recovery Methodology. The primary analysis tool, the structured singular value, is defined and described. The theory of Hankel operators is a critical element of the design method and is reviewed in Chapter 2. Results from the field of convex optimization are briefly described as well. Stability, performance, and robustness analysis of linear feedback systems with structured uncertainty is discussed in Chapter 3. The main contribution of the thesis, the Causality Recovery Methodology, is developed in Chapter 4. Chapter 5 contains two numerical

examples of the CRM design procedure, and the final chapter discusses the results and proposes directions for further research.

1.2 The Formal Synthesis Problem

1.2.1 Introduction

The purpose of this section is to pose the general control problem. The issues of uncertainty and performance will be discussed, and finally the formal feedback synthesis problem will be presented in a rigorous, mathematical framework.

What is the purpose of feedback? This very fundamental question must be examined before we attempt to formulate a synthesis methodology. At the most basic level, we require the dynamic response of some physical process to have certain characteristics or lie in some set of desirable responses. The objective of a compensator is to generate the appropriate inputs (i.e. controls) to the physical process so that the desirable response is achieved. It has long been obvious that feedback (as opposed to open-loop) control is required in the face of open-loop unstable plants, uncertain plant dynamics, and external unmeasurable disturbances . The situation is depicted in Figure 1.1.

The uncertain plant will be modeled as a known nominal system or plant plus some modeling error or perturbation. The precise plant perturbation is unknown; however, it is a member of a known set of possible perturbations. Figure 1.2 embodies this description of the feedback system, which has become standard in the H_∞ control community [6, 16-18, 23]. G represents the nominal plant model, which includes the process to be controlled along with any sensors and actuators. G is a known finite-dimensional, linear, time-invariant (FDLTI) operator, e.g. a transfer function matrix. The compensator transfer function matrix to be designed is K. L is also a FDLTI operator representing the perturbation on G due to the uncertain plant dynamics; when L = 0, we only deal with the nominal plant. The vector time

signals in Figure 1.2 are defined as follows.

d'	Exogenous inputs (commands, disturbances, sensor errors)
e'	Errors, to be made small
u	Controls
y	Measurements
v'	Output from perturbation operator
z'	Input to perturbation operator

The synthesis problem is to specify K to

(1) achieve closed-loop stability

(2) satisfy performance specifications

(3) provide stability and performance robustness with respect to all possible L

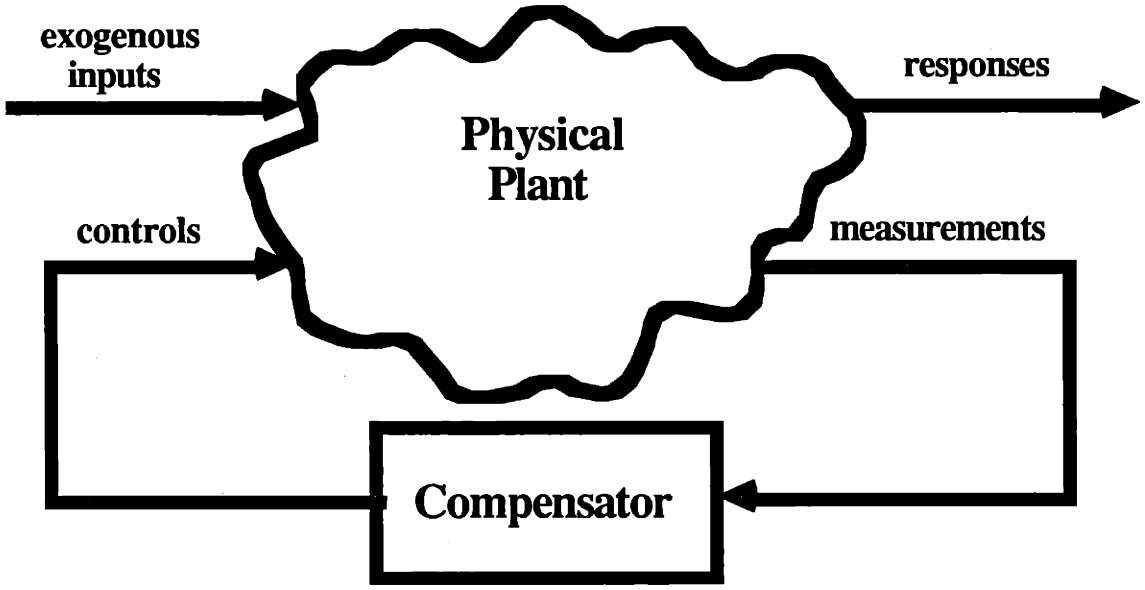

Figure 1.1 The generic feedback problem.

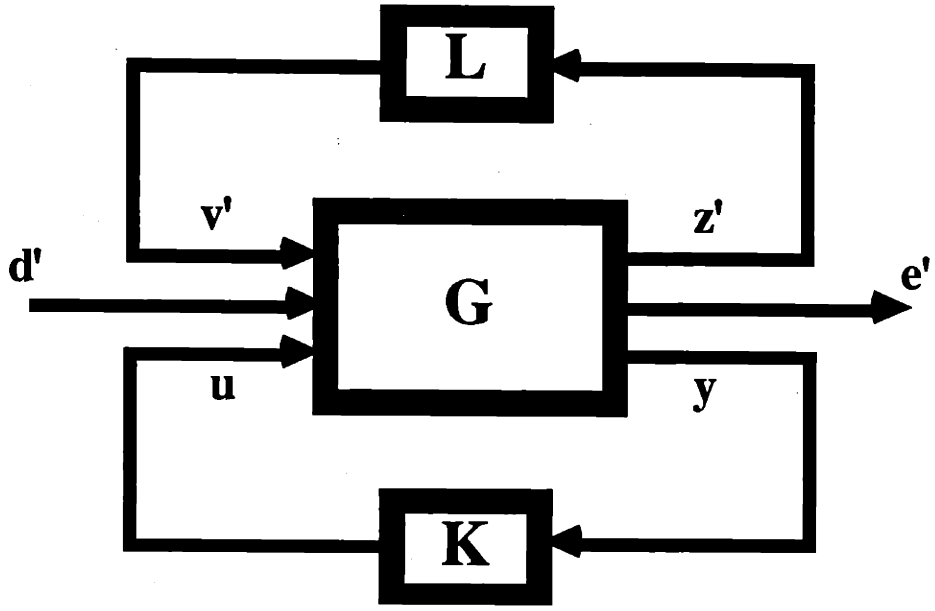

Figure 1.2 A model of the feedback problem.

1.2.2 Nominal Stability

The first requirement for a compensator is that it stabilize the nominal closed-loop system (i.e. for L = 0). Stability implies that bounded inputs produce bounded outputs; that is, internal stability must be achieved. Therefore, K must place all closed-loop poles in the left half plane. In order to meet this requirement, it is evident that stabilizable and detectable design models are needed.

1.2.3 Nominal Performance

Performance is a very broad concept, open to a wide variety of definitions and interpretations. In the context of this thesis and Figure 1.2, performance will roughly mean

that inputs d' in a specified class should produce "small" responses e' that are members of a given set. The input class of interest includes all possible L_2 functions with a bounded norm. This is a common and physically relevant assumption on the exogenous input signals. Bounded L_2 functions correspond to signals of bounded energy. The same assumption is made on the responses e'.

Weighting functions on the input and output signals are used to scale the norm bounds to unity and reflect the varying spatial and frequency content of the input signals and performance specifications. Define new input and output signals d and e (Figure 1.3).

$$d = W_d\, d' \tag{1.1}$$

$$e = W_e\, e' \tag{1.2}$$

W_d and W_e are stable, minimum phase transfer function matrices of appropriate dimension. The weighting functions on each vector provide an extra degree of freedom in the design process, and allow the set of input signals d to be defined independently of the set of desirable responses e.

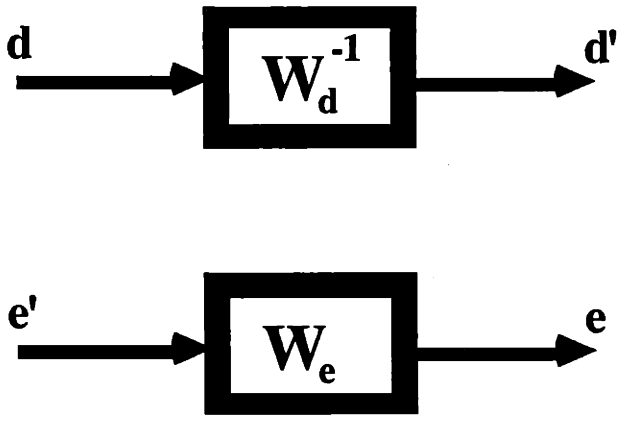

Figure 1.3 Use of weighting functions to define input and output signals.

The frequency response of the largest singular value of a typical input signal (W_d^{-1}) or performance (W_e) weighting function is shown in Figure 1.4. The magnitude is selected by the designer to be large at low frequencies where the references and disturbances are expected to have their energy concentrated. The frequency response declines and levels off at high frequencies where insensitivity to sensor noise and stability-robustness, rather than command-following or disturbance-rejection, are the prime consideration. The nominal performance objective may now be stated.

> Given the plant model G in Figure 1.2 and the weighting functions W_d and W_e (L is assumed to be identically zero), find the internally stabilizing compensator K such that
>
> $$e \in BL_2 \quad \text{for all} \quad d \in BL_2$$
>
> where BL_2 is the set of bounded L_2 functions.

$$BL_2 = \left\{ \; v \;\middle|\; \| v \|_2^2 = \int_{-\infty}^{\infty} \| v(t) \|^2 \, dt < 1 \; \right\} \tag{1.3}$$

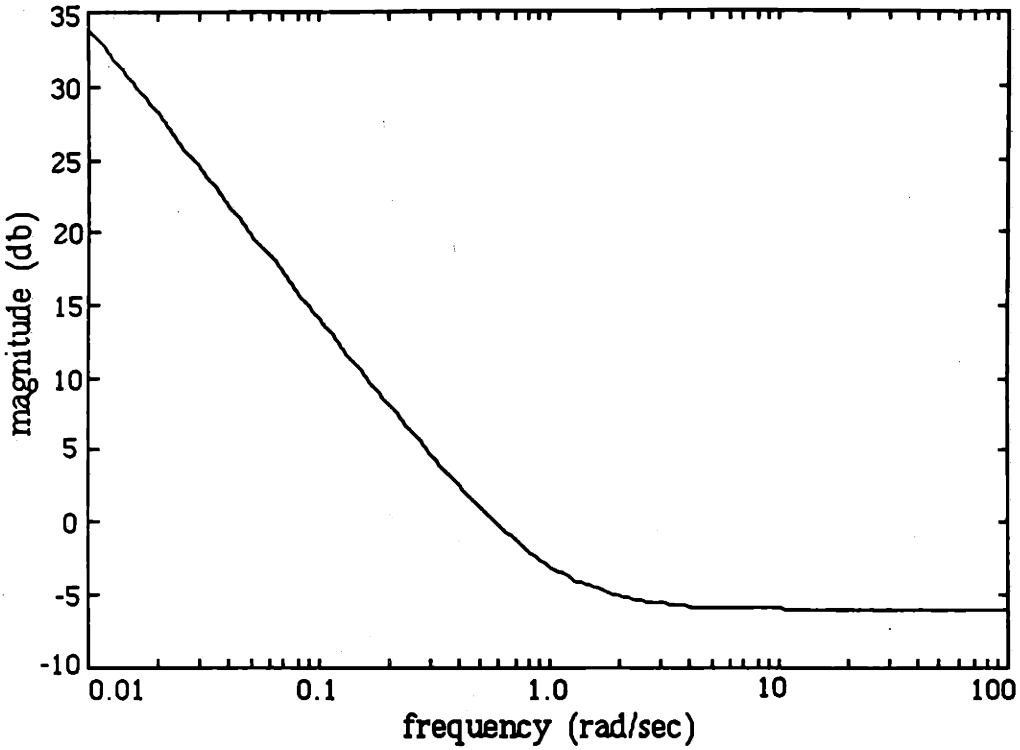

Figure 1.4 Frequency response of a typical performance weighting function.

1.2.4 Uncertainty and Robustness

The operator L in Figure 1.2 arises from the uncertain dynamics associated with the nominal plant model G. L is a result of two generic classes of modeling uncertainty: parameter variations (real) and norm-bounded perturbations (complex). Parameter variations arise from imprecisely known coefficients in the lumped differential equation models of physical systems. Norm-bounded perturbations, also called unstructured uncertainty, are the result of unmodeled dynamics (high-frequency stable poles, far-away minimum and nonminimum phase zeros) and other neglected phenomena (small delays, nonlinear effects, etc.).

We will only be concerned with norm-bounded uncertainty in the sequel. This restriction is not unreasonable, at the present time, because the structured singular value analysis of systems with real parameter variations (the real-μ problem) is relatively crude [16]. It would be fruitless to attempt the formulation of a synthesis methodology without having the rigorous analysis tools as a foundation. In addition, real parameter variations may be handled by "covering" the real perturbation with a complex uncertainty block. Of course, this introduces some conservatism into the design process; however, limited practical experience suggests this procedure is only slightly conservative [21].

When the feedback problem is posed as in Figure 1.2, multiple unstructured uncertainty blocks present at various locations in the feedback loop model give rise to a perturbation L with a block diagonal structure [4].

$$L = \text{diag}(L_1, L_2, ..., L_n) \tag{1.4}$$

As with the input and output signals, weighting functions on the individual perturbations are essential in capturing the spatial and frequency charateristics of L_i. Define the weighted perturbation vectors v_i and z_i (Figure 1.5), for i = 1 to n.

$$v_i = W_{v_i} v_i' \tag{1.5}$$

$$z_i = W_{z_i} z_i' \tag{1.6}$$

Describe the perturbation L in Eqn. (1.4) and Figure 1.2 in terms of a norm-bounded uncertainty Δ and the above weighting functions.

$$L_i = W_{v_i}^{-1} \Delta_i W_{z_i} \tag{1.7}$$

where

W_{v_i} and W_{z_i} are stable, minimum phase FDLTI weighting transfer function matrices

$\Delta_i \in \mathbb{P}$

$\mathbb{P} = \{ \Delta \mid \Delta \text{ stable}, \ \| \Delta \|_\infty < 1 \}$

$$\| \Delta \|_\infty = \sup_\omega \bar{\sigma}[\Delta(j\omega)]$$

The frequency response of the largest singular value of a typical uncertainty weighting function ($W_{v_i}^{-1}$ or W_{z_i}) is shown in Figure 1.6. This typical shape reflects the fact that modeling errors are generally small at low frequencies, where a good understanding of the physical phenomenon exists, and rise as neglected, high-frequency effects become significant.

The robustness requirement states that the compensator K must satisfy the stability and performance objectives in the presence of all possible perturbations. That is, for all L under consideration

(1) Stability-Robustness: The closed-loop transfer function matrix from d to e must have all its poles in the left half plane.

(2) Performance-Robustness: $e \in BL_2$ for all $d \in BL_2$

Chapter 3 contains the analysis tests that ensure (1) and (2) are satisfied.

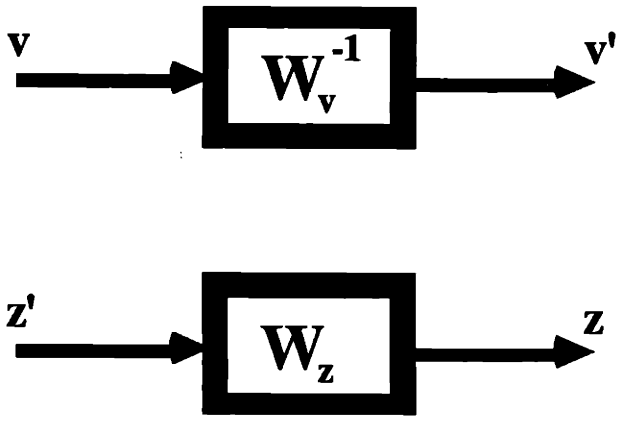

Figure 1.5 Uncertainty weighting functions.

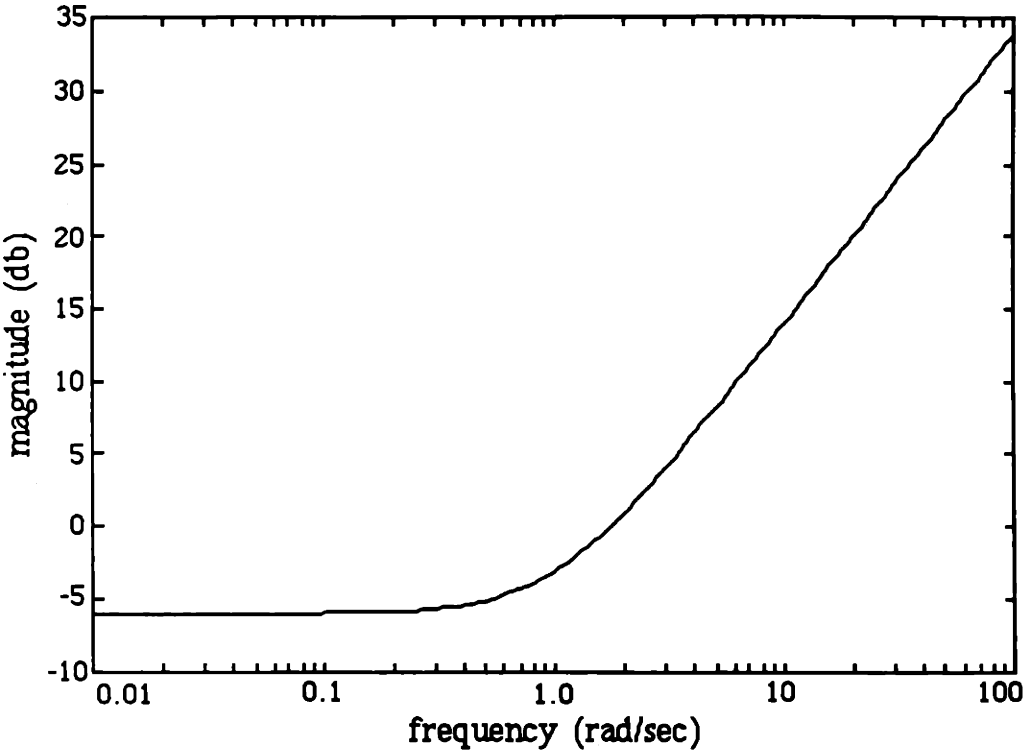

Figure 1.6 Frequency response of a typical uncertainty weighting function.

1.2.5 Formal Design Framework

The uncertainty and performance weighting functions defined in the previous sections can be incorporated into the plant model G to yield the block diagram in Figure 1.7. The FDLTI operator P will be referred to as the design plant model. P consists of the control plant model G and the uncertainty and performance weighting functions W_v , W_z , W_d , and W_e. Note that the design objectives have been (partially) reflected in these weighting functions, and hence in P. So the simplicity of the formal design framework is somewhat misleading, because the frequency-domain stability/performance tradeoffs are assumed fixed. Δ is a unity norm-bounded, diagonal perturbation and is a member of the set $\mathbb{\Delta}$, where

$$\mathbb{\Delta} = \{ \ \Delta \mid \Delta = \text{diag}(\Delta_1, \Delta_2, ..., \Delta_n) \ , \Delta_i \in \mathbb{P} \ \} \qquad (1.8)$$

$$\mathbb{P} = \{ \ \Delta \mid \Delta \text{ stable}, \ \| \Delta \|_\infty < 1 \ \}$$

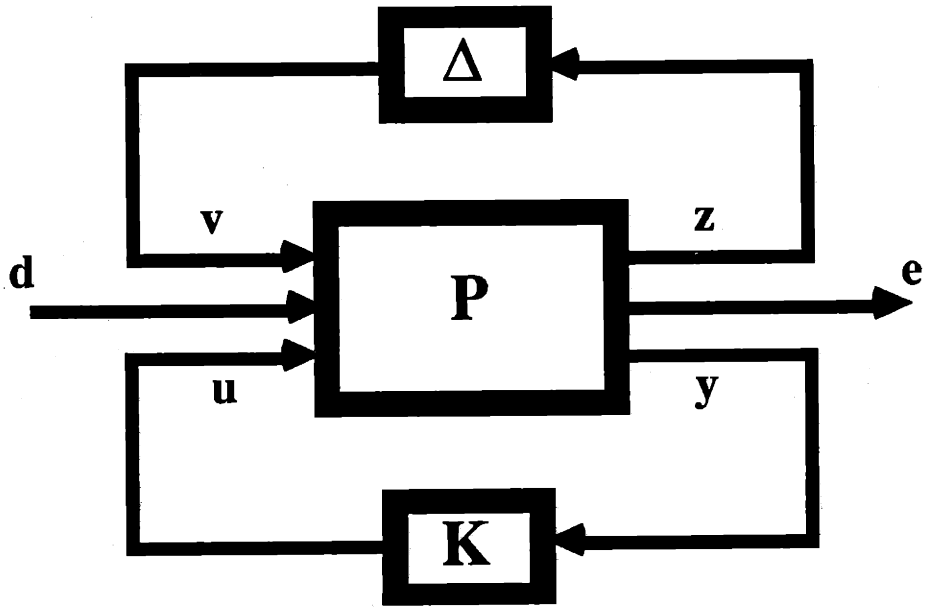

Figure 1.7 General framework for feedback design problem.

Any linear interconnection of components, inputs, outputs, and perturbations may be put into the structure of Figure 1.7. The block diagram contains the following relationships, where the P_{ij} are transfer function matrices of suitable dimensions.

$$\begin{bmatrix} z \\ e \\ y \end{bmatrix} = \begin{bmatrix} P_{11} & P_{12} & P_{13} \\ P_{21} & P_{22} & P_{23} \\ P_{31} & P_{32} & P_{33} \end{bmatrix} \begin{bmatrix} v \\ d \\ u \end{bmatrix} \tag{1.9}$$

$$u = Ky \tag{1.10}$$

$$v = \Delta z \tag{1.11}$$

The compensator K in Figure 1.7 can be incorporated with the plant P via a lower linear fractional transformation to yield the closed-loop transfer function matrix S (Figure 1.8), i.e. $S = F_l(P, K)$.

$$S = \begin{bmatrix} S_{11} & S_{12} \\ S_{21} & S_{22} \end{bmatrix} \tag{1.12}$$

$$\begin{bmatrix} z \\ e \end{bmatrix} = \begin{bmatrix} S_{11} & S_{12} \\ S_{21} & S_{22} \end{bmatrix} \begin{bmatrix} v \\ d \end{bmatrix} \tag{1.13}$$

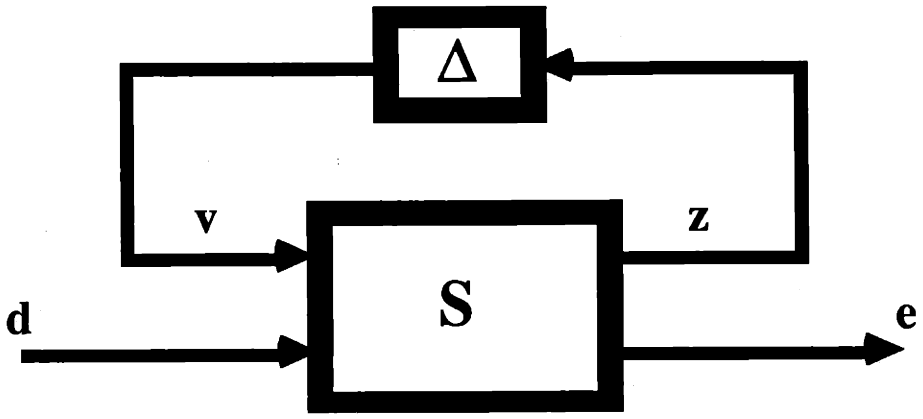

Figure 1.8 Block diagram for closed-loop system.

We now have a formal framework in which to handle the feedback control problem. The concept of performance has been rigorously defined, and the type of modeling uncertainty to be encountered is known. In the sequel a methodology is developed to find a compensator K that satisfies all the objectives discussed in this section.

1.2.6 A Standard Feedback Problem

At this point, it is a worthwhile exercise to interpret the formal feedback problem of the previous section (Figure 1.7) in terms of the more conventional feedback structure in Figure 1.9. We will see that the standard problem in Figure 1.9 is simply a special case of the more general framework presented in Section 1.2.5.

The plant G and the compensator K are FDLTI systems such that the closed-loop system is nominally stable. For the sake of clarity, the only exogenous input to be considered is the reference command d. Other exogenous inputs, such as disturbances and sensor noises, are handled in a similar manner. The unweighted tracking error is denoted by

e' (and y), the control signal generated by the compensator is u, and y' is the plant output. This notation was adopted so as to maintain consistency with that in Figure 1.7. It follows from the block diagram in Figure 1.9 that

$$e' = (I + GK)^{-1} d \tag{1.14}$$

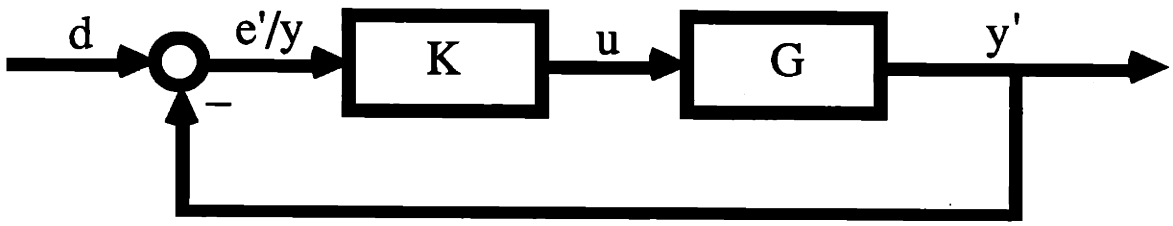

Figure 1.9 Standard feedback configuration.

Define the standard (output) sensitivity transfer function matrix R.

$$R = (I + GK)^{-1} \tag{1.15}$$

It is clear from Eqn. (1.14) that the tracking error will be small if R is small in the frequency range where the commands have their energy (typically low frequencies). A typical performance specification defined with respect to the sensitivity transfer function matrix R is

$$\bar{\sigma} [R(j\omega)] < | w_e^{-1} (j\omega) | \qquad \forall\omega \tag{1.16}$$

where w_e (s) is a single-input, single-output (SISO), proper transfer function that is stable

and minimum phase. $| w_e^{-1} (j\omega) |$ serves to bound the magnitude of the sensitivity over frequency. The Bode plot of a typical sensitivity bounding function, $| w_e (j\omega) |$, is shown in Figure 1.4. The magnitude is large (i.e. small sensitivity) in the low frequency range, where good command-following is desired.

In any realistic problem, there is some modeling error associated with the plant G in Figure 1.9. Describe this error with a multiplicative, norm-bounded (unstructured) uncertainty at the plant input. That is, the perturbed plant $\tilde{G}$ has the representation

$$\tilde{G} = G[I + L] \tag{1.17}$$

where

$$\bar{\sigma} [L(j\omega)] < | w_z (j\omega) | \qquad \forall\omega \tag{1.18}$$

The SISO transfer function $w_z (s)$ is also stable and minimum phase, and bounds the magnitude of the perturbation over frequency. Refer to Figure 1.6 for the magnitude Bode plot of a typical uncertainty bounding function. The modeling error is generally small at low frequencies, and increases with ω.

The compensator K must maintain stability in the presence of L. That is, the closed-loop system in Figure 1.9 must have all its poles in the left half plane when G is replaced by $\tilde{G}$, for all $\tilde{G}$ described by Eqns. (1.17) and (1.18). The stability-robustness condition for a multiplicative perturbation at the plant input is well-known [3]. Define the standard (input) complementary sensitivity

$$C = KG(I + KG)^{-1} \tag{1.19}$$

Then, the closed-loop system is stable for all possible $\tilde{G}$ if

$$\bar{\sigma} [C(j\omega)] < | w_z^{-1} (j\omega) | \qquad \forall\omega \tag{1.20}$$

However, nominal performance (Eqn. 1.16) and stability-robustness (Eqn. 1.20) does not constitute a complete set of requirements for the closed-loop system. A certain level of performance must be guaranteed for all possible L, as well. Let the perturbed (output) sensitivity $\tilde{R} = (I + \tilde{G}K)^{-1}$. Then, the robust performance problem is to find a K such that

$$\bar{\sigma} [\tilde{R}(j\omega)] < | w_e^{-1} (j\omega) | \qquad \forall\omega \tag{1.21}$$

for all $\tilde{G}$ described by Eqns. (1.17) and (1.18). Compare the specifications in (1.16) and (1.21).

Structured singular value analysis and the formal design framework in Section 1.2.5 were developed to handle the robust performance problem. We will now take the standard problem just described and put it into the formal framework. The weighting functions in Eqns. (1.1) and (1.2) can be defined directly from the statement of the conventional problem. Given the block diagram in Figure 1.9 and the performance specification in (1.21),

$$W_d = I \tag{1.22}$$

$$W_e = w_e I \tag{1.23}$$

where I is the identity matrix of appropriate dimension. From Eqn. (1.7) and condition (1.18), the uncertainty weights in (1.5) and (1.6) are defined.

$$W_v = I \tag{1.24}$$

$$W_z = w_z I \tag{1.25}$$

Then,

$$L = \Delta W_z \tag{1.26}$$

where Δ is a stable operator with $\| \Delta \|_\infty < 1$. L obviously satisfies the inequality in (1.18).

The modeling uncertainty at the plant input and the weighting functions can be incorporated into the block diagram shown in Figure 1.9. The complete block diagram (with the uncertainty and weights) has been manipulated in Figure 1.10 to conform to the formal design framework (Figure 1.7). The design plant model P can now be defined in terms of the specific structure shown in Figure 1.10.

$$P = \begin{bmatrix} 0 & 0 & W_z \\ -W_eG & W_e & -W_eG \\ -G & I & -G \end{bmatrix} \tag{1.27}$$

The closed-loop transfer function $S = F_l(P, K)$ is

$$S = \begin{bmatrix} -W_zKG(I+KG)^{-1} & W_zK(I+GK)^{-1} \\ -W_eG(I+KG)^{-1} & W_e(I+GK)^{-1} \end{bmatrix} \tag{1.28}$$

Note that S_{11} is the product of the uncertainty weight and the complementary sensitivity, and S_{22} is the weighted sensitivity. We will see in Chapter 3 that the nominal performance and stability-robustness analysis of S produces precisely the same constraints as in Eqns. (1.16) and (1.20), respectively. The performance-robustness requirement in Eqn. (1.21) is equivalent to a frequency-domain inequality involving the structured singular value of S (see Section 3.4.2).

It is hoped that this section has given the reader some insight into the formal synthesis problem. The performance and uncertainty weighting functions have been defined in terms

of the classical notions of sensitivity reduction and norm-bounded, multiplicative error. Finally, the objectives of the formal synthesis problem (i.e. stability and performance robustness) have been related to conventional feedback requirements.

Note that the numerical examples in Chapter 5 will be solved in terms of the standard configuration in Figure 1.9.

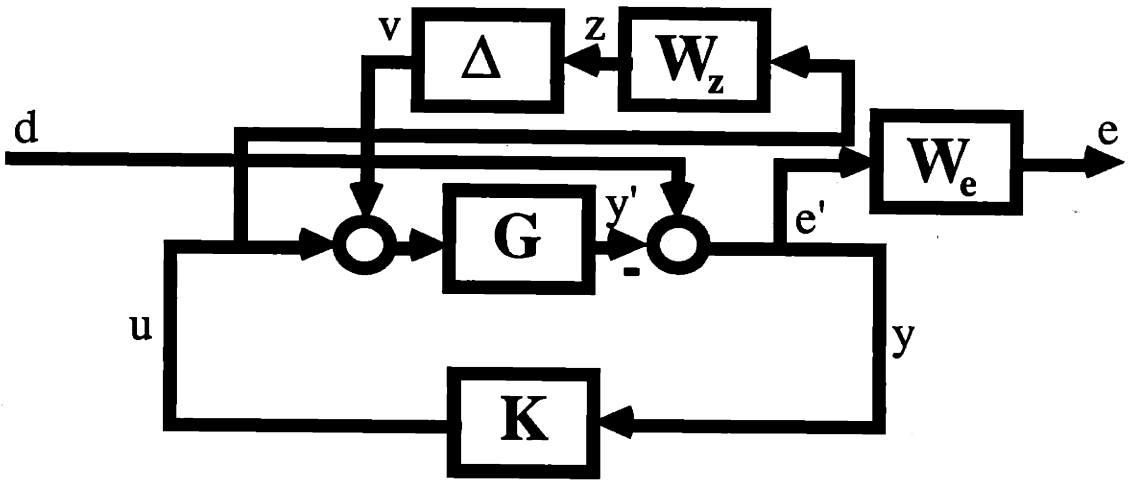

Figure 1.10 Standard feedback configuration put into the formal design framework; compare with Figures 1.7 and 1.9.

1.3 Previous Work and Related Literature

1.3.1 Background Theory

Several aspects of modern feedback theory provide the foundation for this research. The general framework for considering the problem of robust synthesis is well-established [5, 6, 16, 21, 24].

For the analysis of feedback system robustness we rely on the structured singular value μ. This analysis tool, developed by Doyle [5], is a generalization of the ordinary singular value that provides a necessary and sufficient condition for robust stability *and* performance. It removes the conservatism associated with singular value analysis of systems containing structured uncertainty. A frequency-domain performance criterion in terms of μ is central to the CRM.

The synthesis methodology developed in this thesis relies on results from several other areas of systems and control theory. The foundation of the causality recovery approach is the parameterization of all stabilizing compensators conceived by Youla, Jabr, and Bongiorno [25], and refined by Desoer, Liu, Murray, and Saeks [26]. This formula characterizes all stabilizing compensators in terms of a causal, stable operator Q. The resulting closed-loop map is internally stable and an affine function of Q. As we shall see in Chapter 4, this structure plays a key role in the design process.

We also rely heavily on the H_∞ theory pioneered by Zames [27-30] and formalized by Francis and Doyle [17, 18]. The μ-synthesis method (DK iteration), invented by Doyle [6], figures prominently in the CRM, as well. As we shall see in the sequel, H_∞ and (nonconverged) DK iteration compensators provide good starting designs for the CRM.

The theory of Hankel operators [17, 31, 32] is an integral part of the H_∞ feedback paradigm, and it turns out to be equally crucial to the CRM approach. The norm of a Hankel

operator measures the distance of the operator from the H_∞ space or, equivalently, it is a measure of noncausality. Minimizing a Hankel norm over some feasible set is the key concept in the Causality Recovery Methodology. Thus, optimization [33] is also a critical part of the design process.

1.3.2 Approaches to Robust Linear Control

The idea of designing feedback systems to be robust with respect to modeling uncertainties is certainly not new [2]. In fact, various techniques to deal with uncertainty have been proposed throughout the years. Horowitz [34, 35] developed the so-called Horowitz templates that represent, at a particular frequency, the gain and phase changes associated with parameter variations as a region on a Nichols chart. A loop transfer function is derived via classical, graphical techniques from the templates. This procedure is supposed to ensure closed-loop stability and a certain amount of performance over the possible range of parameters. While it is claimed to be a general multivariable method, the procedure is extremely tedious for more than a few frequency points and a great deal of judgment is required on the part of the designer.

Sideris and Safonov [36] approach the problem of structured uncertainty by examining a plant template in the complex plane. A series of transformations at each frequency is performed that maps the irregularly shaped region in the complex plane onto the unit disk. The directional properties of the uncertainty are eliminated, and the transformed problem is essentially a design with unstructured uncertainty. Nevanlinna-Pick interpolation is then used to find a robust compensator such that it is a solution to the original problem.

Khargonekar and Tannenbaum address the problem of robust stabilization of SISO systems in the presence of parameter uncertainty [37]. The authors do not deal with performance issues directly and simultaneous variations in the poles and zeros cannot be

considered within the present framework. Robust stabilization has been investigated by a number of other researchers as well [32, 38, 39]. In fact, Vidyasagar and Kimura [39] have derived necessary and sufficient conditions for a particular compensator to achieve robust stabilization, and necessary and sufficient conditions for the existence of such a controller. However, performance guarantees in the presence of uncertainty are not examined.

Adaptive control has been proposed as a solution to the robust control problem. The concept of identifying the uncertain plant on-line and adjusting the controller accordingly is certainly appealing from an intellectual viewpoint. Unfortunately, it is the plant unstructured uncertainty that may cause the adaptive algorithm to become unstable [7].

1.3.3 μ-Synthesis

The μ-synthesis technique developed by Doyle [6, 16] appears to be (at least for the present time) the most promising approach to the problem of formal robust synthesis. In fact, it has actually been successfully applied to some realistic problems [21]. This procedure, referred to as DK iteration, exploits the fact that the structured singular value is a scaled version of the singular value with a block structured scaling matrix. DK iteration involves the solving of a sequence of scaled H_∞ feedback problems. Hence, its computational complexity is directly tied to the ease with which H_∞ synthesis problems can be solved.

The aim is to find a stabilizing compensator K and a scaling transfer function D such that the infinity norm of the scaled closed-loop map is less than unity (i.e. the condition for robust performance is satisfied). One way to accomplish this is to alternately minimize the scaled closed-loop with respect to K or D while holding the other one fixed. For fixed scaling D, an H_∞ control problem results which appears to be solved easily by very recent techniques [22]; see also Sections 1.1.3 and 4.2.1. When the compensator K is fixed, the

minimization with respect to D is a convex optimization problem at each frequency. The resulting D is approximated by a stable, stably invertible, rational transfer function and the process is repeated until it converges. Unfortunately, this iterative scheme is not jointly convex in K and D and, therefore, is not guaranteed to converge to the globally optimal K and D.

1.4 Introduction to the Causality Recovery Methodology

With the invention of the parameterization of all stabilizing compensators [25, 26], FDLTI feedback design may be interpreted as a search over all stable and causal (i.e. H_∞) functions to satisfy some performance specification. The performance criterion of interest to the CRM is the requirement for robust stability and performance. This leads to a frequency-domain inequality on the closed-loop transfer function in terms of the structured singular value. The aim of the CRM is to find a $Q \in H_\infty$ that meets the inequality constraint.

We will show that the function that optimizes the robustness of the feedback system may be easily computed using only complex matrix arithmetic. The caveat is that this function is not causal (i.e. not in H_∞), in general. The aim of the CRM is to find a stable, causal transfer function matrix that will closely approximate the robustness characteristics of the optimal solution. This process may be thought of as recovering the causality of the optimal solution while retaining its beneficial frequency-domain properties; hence, the methodology's name.

The Causality Recovery Methodology

Step 0 (A priori Information)

The CRM requires a finite-dimensional realization of the design plant P in Figure 1.7. Recall that P includes a model of the plant to be controlled, as well as any performance and

uncertainty weighting functions.

Step 1 (Nominal Compensator Design)

Compute a nominal compensator K_{nom} using any existing synthesis methodology. The resulting closed-loop system S_{nom} provides a lower bound on system performance. That is, the CRM will guarantee a closed-loop system whose robustness is no worse than, and hopefully superior to, that of the nominal design.

Step 2 (Parameterization of all Stabilizing Compensators)

Compute the parameterization of all stabilizing compensators in terms of a free transfer function matrix parameter $Q \in H_\infty$ using the plant P and the nominal compensator K_{nom}. The resulting closed-loop transfer function matrix S is affine in Q.

$$S = T_{11} + T_{12}QT_{21}$$

where $T_{11} = S_{nom}$.

The CRM will use Q to fine-tune the nominal design and improve robustness.

Step 3 (Optimal Noncausal Design)

At this point the restriction that Q lie in H_∞ is removed. This allows the designer to examine the robust synthesis problem by finding a complex matrix at each and every frequency. The complex matrix that maximizes the robustness margin, Q^*, is computed at each frequency via a convex optimization program. In general, Q^* corresponds to a noncausal system and will serve as the starting point in the causality recovery process (Step 4). The robustness of the noncausal closed-loop is, of course, an upper bound on the robustness we can expect from a $Q \in H_\infty$.

Step 4 (Causality Recovery)

A feasible set of Q's in the space of complex matrices satisfying the robustness specification is constructed at each frequency. Causality recovery refers to the process of searching over the feasible set, starting at Q^*, for the Q or Q's that are stable and causal. The search for such an H_∞ function in the feasible set is posed as an optimization problem with the objective function being the Hankel norm, which acts as the measure of noncausality. The optimization is an infinite-dimensional convex program whose aim is to minimize the Hankel norm over the feasible set. If the problem is well-posed (i.e. the desired performance is consistent with the uncertainty), the Hankel norm will be reduced to zero and the resulting argument is a Q in H_∞. This Q produces a stable closed-loop system that is at least as robust as the nominal design.

Step 5 (Construction of Compensator)

The compensator is computed as a function of the transfer function matrix $Q \in H_\infty$, the nominal compensator K_{nom}, and the plant P. The closed-loop transfer function S can also be computed directly.

The above procedure is meant to be a methodology for the (off-line) synthesis of robust feedback systems. Hence, the sequel will focus on the development of computable algorithms to implement the CRM. Unfortunately, the computational burden will prove to be quite severe.

CHAPTER 2. MATHEMATICAL BACKGROUND

2.1 The Structured Singular Value

2.1.1 Definition and Description

The structured singular value μ, developed by Doyle in [5], is a function of a complex matrix and plays a key role in the analysis of feedback systems with structured uncertainty. In this section we will describe the mathematical properties and characteristics of μ and discuss various approximations used in its computation. The μ-analysis of feedback systems is covered in section 3.4.

The function μ is essentially a measure of the distance to singularity of a complex matrix with respect to a set of perturbations of fixed structure. In the context of feedback systems, the structured singular value will be used to analyze the stability of the closed-loop system in Figure 2.1. The complex matrix M represents the transfer function (at a specific frequency) from the perturbation outputs to the perturbation inputs. Δ is a complex matrix perturbation. Stability analysis simply ensures that I-MΔ remains non-singular at all frequencies and for all Δ under consideration.

The positive real-valued function μ satisfies the following condition.

$$\det (I - M\Delta) \neq 0 \quad \forall \Delta \in \mathbb{\Delta}, \ \overline{\sigma}(\Delta) < \gamma \quad \text{iff} \quad \gamma\mu(M) \leq 1 \tag{2.1}$$

$\mathbb{\Delta}$ is the set of possible perturbations Δ of given structure. The function μ of M depends on that structure; however, this dependency is not represented explicitly for notational convenience.

If $\mu(M)\neq 0$, (i.e. $\exists \Delta \in \mathbf{\Delta}$ such that $\det (I - M\Delta) = 0$) then

$$\mu(M) = \left[\min_{\Delta \in \mathbf{\Delta}} \{ \bar{\sigma}(\Delta) \mid \det (I - M\Delta) = 0 \} \right]^{-1} \qquad (2.2)$$

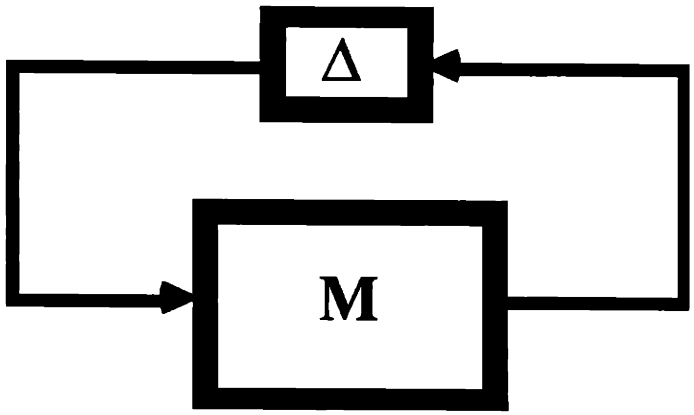

Figure 2.1 Feedback diagram for interpretation of the structured singular value.

Remark 1 The structured singular value is the appropriate tool for analyzing the stability and performance robustness of feedback systems. Realistic modeling uncertainty, as well as closed-loop performance specifications, results in a perturbation Δ of known (block diagonal) structure.

Remark 2 Standard singular value techniques may be used to derive a sufficient condition for the stability of the system in Figure 2.1. This analysis has a serious limitation in that the structure of Δ is completely ignored (i.e. Δ is assumed to be a full matrix perturbation) and the test may be arbitrarily conservative.

Remark 3 While μ results in an "if and only if" robustness condition, a price is paid for such a nonconservative test. The structured singular value is essentially a definition, i.e. search over all possible perturbations of given structure and find the smallest one (in the singular value sense) that makes $I-M\Delta$ singular. Unfortunately, this definition of μ does not satisfy the mathematical definition of a norm. The rich mathematical structure and results which accompany a norm are not available, and this greatly complicates the feedback synthesis problem.

Remark 4 In the sequel we will restrict the problem to the case where $\mathbf{\Delta}$ consists of block diagonal, complex matrices. This represents a very significant class of feedback problems. Such perturbations arise when there are *multiple* norm-bounded (unstructured) uncertainty blocks located at various points in the feedback loop. Unstructured perturbations typically result from unmodeled dynamics, i.e. neglected high-frequency poles and zeros, delays, and nonlinear effects, and worst-case performance specifications. Although real parameter variations are not handled directly, they may be incorporated into this structure in a conservative manner by treating the variations as complex perturbations.

Remark 5 Although equation 2.2 is a suitable definition for the structured singular value, it is not useful for actually computing μ. The implied optimization is nonconvex and may have multiple local minima. Techniques for the calculation of μ are discussed in the next section.

2.1.2 Approximation and Computation

This section presents approximations to μ that lead to reasonable methods for computation in the case of block diagonal, complex perturbations. A more complete treatment can be found in [24]. Assume that $\mathbf{\Delta}$ is a set of matrices such that

$$\mathbf{C}^{N\times N} \supset \Delta \supset \{ \lambda I \mid \lambda \in \mathbf{C} \} \tag{2.3}$$

The two limiting cases provide some insight into the function μ as a generalization of the notions of spectral radius and spectral norm.

$$\Delta = \{ \lambda I \mid \lambda \in \mathbf{C} \} \Rightarrow \mu(M) = \rho(M) = |\overline{\lambda}(M)| \tag{2.4}$$
$$\Delta = \mathbf{C}^{N\times N} \Rightarrow \mu(M) = \overline{\sigma}(M)$$

Bounds on μ in the general case can be obtained from the formulas in (2.4) and from the special properties of Δ. Suppose that $\mathbb{U}$ and $\mathbb{D}$ are sets such that for any $\Delta \in \Delta$

$$U \in \mathbb{U} \Rightarrow \overline{\sigma}(U\Delta) = \overline{\sigma}(\Delta) \tag{2.5}$$
$$D \in \mathbb{D} \Rightarrow D^{-1}\Delta D = \Delta$$

Then, from the definition of μ it follows that

$$U \in \mathbb{U} \Rightarrow \mu(MU) = \mu(M) \tag{2.6}$$
$$D \in \mathbb{D} \Rightarrow \mu(DMD^{-1}) = \mu(M)$$

Based on (2.4) through (2.6), it is shown in [5] that

$$\sup_{U\in\mathbf{U}} \rho(MU) \le \mu(M) \le \inf_{D\in\mathbf{D}} \overline{\sigma}(DMD^{-1}) \tag{2.7}$$

For the case of nonrepeated, complex blocks, we have the following sets.

$$\mathbb{\Delta} = \{ \text{diag}(\Delta_1,\Delta_2, ..., \Delta_n) \mid \Delta_j \in \mathbf{C}^{m_j \times m_j} \}$$
$$\mathbb{U} = \{ \text{diag}(U_1,U_2, ... ,U_n) \mid U_j^* U_j = I \}$$
$$\mathbb{D} = \{ \text{diag}(d_1 I,d_2 I, ... ,d_n I) \mid d_j \in \mathbf{R}_+ \}$$

The bounds in (2.7) provide a means to compute μ, and the key theorems in [5] reveal when these bounds are useful. The lower bound in (2.7) is actually an equality for all M and Δ. However, the optimization problem posed by the lower bound is not convex. Therefore, it may have multiple local maxima and is not very useful as a computational algorithm. The upper bound is an equality in the case of three or fewer blocks or if M is real. In addition, the upper bound optimization problem is convex in ln(D) and has only global minima [For proof see 18]. This fact makes the upper bound a useful computational scheme, and experience has shown that this bound is reasonably tight even when $n > 3$ [6].

For the two block case (i.e. $n = 2$), Doyle has developed two reasonable approximations to the equation

$$\mu(M) = \inf_{D \in \mathbb{D}} \bar{\sigma}(DMD^{-1}) \tag{2.8}$$

In this case, $M = \begin{bmatrix} M_{11} & M_{12} \\ M_{21} & M_{22} \end{bmatrix}$ and $D = \begin{bmatrix} d & 0 \\ 0 & 1 \end{bmatrix}$. The approximations to the infimum are

$$d = \sqrt{\frac{\bar{\sigma}(M_{21})}{\bar{\sigma}(M_{12})}} \tag{2.9}$$

$$d = \sqrt{\frac{\| M_{21} \|_F}{\| M_{12} \|_F}} \tag{2.10}$$

If the matrix M is 2x2 (not block), then these approximations are exact. If M is larger (i.e. block 2x2), then the above equations provide a reasonable approximation to the infimum and are a good starting point in the convex optimization in Eqn. (2.8).

Remark The structured singular value cannot be computed directly. The most effective method for computing an approximation to μ is the convex optimization problem associated with the upper bound in Eqn. (2.5). Therefore in the sequel when we refer to μ, we actually are referring to the quantity that may be computed, i.e. the upper bound. This introduces an unavoidable, but small, degree of conservatism into the design process.

2.2 Hankel Operators

2.2.1 Definition and Description

The theory of Hankel operators plays a central role in the modern, functional analysis based control methodologies (i.e. H_2, H_∞) [6, 16-20, 23, 31]. The Causality Recovery Methodology also depends very heavily on this theory; however, in a fundamentally different way. The H_2 and H_∞ methodologies reduce the control design problem to a general distance problem [19]. That is, the best H_∞ approximation to an L_∞ function must be found. The goal of the CRM is to find an H_∞ function in a given set of L_∞ functions that satisfy some performance specification. References [17, 18] are thorough and lucid treatments of the subject of H_∞ control design and we will rely primarily on these accounts for the discussion

of Hankel operators presented here.

In order to define the Hankel operator we first must introduce the Laurent operator.

Definition 2.1 For $F \in L_\infty$ the *Laurent operator with symbol F*, denoted Λ_F, is a mapping from L_2 to L_2 via

$$\Lambda_F g := Fg \tag{2.11}$$

The Laurent operator with symbol F represents multiplication by F. Λ_F is linear and bounded and $\| \Lambda_F \| = \| F \|_\infty$. A related operator is $\Lambda_F | H_2$, the restriction of Λ_F to H_2, which maps H_2 to L_2. The Hankel operator can now be defined in terms of the restriction of Λ_F to H_2.

Definition 2.2 For $F \in L_\infty$ the *Hankel operator with symbol F*, denoted Γ_F, is a mapping from H_2 to $H_2^\perp$ via

$$\Gamma_F g := \Pi \Lambda_F | H_2 \, g \tag{2.12}$$

where Π is the orthogonal projection from L_2 to $H_2^\perp$.

Γ_F may be thought of as taking a transfer function in H_2 (i.e. strictly proper and stable) and mapping it into an antistable transfer function through the action of the symbol F. The Hankel operator has a time-domain interpretation as well. Assume F(s) is analytic in a strip containing the imaginary axis. This is always the case if F(s) is rational. Let f(t) denote the inverse bilateral Laplace transform of F(s) with this strip being the region of convergence. The linear system with impulse response f(t) is stable, but noncausal in general. That is, the f(t) is two-sided. The time-domain operator maps a function u in $L_2[0,\infty)$ into a function y in $L_2(-\infty,0]$ according to the convolution equation

$$y(t) = \int_0^\infty f(t-\tau)\, u(\tau)\, d\tau \ , \quad t<0 \tag{2.13}$$

2.2.2 The Hankel Norm and Nehari's Theorem

The norm of a Hankel operator will be computed in this section and the significance of the norm discussed. It will be assumed throughout that the symbol F is finite-dimensional and rational. This allows the norm of the operator Γ_F to be computed by standard state-space methods.

Let F be a matrix function in RL_∞. There is a unique factorization

$$F = F_1 + F_2 \tag{2.14}$$

where F_1 is strictly proper and analytic in Re $s \leq 0$ and F_2 is proper and analytic in Re $s \geq 0$, i.e. $F_2 \in RH_\infty$. This factorization is accomplished with a state-space realization of F. The Schur decomposition with eigenvalue ordering and the solution to a Sylvester equation are used to compute the appropriate similarity transformation [20] to arrive at the factorization in Eqn. (2.14).

Introduce a minimal realization of $F_1 = [A,B,C,0]$. The controllability and observability gramians are defined as follows:

$$L_c = \int_0^\infty e^{-At} BB^T e^{-A^T t}\, dt \tag{2.15}$$

$$L_o = \int_0^\infty e^{-A^T t} C^T C e^{-A t} \, dt \tag{2.16}$$

It is well known that L_c and L_o are the unique solutions of the Lyapunov equations

$$AL_c + L_c A' = BB' \tag{2.17}$$

$$A'L_o + L_o A = C'C \tag{2.18}$$

The eigenvalues of $L_c L_o$ are real and nonnegative, and the norm of the Hankel operator is readily computed by

$$\| \Gamma_F \| = \sqrt{\bar{\lambda}(L_c L_o)} \tag{2.19}$$

One of the most significant results in the theory of Hankel operators is Nehari's theorem. This theorem provides the theoretical foundation for the causality recovery process.

Theorem 2.1 [40] There exists a closest $X \in H_\infty$ to a given $F \in L_\infty$, and

$$\| F - X \|_\infty = \| \Gamma_F \|$$

This theorem provides a measure of the distance of an L_∞ function F from the space H_∞. In frequency-domain terms, $\| \Gamma_F \|$ is the distance from an unstable transfer function to the closest stable one. In fact, the Hankel norm is the radius of the smallest tube with center F in complex matrix space versus frequency that contains an H_∞ function. Nehari's theorem interpreted in the time-domain states that the distance from the noncausal system with impulse

response f(t) to the nearest causal system is given by the norm of the Hankel operator.

Remark The fact that the Hankel norm serves as a measure of noncausality will be exploited by the Causality Recovery Methodology. The heart of the CRM is an optimization problem to find a causal, stable (H_∞) transfer function. This is accomplished by minimizing the $\| \Gamma_F \|$ over some feasible set.

2.2.3 Best Approximation

The "best approximation" problem is presented and discussed in this section. We see that the Hankel operator plays a key role. The problem is formally stated as follows.

Let F be a function in L_∞. Find the function X in H_∞ that minimizes $\| F - X \|_\infty$.

Nehari first solved this problem for the case of scalar discrete systems [40]. Glover considers the special case where the function to be approximated is real-rational, i.e. $F \in RL_\infty$, and has developed an efficient, state-space solution to the problem [31]. Glover's algorithm is reviewed here following the treatment in [20].

Consider the best approximation problem for the real-rational case. Then for $F \in RL_\infty$, the solution X is in RH_∞ [For proof see 23, 31].

Theorem 2.2 If $F \in RL_\infty$, then there exists a best approximation X_{opt} in RH_∞.

Theorem 2.3 Let X_{opt} be the best approximation to mxp matrix function F, then

(1) if m = 1 or p = 1, X_{opt} is unique and (F - X_{opt}) is all-pass.

(2) if m ≠ 1 and p ≠ 1, then X_{opt} is not unique and

$$\overline{\sigma}(F - X_{opt})(j\omega) = \| \Gamma_F \| \qquad \forall\, \omega \in \mathbf{R}.$$

Assume, without loss of generality, that F is strictly proper, anti-stable, and square. If F is not anti-stable, it is factored as in Eqn. (2.14) and the stable part is absorbed into X. Rows or columns of zeros are added if F is not square. Introduce a minimal realization F = [A, B, C, 0]. Construct X_{opt} in RH_∞ as follows.

Best Approximation

Step 1

Compute a balanced realization of F [41]. This is simply a similarity transformation of the original realization such that the controllability and observability gramians are diagonal and equal. Let [A, B, C, 0] denote the balanced realization of F. The gramians are

$$L = \begin{bmatrix} \sigma I_r & 0 \\ 0 & \Sigma \end{bmatrix}$$

where $\sigma > \|\Sigma\|$, and r is the multiplicity of σ. Partition A, B, and C according to the structure of L. Then,

$$A = \begin{bmatrix} A_{11} & A_{12} \\ A_{21} & A_{22} \end{bmatrix}, \quad B = \begin{bmatrix} B_1 \\ B_2 \end{bmatrix}, \quad \text{and} \quad C = \begin{bmatrix} C_1 & C_2 \end{bmatrix}.$$

Step 2

Choose $\hat{D}$ such that

$$\hat{D}B_1^T + \sigma C_1 = 0$$

$$\hat{D}\hat{D}^T = \sigma^2 I$$

Step 3

Compute

$$\hat{B} = -(\sigma^2 I - \Sigma^2)^{-1}(\Sigma B_2 + \sigma C_2^T \hat{D})$$

$$\hat{A} = (-A_{22} + B_2\hat{B}^T)^T$$

$$\hat{C} = C_2\Sigma + \hat{D}B_2^T$$

Step 4

$$X_{opt} = [\hat{A}, \hat{B}, \hat{C}, \hat{D}].$$

2.3 Convex Optimization

2.3.1 Definitions and Key Results

The process of optimization has become an integral part of almost all design algorithms, and the CRM is no exception. An optimization problem consists of two elements: the objective function and the feasible set. The goal is to minimize the objective function over the elements contained in the feasible set. The property of convexity eliminates the possibility of having local minima.

Definition 2.8 A *set* C is *convex* if, for all elements x_1 and x_2 in C and every real θ satisfying $0 < \theta < 1$, we have $\theta x_1 + (1 - \theta)x_2$ in C.

Definition 2.9 A real-valued *functional* f defined on a convex subset C of a linear vector space is said to be *convex* if $f(\theta x_1 + (1 - \theta)x_2) \leq \theta f(x_1) + (1 - \theta)f(x_2)$.

Theorem 2.4 [33] Let f be a convex functional defined on a convex subset C of a normed space. Let $\alpha = \{ \inf f(x) \mid x \in C \}$. Then

(1) The subset X of C where $f(x) = \alpha$ is convex.

(2) If x_0 is a local minimum of f, then $f(x_0) = \alpha$ and, hence x_0 is a global minimum.

The above theorem establishes the importance of convexity of both the objective function and of the feasible set in an optimization problem. A convex optimization problem has only global minima and a simple gradient search algorithm that monotonically reduces the objective function is guaranteed to find (or come arbitrarily close to) the infimum.

A simple, but important, result that will be needed in the sequel is contained in the following theorem.

Theorem 2.5 $\| \Gamma_F \|$ is a convex functional of F.

Proof: Let $F = \theta F_1 + (1-\theta)F_2$, $0 < \theta < 1$.

By Nehari's Theorem, $\| \Gamma_F \| = \inf \| \theta F_1 + (1-\theta)F_2 - X \|_\infty$.

Let $X = \theta X_1 + (1-\theta)X_2$ and substitute. Then,

$$\begin{aligned} \| \Gamma_F \| &= \inf \| \theta(F_1 - X_1) + (1-\theta)(F_2 - X_2) \|_\infty. \\ &\leq \inf \{ \| \theta(F_1 - X_1) \|_\infty + \| (1-\theta)(F_2 - X_2) \|_\infty \} \\ &= \inf \| \theta(F_1 - X_1) \|_\infty + \inf \| (1-\theta)(F_2 - X_2) \|_\infty \\ &= \theta \| \Gamma_{F_1} \| + (1-\theta) \| \Gamma_{F_2} \| \end{aligned}$$

Remark 1 Several steps of the CRM are posed as convex optimization problems. From Theorem 2.4 convergence to the global minimum is guaranteed in each case.

Remark 2 A simple search technique that monotonically reduces the objective function may be used to find the minimum of a convex optimization program. We will rely on the modified pattern search algorithm of Hooke and Jeeves [42, 43] to solve the numerical examples posed in Chapter 5. The pattern search is not a gradient algorithm because no derivatives are computed; rather, a search along the coordinate axes in the optimization parameter space is performed. This algorithm was chosen primarily for its simplicity and ease of implementation, rather than its computational speed and efficiency.

2.3.2 Applications to Feedback System Design

The concept of convex optimization in feedback system design is hardly new. The most recent application of optimization theory to feedback design is contained in [44]. Boyd, et al develop a new computer-aided design method for linear, time-invariant controllers. The technique is based on the parameterization of all stabilizing controllers in terms of the free parameter $Q \in H_\infty$. This compensator description leads to a closed-loop transfer function which is affine in Q. Constraints on the closed-loop such as asymptotic tracking, decoupling, limits on peak excursions of variables, step response limits, settling time, and overshoot, as well as frequency-domain inequalities, define a convex program.

The problem is posed in discrete-time and Q is parameterized as a finite impulse response (FIR) filter. Stability and causality of Q are easily handled with this FIR structure. The framework is quite general, with the LQG and H_∞ problems as special cases. The price paid for such generality is increased computational burden due to the fact that the optimization does not take advantage of any special properties of the control problem, beyond convexity.

There is somewhat of a dual relationship between Boyd's CAD method and the CRM. Causality recovery is posed in continuous-time and Q is essentially parameterized as a frequency response. The frequency-domain performance specification defines a convex set of feasible Q's in the space of complex matrices. In many cases (i.e. H_2 and H_∞) the feasible set is convex. The convex objective functional is the Hankel norm or measure of noncausality. In the continuous-time case the problem is essentially infinite-dimensional due to the frequency response parameterization of Q. We will see in Chapter 4 that the infinite-dimensional convex program may be approximated by a finite-dimensional problem.

2.4 Concluding Remarks

This chapter has laid the mathematical foundation for the CRM. The structured singular value of a complex matrix was defined, and methods of computing an upper bound via a convex optimization program were discussed. We will see in the next chapter how the structured singular value is used for the analysis of feedback systems. A necessary and sufficient frequency-domain condition for stability and performance robustness will be derived.

A brief review of the theory of Hankel operators was presented. The Hankel norm was computed using standard state-space methods, and an interpretation of the norm as a measure of noncausality was given. Finally, convexity was shown to be an important property of an optimization program. Chapter 4 combines the Hankel operator theory with the optimization results to form the basis of the CRM.

CHAPTER 3. ANALYSIS: STABILITY, PERFORMANCE, AND ROBUSTNESS

3.1 Introduction

In section 1.2 the synthesis problem was formalized in terms of the general block diagram (Figure 1.7). The compensator objectives were stated as the following requirements on the closed-loop system:

(1) Nominal Stability

(2) Nominal Performance

(3) Robustness

The analysis tests that determine if the above objectives have been met are the focus of this chapter.

The compensator K in Figure 1.7 is assumed known for the purposes of analysis. It can then be incorporated with the plant P via a lower linear fractional transformation to yield the closed-loop operator S (Figure 3.1), i.e. $S = F_l(P,K)$.

$$S = \begin{bmatrix} S_{11} & S_{12} \\ S_{21} & S_{22} \end{bmatrix} \tag{3.1}$$

where

$$\begin{aligned} z &= S_{11}v + S_{12}d \\ e &= S_{21}v + S_{22}d \end{aligned} \tag{3.2}$$

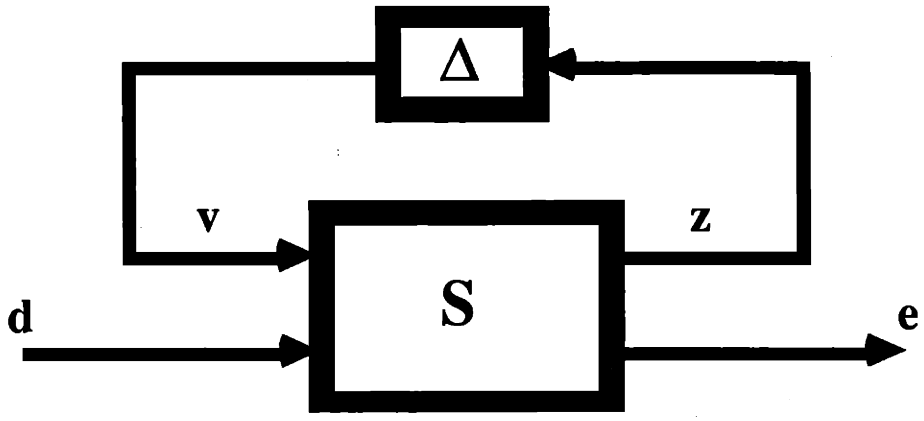

Figure 3.1 Analysis block diagram.

3.2 Nominal Stability

The first requirement for any compensator K is that it stabilize the plant P for the nominal case of Δ identically equal to 0. A standard test for nominal stability is the multivariable Nyquist criterion. This test relies on Cauchy's integral theorem and the Principle of the Argument to determine if any closed-loop poles are in the right half plane. For a given K, we can immediately determine the stability of the closed-loop by plotting the Nyquist diagram of the loop transfer function and examining the number of encirclements of the critical point.

The parameterization of all internally stabilizing compensators, first put forth by Youla, et al [25], allows the issue of nominal stability to be easily handled. All stabilizing compensators are described in terms of coprime factorizations of the plant P and a free parameter (transfer function matrix) $Q \in H_\infty$. This compensator structure results in an internally stable closed-loop map S that is affine in the free parameter Q.

$$S = T_{11} + T_{12} Q T_{21} \tag{3.3}$$

where T_{ij} is a function of the plant P and is in H_∞. The key results and theorems associated with the Youla parameterization will be presented in the synthesis chapter (Section 4.3).

Remark The requirement of nominal stability is transformed to the constraint that Q be *any* stable, causal transfer function matrix. The task of feedback synthesis boils down to finding the appropriate $Q \in H_\infty$ such that S meets stated performance objectives.

3.3 Nominal Performance

In section 1.2.3 performance was defined generally as unity norm-bounded L_2 input signals producing unity norm-bounded L_2 outputs. In this section we state the necessary and sufficient analysis test that determines if the feedback system achieves the desired performance. This is a nominal performance test because we do not take into account the effect of the perturbation Δ.

Nominal Performance Theorem 3.1 [24]

$e \in BL_2$ for all $d \in BL_2$ if and only if

$$\| S_{22} \|_\infty \leq 1$$

The above theorem demonstrates how $\| \cdot \|_\infty$ norm arises naturally in feedback system design when dealing with bounded energy signals. In fact there are a variety of other assumptions on the input and output signals (i.e. bounded power) that lead to identical performance analysis theorems [24]. Thus the $\| \cdot \|_\infty$ norm will provide the appropriate vehicle for performance determination in the sequel. While this norm does not capture all the

features of both time and frequency domain performance objectives, the weighted, frequency $\| \cdot \|_\infty$ norm is arguably the best compromise. As we shall see in the following section, the $\| \cdot \|_\infty$ is critical when dealing with modeling uncertainty and robustness.

3.4 Robustness

In this section we analyze the robustness of a feedback system in the presence of structured uncertainty. The closed-loop map S (Figure 3.1) is assumed to be stable and satisfy the condition in the Nominal Performance Theorem 3.1.

3.4.1 Stability-Robustness

Modeling uncertainty in various components of a feedback system will give rise to a block-diagonal perturbation Δ. The exact perturbation is unknown; however, as discussed in Section 1.2.5 Δ will be a member of the set

$$\mathbb{\Delta} = \{ \ \Delta \mid \Delta = \text{diag}(\Delta_1, \Delta_2, ..., \Delta_n) \ , \Delta_i \in \mathbb{P} \ \} \tag{3.4}$$

$$\mathbb{P} = \{ \ \Delta \mid \Delta \text{ stable}, \ \| \Delta \|_\infty < 1 \ \} \tag{3.5}$$

The following theorem states the necessary and sufficient condition for robust stability in the presence of structured uncertainty. Stability robustness implies that the perturbed system has no poles in the closed right half plane.

Robust Stability Theorem 3.2 [24]

The system in Figure 3.1 is stable for all $\Delta \in \mathbb{\Delta}$ if and only if

$$\| \mu(S_{11}) \|_\infty \leq 1$$

Remark This theorem is a generalization of the familiar singular value robustness tests [3]. The advantage of using μ over $\overline{\sigma}$ is derived from the exploitation of structural information associated with Δ. This leads to a necessary and sufficient condition, as opposed to the arbitrarily conservative singular value test which represents only a sufficient condition. $\| S_{11} \|_\infty$ may be very large, but no structured perturbation leads to instability. Thus, μ is a necessary tool in dealing with systems with structured modeling error (i.e. parameter variations and/or multiple norm-bounded perturbations). We will see in the next section that even in the case of a single unstructured modeling uncertainty, μ is essential in dealing with the issue of robust performance in a nonconservative manner.

3.4.2 Performance-Robustness

To satisfy the requirement of robust performance the closed-loop transfer function from disturbances d to errors e, $F_u(S, \Delta)$, must be small *for all possible* Δ. The robust performance specification is formally stated as

$$\| F_u(S, \Delta) \|_\infty \leq 1 \tag{3.6}$$

for all $\Delta \in \mathbb{\Delta}$. The upper linear fractional transformation F_u forms the closed-loop system from d to e in Figure 3.1.

This requirement may be interpreted as a stability condition on the perturbed system.

$$\text{Let } \widetilde{S} = F_u(S, \Delta). \tag{3.7}$$

Theorem 3.3 $\| \tilde{S} \|_\infty \leq 1$ if and only if

(1) $\tilde{S}$ is stable, and

(2) the system in Figure 3.2 is stable for all $\Delta_p \in \mathbb{P}$

where $\mathbb{P}$ is defined in (3.5)

Remark This is just a stability robustness theorem stated "in reverse", with respect to a "performance perturbation" Δ_p.

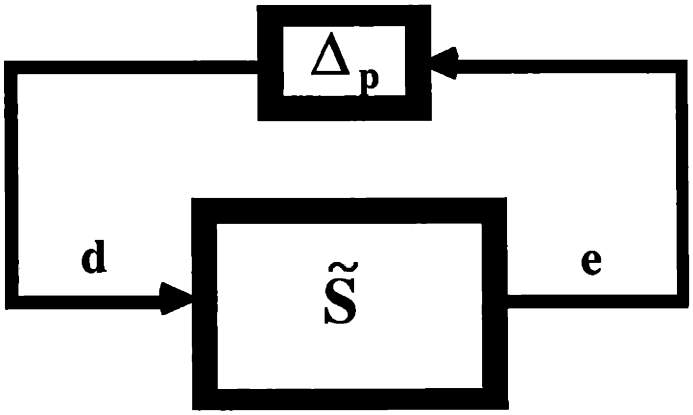

Figure 3.2 The perturbed closed-loop system $\tilde{S}$ with performance block Δ_p.

Theorem 3.3 is equivalent to a stability-robustness condition on an augmented system (Figure 3.3), and the results of the previous section apply. Stability and performance robustness are achieved simultaneously if and only if the feedback system is stable for all perturbations with the (2x2) block-diagonal structure in Figure 3.3.

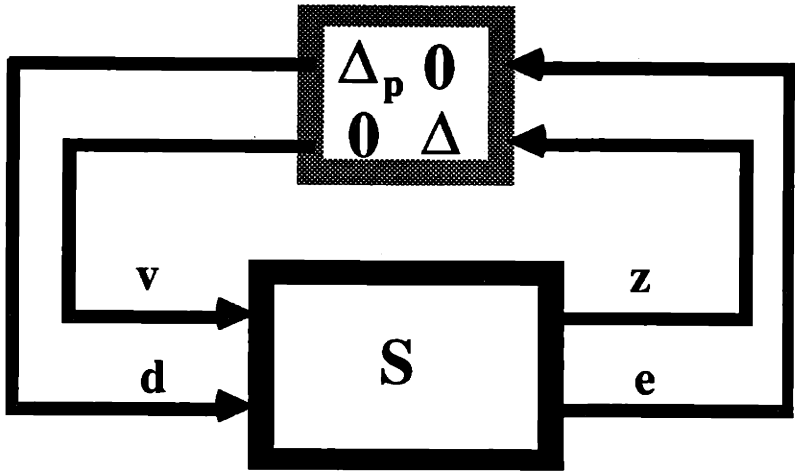

Figure 3.3 Stability and performance robustness viewed as a stability condition.

Robust Performance Theorem 3.4 [24]

$F_u(S, \Delta)$ is stable and $\| F_u(S, \Delta) \|_\infty \leq 1 \;\; \forall \Delta \in \mathbb{\Delta}$ if and only if

$$\| \mu(S) \|_\infty \leq 1$$

where μ is computed with respect to the augmented block structure

$$\mathbb{\Delta} = \{ \text{diag} (\Delta, \Delta_p) \mid \Delta \in \mathbb{\Delta} \}$$

Remark 1 The theorem demonstrates that simultaneous stability and performance robustness is guaranteed by a necessary and sufficient stability condition. This leads naturally to a block structured perturbation, regardless of the modeling uncertainty structure Δ, which requires the use of the structured singular value. The result in the above theorem guarantees stability *and* performance for a whole set of possible plants.

Remark 2 The results of this section have a simple interpretation in a (SISO) setting. Refer to the standard feedback problem described in Section 1.2.6. Assume that the number of encirclements of the critical point (-1,0) in the complex plane by the loop transfer function $g(j\omega)k(j\omega)$ is consistent with nominal stability (i.e. the Nyquist criterion is satisfied). Stability-robustness requires that the number of encirclements of the critical point remains constant in the presence of the multiplicative uncertainty $(1+\Delta w_z)$. This is ensured if the worst-case distance to the critical point of the perturbed plant is greater than zero for all frequencies, i.e.

$$| 1 + g(j\omega)k(j\omega) | - | g(j\omega)k(j\omega)w_z(j\omega) | > 0$$

Note that this condition is equivalent to that in Eqn. (1.20).

Performance (i.e. the magnitude of the sensitivity function R) may be interpreted in terms of the distance to the critical point, as well. From Eqn. (1.15) it is clear that the sensitivity is simply the reciprocal of the distance to the critical point. Performance-robustness requires that the worst-case distance to the critical point at each frequency to be larger than some positive value defined by the performance weighting function $w_e(s)$, i.e.

$$| 1 + g(j\omega)k(j\omega) | - | g(j\omega)k(j\omega)w_z(j\omega) | > | w_e(j\omega) |$$

In fact, the structured singular value in the SISO case is simply a measure of the distance to the critical point.

$$\mu = | w_e(j\omega)r(j\omega) | + | w_z(j\omega)c(j\omega) |$$

where r and c are the standard sensitivity and complementary sensitivity transfer functions, respectively, defined in Section 1.2.6.

This discussion is shown graphically in Figure 3.4.

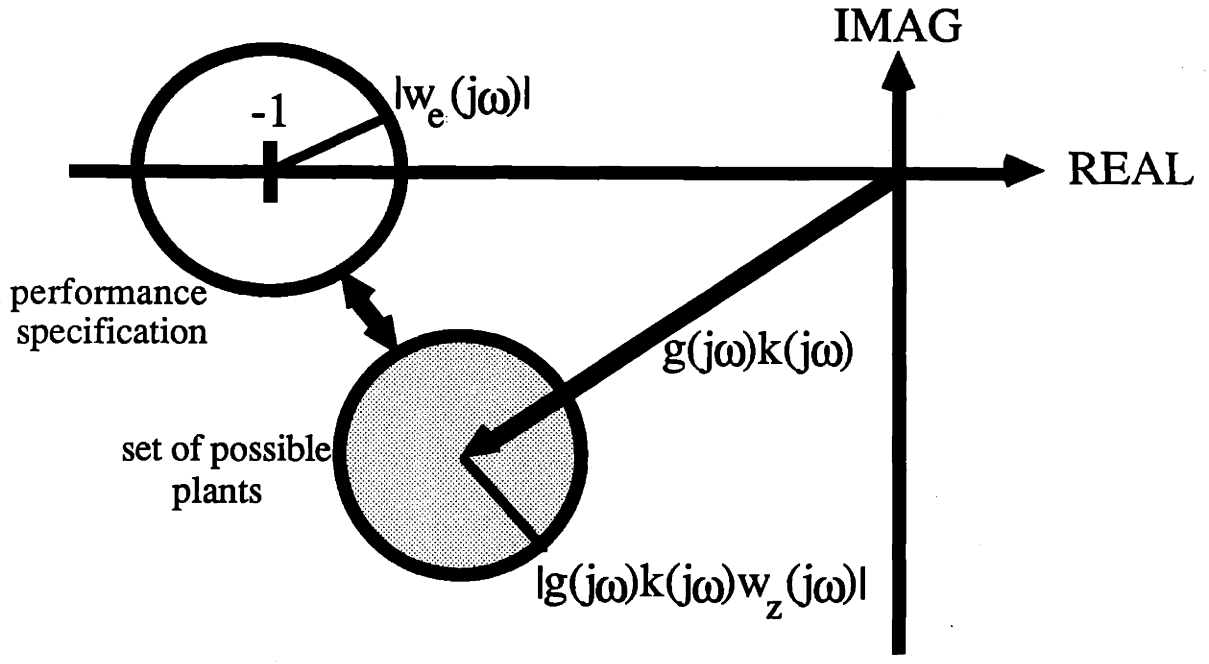

Figure 3.4 Complex plane interpretation of performance-robustness in SISO case.

It will be convenient to have a quantitative measure of the robustness of a feedback system.

Definition 3.1 The *robustness margin* ρ of an LTI feedback system S is defined with respect to Figure 3.3 as

$$\rho(S) = [\ \| \mu(S) \|_\infty\ ]^{-1}$$

Remark The quantity ρ measures the simultaneous stability and performance robustness of a system S. We will see in the sequel that the aim of the CRM is to increase ρ.

3.5 Concluding Remarks

This chapter has laid the analysis foundation for dealing with structured uncertainty in feedback systems. We have seen that this type of uncertainty always arises when considering the problem of robust performance. The synthesis methodology developed in the next chapter will rely on the analysis theorems presented here.

As we shall see in section 4.3, the parameterization of all stabilizing compensators yields a closed-loop transfer function S that is guaranteed to be nominally stable and affine in the free parameter Q.

$$S = T_{11}+T_{12}QT_{21} \tag{3.8}$$

where T_{ij} are functions of P in H_∞.

The Robust Performance Theorem imposes the constraint

$$\| \mu(T_{11}+T_{12}QT_{21}) \|_\infty \leq 1 \tag{3.9}$$

From the properties of the structured singular value, the inequality in Eqn. (3.9) is satisfied if

$$\| D(T_{11}+T_{12}QT_{21})D^{-1} \|_\infty \leq 1 \tag{3.10}$$

for some diagonal scaling transfer function D.

The next chapter presents a methodology for finding a $Q \in H_\infty$ such that Eqn. (3.10) is satisfied. This results in a nominally stable closed-loop system with robust stability and performance.

CHAPTER 4. SYNTHESIS: THE CAUSALITY RECOVERY METHODOLOGY

4.1 Introduction

This chapter presents the Causality Recovery Methodology and the main results of the thesis. The familiar block diagram in Figure 1.7 represents the general framework for consideration of the feedback synthesis problem in the presence of modeling uncertainty. The objective is to find a compensator K to

(1) achieve closed-loop stability

(2) yield some desired level of performance

(3) provide robustness with respect to the modeling uncertainty Δ.

The nature (i.e. $\| \Delta \|_\infty < 1$) and structure of the perturbation Δ impose known constraints on the lower feedback loop in Figure 1.7. Therefore, the synthesis process will be discussed in terms of Figure 4.1. The disturbance vector d is a composite of the vectors v and d from Figure 1.7. Similarly, the error vector e in Figure 4.1 consists of z and e from Figure 1.7.

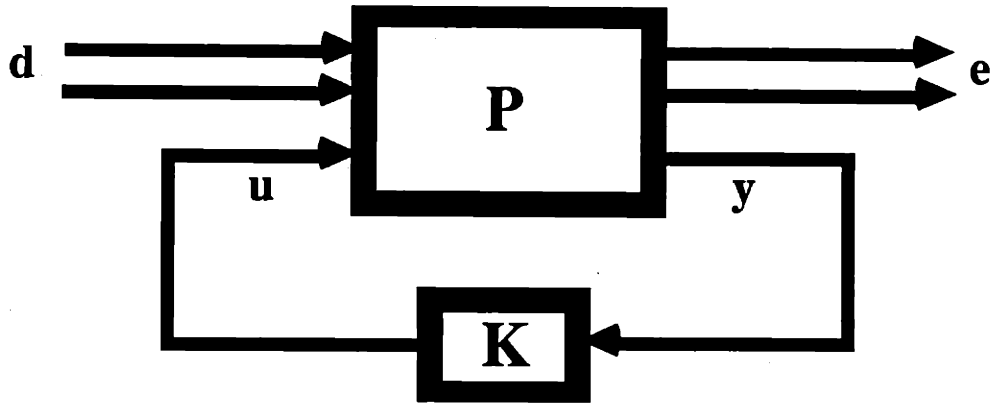

Figure 4.1 Synthesis block diagram.

From the previous chapter on analysis we know the three objectives are satisfied if a transfer function matrix Q exists such that

$$Q \in H_\infty \tag{4.1}$$

$$\| DSD^{-1} \|_\infty \leq \gamma \tag{4.2}$$

At each frequency, D is a real, diagonal scaling matrix (see Section 2.2.2). S, the closed-loop transfer function from d to e (Figure 4.1), can be expressed as an affine function of Q.

$$S = T_{11}+T_{12}QT_{21} \tag{4.3}$$

Note that γ is just a scaling factor to ensure the synthesis problem has a solution. The CRM will find the smallest γ and a transfer function matrix Q that satisfies (4.1) and (4.2). The compensator K in Figure 4.1 is then computed as a function of the Q parameter and the coprime factorization of P.

There is a simple prescription for satisfying the constraints in (4.1) and (4.2), and this will be the starting point for the causality recovery procedure. Choose the most elementary H_∞ function Q = 0. This leads to a compensator that is strictly a function of some plant factorization (see Section 4.3), and the nominal closed-loop transfer function T_{11}. The term "nominal" in this context refers to the fact that Q is identically zero.

Determine the robustness properties of T_{11} by computing the upper bound on $\mu(T_{11})$. This will result in a real, diagonal scaling matrix D_{nom} at each frequency, and a measure of nominal performance γ_{nom}.

$$D_{nom}(\omega) = \arg \inf_{D \in \mathbf{D}} \bar{\sigma} (DT_{11}(j\omega)D^{-1}) \tag{4.4}$$

where $\mathbb{D} = \{ \text{diag}(d_1 I, d_2 I, \ldots, d_n I) \mid d_j \in \mathbf{R}_+ \}$

$$\gamma_{nom} = \| D_{nom} T_{11} D_{nom}^{-1} \|_\infty \tag{4.5}$$

The H_∞ function $Q = 0$ satisfies the performance specification in (4.2) for $\gamma = \gamma_{nom}$.

The particular bound γ_{nom} may or may not represent adequate stability and performance robustness of the feedback system. In either case, the aim of the CRM is to *improve* the closed-loop robustness by exploiting the extra degree of freedom available in Q. The CRM may be thought of as an algorithm to "fine-tune" the nominal design T_{11} by adjusting the frequency response of the free parameter Q . In the remainder of this chapter a procedure will be developed to guarantee the finding of a $Q \in H_\infty$ such that the robustness margin ρ of the resulting closed-loop system is greater than or equal to $\rho(T_{11})$, i.e.

$$\| D_{nom}(T_{11} + T_{12} Q T_{21}) D_{nom}^{-1} \|_\infty \leq \| D_{nom} T_{11} D_{nom}^{-1} \|_\infty \tag{4.6}$$

The implication is clear. Start with a "good" nominal design T_{11}, and the CRM will produce another closed-loop system whose performance is at least as good as the nominal. As we shall see, the price for such improvement is increased compensator complexity.

Remark The scaling D_{nom} is computed as a function of T_{11} (see Eqn. 4.4), and does not change throughout the CRM process. As we shall see, this greatly simplifies the problem and leads to a convex program in Q. However, we are now no longer trying to optimize the structured singular value; the infinity norm of the scaled closed-loop system will be minimized (for the fixed scaling D_{nom}). Since the scaled singular value serves as an upper bound on μ, some conservatism is introduced into the design.

Once a new compensator has been computed by the CRM, T_{11} may be redefined to

incorporate this new design. The scaling D_{nom} is recomputed, and the causality recovery process repeated. This is just a different approach to the DK iteration described in Section 1.3.3. As such, the procedure is nonconvex and convergence to the globally optimal compensator and scaling is not guaranteed.

The CRM consists of several distinct steps. First, design a stabilizing compensator K_{nom} for the design plant model P. Let S_{nom} denote the closed-loop transfer function. Section 4.2 discusses the preliminary design step and the methods that yield a "good" nominal design. The Youla parameterization and coprime factorization are covered in section 4.3. This results in a closed-loop transfer function S that is affine in the free parameter Q and equal to S_{nom} when $Q = 0$.

$$S = T_{11}+T_{12}QT_{21} \tag{4.7}$$

where $T_{11} = S_{nom}$.

Section 4.4 describes the design of the closed-loop system with optimal performance-robustness. The optimal system is noncausal in general, and imposes a limit on achievable closed-loop performance. The procedure for finding a causal closed-loop transfer function is described in section 4.5, and section 4.6 presents an algorithm for the implementation of the causality recovery process.

4.2 Nominal Design

This section presents two existing methods for achieving a "good" initial feedback design. The goal is to design a compensator that has reasonable performance-robustness properties. This nominal design will serve as the starting point for the CRM.

4.2.1 H_∞ Synthesis

It is known from section 2.2 that the largest singular value of any matrix M is an upper bound on the structured singular value, where μ is computed with respect to some known perturbation structure.

$$\mu(M) \leq \bar{\sigma}(M) \tag{4.8}$$

The relationship in (4.8) suggests a compensator that satisfies some H_∞ optimality criterion will be a reasonable nominal design. That is,

$$\| S \|_\infty \leq \gamma \Rightarrow \| \mu(S) \|_\infty \leq \gamma \tag{4.9}$$

where S is the closed-loop transfer function matrix.

The standard H_∞ feedback problem is to find a stabilizing K to minimize the H_∞ norm of the transfer matrix from disturbances d to errors e (Figure 4.1). In conjunction with the Youla parameterization, this translates into the following optimization problem.

$$\min_{Q \in H_\infty} \| T_{11} + T_{12} Q T_{21} \|_\infty \tag{4.10}$$

In general, the optimal solution involves an infinite-dimensional eigenvalue problem that cannot be computed directly [20]. However an iterative scheme, referred to as γ-iteration, has been formulated to find the minimum γ and solve the suboptimal problem:

$$\text{Find a } Q \in H_\infty \text{ such that } \| T_{11} + T_{12} Q T_{21} \|_\infty \leq \gamma \tag{4.11}$$

The solution to this problem is well-established and is arbitrarily close to optimal [17-20].

The latest results in the area of H_∞ synthesis have been put forth by Doyle and Glover [22]. These researchers have extended the Youla parameterization to a parameterization of all stabilizing compensators *that satisfy an H_∞ performance criterion.* Consider the problem framework in Figure 4.1. P represents a block 2x2 transfer function matrix with the following relationships among the signals.

$$P = \begin{bmatrix} P_{11} & P_{12} \\ P_{21} & P_{22} \end{bmatrix} \tag{4.12}$$

$$\begin{aligned} e &= P_{11}d + P_{12}u \\ y &= P_{21}d + P_{22}u \end{aligned} \tag{4.13}$$

Introduce a stabilizable and detectable realization of P using the shorthand transfer function notation with the state-space parameters ($\dot{x} = Ax + Bu$, $y = Cx + Du$).

$$P = [\, A, B, C, D] \tag{4.14}$$

where

$$B = [B_1\ B_2]$$

$$C = \begin{bmatrix} C_1 \\ C_2 \end{bmatrix}$$

$$D = \begin{bmatrix} D_{11} & D_{12} \\ D_{21} & D_{22} \end{bmatrix}$$

Each transfer function in (4.12) has a state space representation in terms of (4.14).

$$P_{ij} = [\ A, B_j , C_i , D_{ij}\ ] \quad ; \quad i,j = 1,2 \tag{4.15}$$

Remark The Doyle/Glover parameterization, as presented in [22] and here, requires the D matrix to have certain properties. The diagonal feedthrough terms, D_{11} and D_{22}, must be identically zero. This constraint is met by strictly proper plants P_{11} and P_{22}. The cross diagonal terms must satisfy

$$\begin{aligned} D_{12}^T D_{12} &= I \\ D_{21} D_{21}^T &= I \end{aligned} \tag{4.16}$$

The conditions in (4.16) will require P_{12} and P_{21} to be proper, but not strictly proper. More specifically, D_{12} must have full column rank and D_{21} full row rank. Then, Eqns. (4.16) can always be satisfied by proper scaling of the controls u and measurements y.

The goal is to parameterize all internally stabilizing compensators K such that

$$\| F_l(P, K) \|_\infty \leq \gamma \tag{4.17}$$

where F_l is the lower linear fractional transformation that forms the closed-loop transfer function matrix in Figure 4.1.

Remark The performance measure γ can be set equal to unity, without loss of generality, by scaling the disturbances d and the errors e.

The compensator structure is shown in Figure 4.2. The parameterization of all stabilizing compensators K satisfying (4.17) follows.

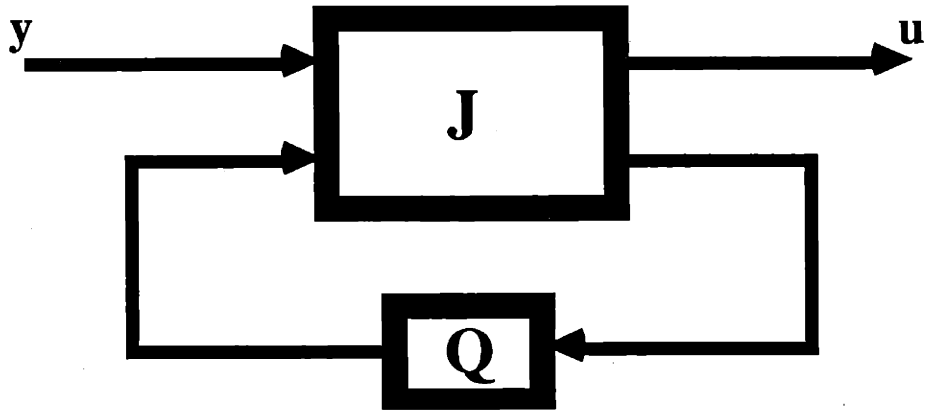

Figure 4.2 The compensator structure for the Doyle/Glover parameterization.

$$K = F_l(J, Q) \tag{4.18}$$

where Q is *any* function in H_∞ such that $\| Q \|_\infty \leq 1$ (4.19)

$$J = [A_J, B_J, C_J, D_J] \tag{4.20}$$

where

$$A_J = A - K_F C_2 - B_2 K_C + Y_\infty C_1^T (C_1 - D_{12} K_C)$$

$$B_J = [K_F \quad K_{Fl}]$$

$$C_J = \begin{bmatrix} -K_C \\ K_{Cl} \end{bmatrix}$$

$$D_J = \begin{bmatrix} 0 & -I \\ I & 0 \end{bmatrix}$$

$$K_C = (B_2^T X_\infty + D_{12}^T C_1) (I - Y_\infty X_\infty)^{-1}$$

$$K_{Cl} = (D_{21} B_1^T - C_2) (I - Y_\infty X_\infty)^{-1}$$

X_∞ is the unique, real, symmetric solution of the Algebraic Riccati Equation

$$(A - B_2 D_{12}^T C_1)^T X_\infty + X_\infty (A - B_2 D_{12}^T C_1) - X_\infty (B_2 B_2^T - B_1 B_1^T) X_\infty + \tilde{C}_1^T \tilde{C}_1 = 0$$

$$\tilde{C}_1 = (I - D_{12} D_{12}^T) C_1$$

$$K_F = (Y_\infty C_2^T + B_1 D_{21}^T)$$

$$K_{Fl} = (Y_\infty C_1^T D_{12} + B_2)$$

Y_∞ is the unique, real, symmetric solution of the Algebraic Riccati Equation

$$(A - B_1 D_{21}^T C_2) Y_\infty + Y_\infty (A - B_1 D_{21}^T C_2)^T - Y_\infty (C_2^T C_2 - C_1^T C_1) Y_\infty + \tilde{B}_1 \tilde{B}_1^T = 0$$

$$\tilde{B}_1 = B_1 (I - D_{21}^T D_{21})$$

Remark 1 Three conditions must be met in order for the above parameterization to be valid.

(1) $X_\infty \geq 0$

(2) $Y_\infty \geq 0$

(3) $\overline{\lambda}(Y_\infty X_\infty) \leq 1$

The minimum γ in Eqn. (4.17) should be found (by some iterative procedure) to satisfy these conditions.

Remark 2 A compensator satisfying the H_∞ criterion in Eqn. (4.17) is computed via the solution of two Riccati equations. It is no more difficult to design a compensator that meets an H_∞ optimality criterion than it is to compute an LQG solution.

Remark 3 The Youla parameterization describes all stabilizing compensators as a function of a free parameter $Q \in H_\infty$. However, the parameterization does not establish any guidelines as to how Q should be chosen in a given situation. While $Q = 0$ is a stabilizing solution, the performance of the resulting closed-loop system is unknown. The Doyle/Glover parameterization makes the zero function a legitimate choice for the free parameter from a performance perspective. That is,

$$J_{11} = [\, A_J, K_F, K_C, 0 \,] \tag{4.21}$$

is a compensator that achieves

$$\| F_l(P, J_{11}) \|_\infty \leq \gamma \tag{4.22}$$

It is important to note that, unlike the Youla parameterization, the closed-loop map $F_l[P,F_l(J,Q)]$ is no longer affine in Q; it is contractive, however.

For the sake of clarity, it is worth reviewing the above design process. Assume that the design plant P (Eqn. 4.13) is given. If D_{11} and D_{22} are not identically zero, add high frequency poles to make P_{11} and P_{22} strictly proper. P_{12} and P_{21} must be proper so that D_{12} has full column rank and D_{21} has full row rank.

H_∞ Synthesis via the Doyle/Glover Parameterization

Step 1

Guess the level of achievable performance γ.

Step 2

Scale the disturbances d and errors e so that the upper bound in Eqn. (4.17) is unity.

$$B_1 = \frac{1}{\sqrt{\gamma}} B_1$$

$$C_1 = \frac{1}{\sqrt{\gamma}} C_1$$

$$D_{12} = \frac{1}{\sqrt{\gamma}} D_{12}$$

$$D_{21} = \frac{1}{\sqrt{\gamma}} D_{21}$$

Step 3

Scale the cross diagonal D terms so that Eqn. (4.16) is satisfied. S_u is the square, nonsingular, scaling matrix for the controls and S_y is the square, nonsingular, scaling on the measurements. Then,

$$S_u^T S_u = D_{12}^T D_{12}$$

$$S_y^{-1}(S_y^{-1})^T = D_{21} D_{21}^T$$

These equations may be solved for S_u and S_y using the Cholesky decomposition [45]. Scale

the plant matrices as follows.

$$B_2 = B_2 S_u^{-1}$$

$$C_2 = S_y C_2$$

$$D_{12} = D_{12} S_u^{-1}$$

$$D_{21} = S_y D_{21}$$

$$D_{22} = S_y D_{22} S_u^{-1}$$

Step 4

Solve the Riccati equations in (4.20) with the appropriately scaled plant. Check the conditions in Remark 3. If they are not satisfied, adjust γ and go to Step 2.

Step 5

Construct J according to (4.20). Let $K = J_{11}$.

As was discussed previously, the singular value serves as an upper bound for the structured singular value and there may be an arbitrarily large gap between the two quantities. Therefore, the H_∞ compensator may be an overly conservative design in terms of performance-robustness. One way to possibly avoid this problem is discussed in the following section.

4.2.2 μ-Synthesis via DK Iteration

A synthesis procedure has been proposed in [6] to take advantage of the nonconservative μ analysis framework. The objective of μ-synthesis is to find a stabilizing compensator K such that robust stability and performance is achieved.

$$\| \mu[F_l(P, K)] \|_\infty \leq \gamma \tag{4.23}$$

Based on the μ upper bound, a reasonable approximation to this problem is to find a stabilizing K and a real, diagonal scaling matrix D so that

$$\| DF_l(P, K)D^{-1} \|_\infty \leq \gamma \tag{4.24}$$

This suggests an iterative approach to μ-synthesis, referred to as DK iteration. The aim is to minimize the left hand side of the expression in (4.24) by alternatively minimizing over D and K while holding the other constant.

$$\min_{D,K} \| DF_l(P,K)D^{-1} \|_\infty \tag{4.25}$$

For fixed D this is just a scaled H_∞ control problem and may be solved by the Doyle/Glover parameterization above. When K is fixed, (4.25) is minimized with respect to D at each frequency. This constitutes a convex optimization program in D, and all local minima are global [24]. The result is a real, diagonal matrix $D(\omega)$ at each frequency. The magnitude frequency response $D(\omega)$ is fit with a stable, minimum phase, rational transfer function. Note that the phase of D does not effect the norm in (4.25). This procedure is continued until it converges, or until a compensator is found that yields acceptable closed-loop performance (i.e. Eqn. 4.24 is satisfied). DK iteration is summarized below.

DK Iteration

Step 1

Choose an initial transfer function for the scaling D. The most obvious choice is D = I.

Step 2

Find a stabilizing K that minimizes $\| DF_l(P, K)D^{-1} \|_\infty$.

Step 3

Evaluate the μ properties of this solution. This results in a new scaling matrix D at each frequency.

Step 4

Approximate the new D scaling from Step 3 with a rational transfer function matrix (stable, minimum phase), and go to Step 2. Note that this rational approximation must be done accurately to ensure convergence of the DK iteration.

Using the Doyle/Glover H_∞ solution in Step 2, DK iteration becomes an efficient means for attacking the μ-synthesis problem, and could in theory come arbitrarily close to the μ-optimal solution. Unfortunately, the minimization over D and K is not jointly convex. This implies that DK iteration is not guaranteed to converge to the globally optimal D and K. In fact, local minima have been found in numerical studies.

Remark The CRM cannot improve the robustness properties of a compensator resulting from a *converged* DK iteration, even if the solution is a local minimum. This is a direct consequence of the fact that the D scaling remains constant throughout the CRM design

process. However, an intermediate result from the DK iteration should prove to be a good nominal design and starting point for the CRM.

The result of this section is an initial compensator K_{nom}, designed by some existing methodology. S_{nom} is the nominal closed-loop transfer function, and D_{nom} is the associated scaling. The measure of nominal robustness is γ_{nom}.

$$S_{nom} = F_l(P,K_{nom})$$

$$D_{nom}(\omega) = \arg \inf_{D \in \mathbb{D}} \bar{\sigma} \left[D S_{nom}(j\omega) D^{-1} \right]$$

$$\mathbb{D} = \{ \text{diag}(d_1 I, d_2 I, \ldots, d_n I) \mid d_j \in \mathbf{R}_+ \}$$

$$\gamma_{nom} = \| D_{nom} S_{nom} D_{nom}^{-1} \|_\infty$$

4.3 Parameterization of All Stabilizing Compensators

In this section we present the parameterization of all stabilizing controllers and, as a direct consequence, the parameterization of all internally stable closed-loop maps, in terms of a free parameter $Q \in H_\infty$. A technique is described to incorporate a given compensator into the parameterization so that the given closed-loop is achieved when $Q = 0$. State-space formulas for the parameterization are presented. These results have been widely reported [17, 20, 23, 46], and the treatment here closely parallels that in [20].

The concept of coprime factorization of transfer function matrices is an integral part of the Youla parameterization.

Definition 4.1 Two matrices M and N in RH_∞ are *right-coprime* if they have an equal number of columns and there exist matrices X and Y in RH_∞ such that

$$XM + YN = I \tag{4.26}$$

Definition 4.2 Two matrices $\tilde{M}$ and $\tilde{N}$ in RH_∞ are *left-coprime* if they have an equal number of rows and there exist matrices $\tilde{X}$ and $\tilde{Y}$ in RH_∞ such that

$$\tilde{M}\tilde{X} + \tilde{N}\tilde{Y} = I \tag{4.27}$$

Lemma 4.1 For each proper real-rational matrix P there exist eight RH_∞ matrices (nonunique) satisfying

$$P = NM^{-1} = \tilde{M}^{-1}\tilde{N} \tag{4.28}$$

$$\begin{bmatrix} \tilde{V} & -\tilde{U} \\ -\tilde{N} & \tilde{M} \end{bmatrix} \begin{bmatrix} M & U \\ N & V \end{bmatrix} = \begin{bmatrix} I & 0 \\ 0 & I \end{bmatrix} \tag{4.29}$$

where N and M are right-coprime and $\tilde{N}$ and $\tilde{M}$ are left-coprime. Equation (4.29) is known as a Bezout identity.

Once again consider the block diagram in Figure 4.1 and the realizations in (4.12) and (4.15). The following two theorems are well known.

Theorem 4.1 K stabilizes P if and only if K stabilizes P_{22}.

Theorem 4.2 There exists a proper, real-rational transfer function K achieving internal stability if and only if [A , B_2] is stabilizable and [C_2 , A] is detectable.

Remark Theorems 4.1 and 4.2 establish the role of P_{22} in the existence of an internally stable closed-loop system. The sequel assumes that the stabilizability and detectability conditions are satisfied, and the factorizations in Eqns. (4.28) and (4.29) are computed for $P = P_{22}$.

Theorem 4.3 The set of all proper controllers achieving internal stability for the feedback system in Figure 4.1 is parameterized by the formula

$$\begin{aligned} K &= (U + MQ)(V + NQ)^{-1} \\ &= (\tilde{V} + Q\tilde{N})^{-1}(\tilde{U} + Q\tilde{M}) \\ &= K_o + \tilde{V}^{-1} Q (I + V^{-1} NQ)^{-1} V^{-1} \end{aligned} \tag{4.30}$$

where $Q \in H_\infty$ such that $(I + V^{-1} NQ)^{-1}(j\omega)$ is invertible at $\omega = \infty$, and $K_o = UV^{-1} = \tilde{V}^{-1} \tilde{U}$.

K can also be expressed in terms of a linear fractional transformation (Figure 4.2).

$$K = F_l(J, Q) \tag{4.31}$$

where

$$J = \begin{bmatrix} K_o & \tilde{V}^{-1} \\ V^{-1} & -V^{-1}N \end{bmatrix} \tag{4.32}$$

The above theorem parameterizes all stabilizing controllers for the plant P in terms of a free parameter Q. The affine parameterization of the closed-loop transfer function from disturbances d to errors e follows.

Theorem 4.4 The set of all closed-loop transfer function matrices S from d to e achievable by an internally stabilizing proper controller is

$$\mathbb{S} = \{ S \mid S = T_{11} + T_{12} Q T_{21} , Q \in H_\infty , I + D_{22} Q(j\omega) \text{ invertible at } \omega = \infty \}$$

where $T_{11} = P_{11} + P_{12} U \tilde{M} P_{21}$

$T_{12} = P_{12} M$

$T_{21} = \tilde{M} P_{21}$

Remark The closed-loop transfer function is the result of a lower linear fractional transformation with T_{22} identically zero (Figure 4.3), i.e. $S = F_l(T, Q)$.

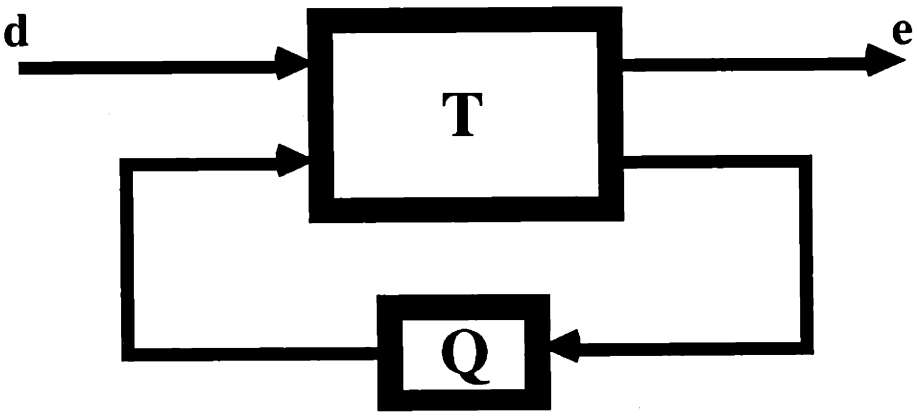

Figure 4.3 Representation of all stable closed-loop transfer functions.

Explicit state-space formulas exist for the computation of all the above coprime factorizations and transfer function matrices. These will be recounted here for the sake of

completeness. We begin with a realization of $P_{22} = [\ A, B_2, C_2, D_{22}\ ]$, where $[\ A, B_2\ ]$ is stabilizable and $[\ C_2, A\ ]$ is detectable. Compute a stabilizing, full-state feedback gain F. It is well known from LQG theory that one such F is

$$F = - B_2^T X \tag{4.33}$$

where

X is the unique, real, symmetric solution of the Algebraic Riccati Equation

$$A^TX + XA - XB_2B_2^TX + C_2^TC_2 = 0$$

Then,

$$M = [\ A + B_2F, B_2, F, I\ ] \tag{4.34}$$

$$N = [\ A + B_2F, B_2, C_2 + D_{22}F, D_{22}\ ] \tag{4.35}$$

The left coprime factorizations can be obtained by a duality argument. Compute a stabilizing filter gain H via a filter Algebraic Riccati Equation.

$$H = - Y C_2^T \tag{4.36}$$

where

Y is the unique, real, symmetric solution of the Algebraic Riccati Equation

$$AY + YA^T - YC_2^TC_2Y + B_2B_2^T = 0$$

Then,

$$\tilde{M} = [\ A + HC_2, H, C_2, I\ ] \tag{4.37}$$

$$\tilde{N} = [\ A + HC_2, B_2 + HD_{22}, C_2, D_{22}\ ] \tag{4.38}$$

The Bezout factors are:

$$V = [\, A + B_2F,\ -H,\ C_2 + D_{22}F,\ I \,] \tag{4.39}$$

$$U = [\, A + B_2F,\ -H,\ F,\ 0 \,] \tag{4.40}$$

$$\tilde{V} = [\, A + HC_2,\ -(B_2 + HD_{22}),\ F,\ I \,] \tag{4.41}$$

$$\tilde{U} = [\, A + HC_2,\ -H,\ F,\ 0 \,]. \tag{4.42}$$

A state-space realization of J can be found from the above results:

$$J = [A_J,\ B_J,\ C_J,\ D_J\,] \tag{4.43}$$

where

$$A_J = A + HC_2 + B_2F + HD_{22}F$$

$$B_J = [\, -H \quad B_2+HD_{22} \,]$$

$$C_J = \begin{bmatrix} F \\ -(C_2 + D_{22}F) \end{bmatrix}$$

$$D_J = \begin{bmatrix} 0 & I \\ I & -D_{22} \end{bmatrix}$$

Equation (4.43) leads to realizations of the closed-loop transfer functions T_{11}, T_{12}, and T_{13}.

$$T_{11} = [A_{T_{11}},\ B_{T_{11}},\ C_{T_{11}},\ D_{T_{11}}\,] \tag{4.44}$$

where

$$A_{T_{11}} = [\, A+B_2F \quad -HC_2\ ;\ 0 \quad A+HC_2 \,]$$

$$B_{T_{11}} = \begin{bmatrix} -HD_{21} \\ B_1 + HD_{21} \end{bmatrix}$$

$$C_{T_{11}} = [\ C_1+D_{12}F \quad C_1\ ]$$

$$D_{T_{11}} = D_{11}$$

$$T_{12} = [A_{T_{12}}, B_{T_{12}}, C_{T_{12}}, D_{T_{12}}] \tag{4.45}$$

where

$$A_{T_{12}} = A+B_2F$$

$$B_{T_{12}} = B_2$$

$$C_{T_{12}} = C_1+D_{12}F$$

$$D_{T_{12}} = D_{12}$$

$$T_{21} = [A_{T_{21}}, B_{T_{21}}, C_{T_{21}}, D_{T_{21}}] \tag{4.46}$$

where

$$A_{T_{21}} = A+HC_2$$

$$B_{T_{21}} = B_1+HD_{21}$$

$$C_{T_{21}} = C_2$$

$$D_{T_{21}} = D_{21}$$

Theorem 4.4 parameterizes all stable closed-loop maps in terms of an H_∞ function Q. The function Q = 0 results in a closed-loop transfer function $S = T_{11}$. While it is guaranteed that this closed-loop map is internally stable, nothing can be said concerning the performance or robustness of the resultant system. The following modification to the Youla parameterization will ensure that T_{11} represents a reasonable closed-loop design. These results will be used to make T_{11} the initial closed-loop design.

Let the compensator K_{nom} and the associated closed-loop transfer function S_{nom} be specified. Since K_{nom} is a stabilizing compensator, Theorem 4.3 states that there exists a $Q_{nom} \in H_\infty$ such that

$$K_{nom} = (U + MQ_{nom})(V + NQ_{nom})^{-1} \tag{4.47}$$

Solving for Q_{nom} yields

$$Q_{nom} = (K_{nom}N - M)^{-1}(U - K_{nom}V) \tag{4.48}$$

Compute U_{nom} and V_{nom} according to

$$U_{nom} = U + MQ_{nom} \tag{4.49}$$

$$V_{nom} = V + NQ_{nom} \tag{4.50}$$

The above manipulations yield the following results.

Theorem 4.5 U_{nom} and V_{nom} are in H_∞ and satisfy the Bezout identity

$$-\tilde{N}U_{nom} + \tilde{M}V_{nom} = I \tag{4.51}$$

Proof: M, N, U, and V are in H_∞ (Lemma 4.1), and Q_{nom} is in H_∞ (Theorem 4.3). Therefore, U_{nom} and V_{nom} are in H_∞. To prove (4.51) substitute (4.49) and (4.50) into the equation and use the Bezout identity in (4.29).

Remark Theorem 4.5 establishes U_{nom} and V_{nom} as legitimate Bezout factors and, as such, they may be used in Theorems 4.3 and 4.4.

Lemma 4.2 The set of all proper controllers achieving internal stability for the feedback system in Figure 4.1 may be parameterized by the formula

$$K = (U_{nom} + MQ)(V_{nom} + NQ)^{-1}$$

This leads to another characterization of the set of all stable closed-loop transfer function matrices S.

$$\mathbb{S} = \{ S \mid S = T_{11} + T_{12} Q T_{21} , Q \in H_\infty , I + D_{22} Q(j\omega) \text{ invertible at } \omega = \infty \}$$

where
$$T_{11} = P_{11} + P_{12} U_{nom} \tilde{M} P_{21}$$
$$= S_{nom}$$
$$T_{12} = P_{12} M$$
$$T_{21} = \tilde{M} P_{21}$$

Proof: $S_{nom} = F_l(P, K_{nom})$ by definition. From the definition of lower linear fractional transformation,

$$F_l(P, K_{nom}) = P_{11} + P_{12} K_{nom} (I - P_{22} K_{nom})^{-1} P_{21}.$$

From (4.47), (4.49), and (4.50), $K_{nom} = U_{nom} V_{nom}^{-1}$. From (4.28), $P_{22} = \tilde{M}^{-1}\tilde{N}$. Substitute the above to equations into $F_l(P, K_{nom})$ and use (4.29) to get the desired result.

Remark We now have a procedure to incorporate the nominal closed-loop S_{nom} into the parameterization of all stable closed-loop transfer functions. First, compute the coprime factorizations of P_{22} and the Bezout factors in (4.28) and (4.29) using the state-space formulas in (4.33) - (4.42). Parameterize all stabilizing compensators in terms of these factors and the free parameter Q (Equation 4.30). Solve for the particular Q_{nom} that will yield

the nominal compensator K_{nom} when applied to Eqn. (4.30). Use Q_{nom} to compute the new Bezout factors U_{nom} and V_{nom}. Form the closed-loop transfer functions T_{11}, T_{12}, and T_{21} according to Theorem 4.4 with U_{nom} in place of U. The result is $T_{11} = S_{nom}$.

The closed-loop transfer function T_{11} represents a reasonable feedback system (i.e. one with known performance and robustness). Now $Q = 0$ is an acceptable choice for the free parameter. The aim of the Causality Recovery Methodology is to find another $Q \in H_\infty$ such that the closed-loop robustness is no worse than the nominal design, and hopefully better. The next three sections describe the CRM in detail.

4.4 Optimal Noncausal Design

At this point it is worth recalling the objectives of the CRM. Simply stated, we would like to find a transfer function matrix Q such that

$$Q \in H_\infty \tag{4.52}$$

$$\| D_{nom}(T_{11}+T_{12}QT_{21})D_{nom}^{-1} \|_\infty \leq \gamma \tag{4.53}$$

Since we are interested in improving the performance robustness of the closed-loop system over the nominal design T_{11}, γ is chosen such that

$$0 < \gamma \leq \gamma_{nom} \tag{4.54}$$

The Causality Recovery Methodology treats the constraints in (4.52) and (4.53) independently. This allows the designer to ignore the causality restriction on Q and examine the synthesis problem at each frequency. The rationale behind this approach can be simply

described in a single-input, single-output context.

A function in H_∞ (i.e. a stable, causal function) is analytic in the right half plane. Cauchy's Integral Theorem applied along the familiar Nyquist contour imposes constraints on the frequency response of such a function (i.e. Bode's gain and phase integral relationships [1]). The phase (gain) of a stable, causal transfer function is completely determined by the gain (phase) over all frequencies. When the stability/causality restriction is lifted, there is no relationship between the gain and phase of a system from one frequency point to the next. Therefore, we can treat each frequency point as independent from every other frequency.

This philosophy allows one to maximize the "robustness" of the feedback system at each frequency using only complex matrix arithmetic. The result is a closed-loop frequency response with optimal performance-robustness. The price paid for such optimality is that the function will not be causal in general. That is, it will be a member of L_∞ not H_∞. However, such a system will represent an upper bound on achievable performance, or equivalently a lower bound on γ.

The frequency by frequency approach to maximizing robustness suggests the following optimization problem for finding the optimal, noncausal Q^*.

$$Q^*(j\omega) = \arg\min_{Q \in C^{mxp}} \bar{\sigma} \{ D_{nom}(j\omega)[T_{11}(j\omega) + T_{12}(j\omega)\, Q\, T_{21}(j\omega)]D_{nom}(j\omega)^{-1} \} \quad (4.55)$$

Theorem 4.7 The optimization in (4.55) is a convex program in Q.

Proof: We must show that the objective function and the feasible set are convex. First prove the objective function is convex. The argument jω will be dropped for convenience.

Let $Q = \theta Q_1 + (1-\theta)Q_2$, for $0 < \theta < 1$.

$$\bar{\sigma} \{ D[T_{11} + T_{12}QT_{21}] D^{-1} \}$$

$$= \bar{\sigma} \{ \theta D[T_{11} + T_{12}Q_1T_{21}] D^{-1} + (1 - \theta)D[T_{11} + T_{12}Q_2T_{21}] D^{-1} \}$$

$$\leq \bar{\sigma} \{ \theta D[T_{11} + T_{12}Q_1T_{21}] D^{-1} \} + \bar{\sigma} \{ (1 - \theta)D[T_{11} + T_{12}Q_2T_{21}] D^{-1} \}$$

$$\leq \theta \bar{\sigma} \{ D[T_{11} + T_{12}Q_1T_{21}] D^{-1} \} + (1-\theta) \bar{\sigma} \{ D[T_{11} + T_{12}Q_2T_{21}] D^{-1} \}$$

Therefore, the objective function is convex.

Next, prove the feasible set is convex. This is trivial, as the sum of any two complex matrices is a complex matrix.

Remark The optimization in Eqn. (4.55) is carried out independently at every frequency. The parameters are the real and imaginary parts of the elements of Q. This results in having to calculate 2mp real, scalar parameters at each frequency.

Define the measure of optimal noncausal performance

$$\gamma^* = \| D_{nom}(T_{11} + T_{12}Q^*T_{21})D_{nom}^{-1} \|_\infty \tag{4.56}$$

The measure γ^* is a lower bound on the performance-robustness that may be achieved by a $Q \in H_\infty$. That is, the γ that allows (4.52) and (4.53) to be satisfied is such that

$$\gamma^* \leq \gamma \leq \gamma_{nom} \tag{4.57}$$

Remark The inequality in (4.57) is an acknowledgement of the fact that robustness defined in terms of $\| D(T_{11} + T_{12}QT_{21})D^{-1} \|_\infty$ must be sacrificed to achieve a causal compensator. The robustness margin of a closed-loop system with a $Q \in H_\infty$ will, in general, be less than $\rho^* = 1/\gamma^*$.

4.5 Causality Recovery

The noncausal function Q^* yields optimal closed-loop robustness as measured by the robustness margin ρ^*. The caveat is that $Q^* \in L_\infty$ and is not necessarily in H_∞. Thus, the restriction imposed by the Youla parameterization is not satisfied and nominal stability of the closed-loop is not achieved. In general, the closed-loop robustness properties associated with Q^* cannot be mimicked by a transfer function $Q \in H_\infty$. In this section we propose an algorithm to find a stable, causal Q such that the closed-loop performance-robustness is no worse than the nominal design, and hopefully better, i.e.

$$\| D_{nom}(T_{11} + T_{12}QT_{21})D_{nom}^{-1} \|_\infty \leq \gamma_{nom} \tag{4.58}$$

The process of causality recovery may be thought of as an adjustment of the frequency

response of Q^* in such a way as to reduce its noncausality, or distance from H_∞, subject to a robustness constraint on the closed-loop. An alternative view is that causality recovery is a search for an H_∞ function over a tube in complex matrix space versus frequency. The robust performance specification dictates the geometry of the tube.

Define the set of frequency responses that satisfy the robustness requirement in (4.53).

$$\Phi = \{ Q \in L_\infty \mid \| D_{nom}(T_{11} + T_{12}QT_{21})D_{nom}^{-1} \|_\infty \leq \gamma \} \tag{4.59}$$

for $\gamma^* \leq \gamma \leq \gamma_{nom}$. At a specific frequency, the feasible set Φ may be interpreted as a set of complex matrices satisfying

$$\bar{\sigma} \{D_{nom}(j\omega)[T_{11}(j\omega) + T_{12}(j\omega)QT_{21}(j\omega)]D_{nom}(j\omega)^{-1}\} \leq \gamma \tag{4.60}$$

The feasible set Φ contains all L_∞ functions that satisfy the robust performance specification. We wish to determine if any of the L_∞ functions in (4.59) are also in H_∞. The fundamental component of the Causality Recovery Methodology is an optimization problem to establish the existence of a $Q \in \Phi \cap H_\infty$. Recall Nehari's Theorem (see Section 2.3) which states that a function Q is in H_∞ if and only if the norm of the Hankel operator with symbol Q ($\| \Gamma_Q \|$) is zero. This suggests the following optimization is the appropriate problem to solve.

$$\min_{Q \in \Phi} \| \Gamma_Q \| \tag{4.61}$$

Theorem 4.8 The optimization in (4.61) is a convex program in Q.

Proof: Theorem 2.5 states that the objective function is convex. The feasible set Φ is proved to be convex as follows.

Let Q_1 and Q_2 be elements of the set Φ as defined in (4.59). Construct Q as

$$Q = \theta Q_1 + (1-\theta)Q_2, \text{ for } 0 < \theta < 1.$$

Prove that Q is in Φ as well.

$$\begin{aligned}
&\| D_{nom}(T_{11} + T_{12}QT_{21})D_{nom}^{-1} \|_\infty \\
&\quad = \|\theta D_{nom}(T_{11}+T_{12}Q_1T_{21})D_{nom}^{-1} + (1-\theta)D_{nom}(T_{11}+T_{12}Q_2T_{21})D_{nom}^{-1}\|_\infty \\
&\quad \le \theta\|D_{nom}(T_{11}+T_{12}Q_1T_{21})D_{nom}^{-1}\|_\infty + (1-\theta)\|D_{nom}(T_{11}+T_{12}Q_2T_{21})D_{nom}^{-1}\|_\infty \\
&\quad \le \theta\gamma + (1-\theta)\gamma \\
&\quad \le \gamma
\end{aligned}$$

Therefore, Q is in Φ and the set is convex.

If an H_∞ function lies within Φ (for a given γ), then the minimum in (4.61) is zero and the argument Q results in a nominally stable closed-loop that achieves the robust performance objective. If γ is too small, a stable, causal function may not lie in the feasible set and the minimum Hankel norm will be some positive number. A binary search over $[\gamma^*, \gamma_{nom}]$ can be used to find the minimum γ that admits an H_∞ function into the feasible set. The search procedure is analogous to the γ-iteration that is performed as part of the H_∞ design process as outlined in Section 4.2.1 and in [17, 19, 20].

Remark 1 We can only guarantee that the closed-loop performance-robustness is no worse than the initial design. That is, the robustness margin ρ will be greater than or equal to ρ_{nom}. For example, if the initial compensator is the result of a *converged* DK iteration, then the CRM cannot improve on the design and $Q = 0$ will be the result. Of course, the usefulness of the CRM is demonstrated when a $Q \in H_\infty$ is found for $\gamma < \gamma_{nom}$.

Remark 2 The minimization in (4.61) is an infinite-dimensional, convex program due to the definition of Φ as a set of L_∞ functions. Practically speaking, only a finite-dimensional solution may be implemented, and an approximation to (4.61) and the CRM γ-iteration will have to be made. We will see in the next section that convexity must be sacrificed in order to develop an algorithm that is numerically tractable.

4.6 An Algorithm for Causality Recovery

This section describes an algorithm that will compute, in finite time, a finite-dimensional, rational transfer function matrix Q with the following properties.

$$(1) \quad \| \Gamma_Q \| \leq \varepsilon$$

$$(2) \quad \| D_{nom}(T_{11} + T_{12}QT_{21})D_{nom}^{-1} \|_\infty \leq \gamma_{nom} - k\varepsilon$$

for any $\varepsilon > 0$, and some $k > 0$.

A Q_H in H_∞ may then be computed that approximates Q in the sense that $\|Q_H - Q\|_\infty \leq \varepsilon$. The closed-loop robustness associated with Q_H is within a multiple of ε of the robustness measure associated with Q.

Define the finite-dimensional feasible set

$$\overline{\Phi} = \{ Q \in RL_\infty(n) \mid \| D_{nom}(T_{11}+T_{12}QT_{21})D_{nom}^{-1} \|_\infty \leq \gamma \} \tag{4.62}$$

where $RL_\infty(n)$ is the set of rational L_∞ functions with real coefficients and McMillan degree less than or equal to n. $\overline{\Phi}$ is no longer a convex set and the optimization problem

$$\min_{Q \in \overline{\Phi}} \| \Gamma_Q \| \tag{4.63}$$

may have multiple local minima. It may be concluded, from a property of rational functions, that as the degree n approaches infinity, $\overline{\Phi}$ becomes "dense" and approaches the convex set Φ. We will see shortly that this is not a critical property. That is, for any degree n, we will be able to construct a sequence of functions in $RL_\infty(n)$ that at least satisfy the *nominal* robustness specification and have Hankel norms approaching zero. Of course, the aim is to find a finite-dimensional function Q in H_∞ that *improves* the feedback system robustness.

The algorithm that will be used to perform the minimization in (4.63) is the modified pattern search procedure described in [43]. It is essentially a sequential search along the coordinate axes in the parameter space. The starting point for the optimization is the noncausal function Q^* that yields optimal performance-robustness. Ideally this function is computed at *every* frequency according to Eqn. (4.55). In practice, some large number of frequency points N is used to compute Q^*, where $N >> n$. An n^{th} order rational approximation $\overline{Q^*}$ is found by performing a weighted, least-squares fit of the frequency response data for each element of Q^* [8]. The lower bound on the robustness measure becomes

$$\overline{\gamma^*} = \| D_{nom}(T_{11} + T_{12}\overline{Q^*}T_{21})D_{nom}^{-1} \|_\infty \tag{4.64}$$

The parameterization of Q in (4.63) is an important issue. The μ analysis framework and the CRM are fundamentally frequency-domain tools. Therefore, an appealing parameterization from a conceptual, as well as a numerical, point of view is the multivariable pole/zero form. For example, in the two-input, two-output case, Q is described as

$$Q(s) = \frac{\begin{bmatrix} k_{11}(s+z_1^{11})(s+z_2^{11})\ldots(s+z_n^{11}) & k_{12}(s+z_1^{12})(s+z_2^{12})\ldots(s+z_n^{12}) \\ k_{21}(s+z_1^{21})(s+z_2^{21})\ldots(s+z_n^{21}) & k_{22}(s+z_1^{22})(s+z_2^{22})\ldots(s+z_n^{22}) \end{bmatrix}}{(s+p_1)(s+p_2)\ldots(s+p_n)} \tag{4.65}$$

where the poles, zeros, and gains are the parameters in the optimization.

From a numerical point of view, the pole/zero parameterization is attractive because the dynamic range of the parameters will be reasonably small (i.e. restricted to the frequency range of interest). In contrast, the coefficients of the numerator and denominator polynomials may exhibit a tremendous range of values [e.g. $(s+10)^{10}$]. Q as a function of the poles and zeros is highly nonlinear; however, since we perform a pattern search, and not a gradient search, this proved not to be a significant disadvantage.

The minimization of the Hankel norm over the feasible set involves an adjustment of the poles and zeros of Q in such a way as to reduce the measure of noncausality subject to the frequency-domain constraint imposed by the feasible set. There are three basic ways to reduce the Hankel norm of the transfer function matrix in Eqn. (4.65).

(1) Move the unstable poles into the left half plane or to infinity

(2) Cancel out the unstable poles with nonminimum phase zeros

(3) Reduce the gain k_{ij} in (4.65)

Remark It is worth noting that the feasible set $\overline{\Phi}$ is never actually constructed as part of the design process; it is a conceptual notion only. The minimization algorithm reduces the Hankel norm by perturbing the poles and zeros of the Q function. The perturbation is admissible if it reduces the Hankel norm *and* is a function in $\overline{\Phi}$. Thus, it is only necessary to check if a particular function is in $\overline{\Phi}$ and not to construct the set itself. This can be done for any n and γ by checking the defining equation (4.62).

The causality recovery process is slightly more complicated in the finite-dimensional case due to the nonconvexity of the problem. If the minimum in (4.63) is not zero, one of three scenarios is possible.

(1) A local minimum has been found.

(2) An $RH_\infty(n)$ function is not contained in $\overline{\Phi}$.

(3) An H_∞ function does not exist to satisfy the robustness constraint.

Only ad hoc methods exist for circumventing situation (1). That is, one can try a different starting point, optimization algorithm (i.e. simulated annealing), parameterization, etc. We will not discuss this case further. As we shall see in Theorem 4.10, it is possible to reduce the minimum Hankel norm and avoid situation (2) by increasing the order n of admissible functions in $\overline{\Phi}$. The third case is remedied by relaxing (i.e. increasing) the robustness specification γ. Before we present the causality recovery algorithm, some preliminary results are required.

Theorem 4.9 Let $\gamma_{nom} = \| D_{nom} T_{11} D_{nom}^{-1} \|_\infty$. Suppose there is a function $Q_o \in RL_\infty(n)$ with Hankel norm $\| \Gamma_{Q_o} \| = \alpha_o > 0$, and a γ_o satisfying

$$\| D_{nom} (T_{11} + T_{12} Q_o T_{21}) D_{nom}^{-1} \|_\infty \leq \gamma_o < \gamma_{nom}$$

Then, there exists a $Q \in RL_\infty(n)$ such that, for any $\varepsilon > 0$ and a $k > 0$,

(1) $\| \Gamma_Q \| \leq \varepsilon$

(2) $\| D_{nom}(T_{11} + T_{12} Q T_{21}) D_{nom}^{-1} \|_\infty \leq \gamma_{nom} - k\varepsilon$

Proof: The most straightforward way to prove the existence of such a Q is to simply construct the function. Let Q be a convex combination of the function Q_o and the zero function, i.e. $Q = \theta Q_o + (1-\theta)(0) = \theta Q_o$ for $0 < \theta < 1$.

Then, $\| \Gamma_Q \| = \theta \| \Gamma_{Q_o} \|$, and the conditions of the theorem are satisfied for a $\theta \leq \varepsilon/\alpha_o$.

$$\| D_{nom}(T_{11} + T_{12} Q T_{21}) D_{nom}^{-1} \|_\infty \leq \theta \| D_{nom}(T_{11} + T_{12} Q_o T_{21}) D_{nom}^{-1} \|_\infty + (1-\theta) \| D_{nom} T_{11} D_{nom}^{-1} \|_\infty$$

$$\leq \theta\gamma_o + (1-\theta)\gamma_{nom}$$

$$\leq \varepsilon\gamma_o/\alpha_o + (1-\varepsilon/\alpha_o)\gamma_{nom}$$

$$\leq \gamma_{nom} - \varepsilon(\gamma_{nom} - \gamma_o)/\alpha_o$$

$$\leq \gamma_{nom} - k\varepsilon$$

Remark Theorem 4.9 guarantees that the CRM algorithm will terminate in finite time with a finite-dimensional function Q of arbitrarily small Hankel norm. The Hankel norm reduction may simply be accomplished by reducing the gain of Q_o. Note that, all other factors being equal, a function Q_o', with Hankel norm $\alpha_o' < \alpha_o$, yields a constant $k' > k$ in Theorem 4.9, and an improved robustness measure. This suggests that we find the function

with minimum Hankel norm before reducing the gain of Q (or equivalently increasing γ). This motivates the following theorem.

Theorem 4.10 Given the feasible sets

$$\overline{\Phi}_n = \{ Q \in RL_\infty(n) \mid \| D_{nom}(T_{11} + T_{12}QT_{21})D_{nom}^{-1} \|_\infty \leq \gamma \}$$

$$\overline{\Phi}_{n+1} = \{ Q \in RL_\infty(n+1) \mid \| D_{nom}(T_{11} + T_{12}QT_{21})D_{nom}^{-1} \|_\infty \leq \gamma \}$$

Let

$$\alpha_n = \min_{Q \in \Phi_n} \| \Gamma_Q \|$$

$$\alpha_{n+1} = \min_{Q \in \Phi_{n+1}} \| \Gamma_Q \|$$

Then, $\alpha_{n+1} \leq \alpha_n$.

Proof: This is a simple consequence of the fact that $\overline{\Phi}_n$ is a subset of $\overline{\Phi}_{n+1}$.

Remark For a fixed performance specification γ, increasing the order of admissible functions in $\overline{\Phi}$ will result in a minimum Hankel norm that is less than or equal to the previous minimum. This suggests a way to possibly reduce the Hankel norm in the causality recovery process.

In light of Theorems (4.9) and (4.10), the finite-dimensional causality recovery algorithm is presented. The following definitions will be needed.

$$\overline{\Phi}_i = \left\{ Q \in RL_\infty(n_i) \mid \| D_{nom}(T_{11} + T_{12}QT_{21})D_{nom}^{-1} \|_\infty \leq \gamma_i \right\}$$

$$\alpha_{i+1} = \min_{Q \in \overline{\Phi}_i} \| \Gamma_Q \|$$

$$Q_{i+1} = \arg\min_{Q \in \overline{\Phi}_i} \| \Gamma_Q \|$$

The starting point for the minimization over the feasible set is Q_i.

The Causality Recovery Algorithm

Choose $\varepsilon_1 > 0, \varepsilon_2 > 0, 0 < \beta < 1$

$Q_0 = \overline{Q^*}$

n_0 = McMillan degree of Q_0

$\gamma_0 = \overline{\gamma^*}$

Compute α_1 and Q_1

$n_1 = n_0 + 1$

$\gamma_1 = \gamma_0$

Compute α_2 and Q_2

$i = 2$

while $\alpha_i > \varepsilon_1$ [begin outer loop]

while $(\alpha_{i-1} - \alpha_i) > \varepsilon_2$ [begin inner loop]

$n_i = n_{i-1} + 1$

$\gamma_i = \gamma_{i-1}$

Compute α_{i+1} and Q_{i+1}

$i = i + 1$

end [end inner loop]

$\gamma_i = (1 - \beta)\gamma_{i-1} + \beta\gamma_{nom}$

Compute α_{i+1} and Q_{i+1}

$i = i + 1$

end [end outer loop]

The algorithm starts with an initial robustness specification γ_0 and McMillan degree n_0 and attempts to find a $Q \in RH_\infty(n_0)$ such that the specification is satisfied. If such a function is not found, the admissible order of Q is increased by adding a stable pole/zero cancellation to each element. The order of Q is increased as long as it results in greater than an ε_2 reduction in the Hankel norm. When this level of improvement in the Hankel norm ceases, the algorithm decides that increasing the order of Q is no longer worthwhile and the robustness specification parameter γ is increased.

Theorem 4.10 guarantees that α_i is a non-increasing sequence. The sequence converges because α_i is bounded below by zero. This ensures that the inner loop (i.e. the loop where the McMillan degree is increased) will eventually terminate. That is, the fact that the α_i sequence converges implies that an ε_2 improvement cannot be maintained indefinitely.

It is clear that a smaller ε_2 will allow the inner loop to reduce the Hankel norm further and will result in a higher dimensional Q parameter. As the McMillan degree is increased, the optimization approaches a convex program and the global minimum Hankel norm (for some γ). Unfortunately, the global minimum is not known a priori, and it is impossible to state how close one is to the global solution as a function of ε_2. However, even in the absence of such knowledge, the inner loop serves a useful purpose. It reduces the Hankel norm for a constant γ and potentially allows more of an improvement in performance-robustness. That is, the constant k in Theorem 4.9 is increased.

The outer loop is where the relaxation of the robustness specification takes place. This may be viewed as a last resort after the option of increasing the order of Q is exhausted. At this stage, the algorithm essentially assumes that no H_∞ function will satisfy the given specification. Theorem 4.9 states that there eventually will exist a $Q \in RL_\infty(n)$ of arbitrarily small Hankel norm in the feasible set if the robustness specification is increased to within $k\varepsilon_1$ of γ_{nom}.

The difference equation in the outer loop generates a γ_i sequence that approaches γ_{nom}

exponentially from the initial condition $\overline{\gamma^*}$, and is within $k\varepsilon_1$ of γ_{nom} in a finite time. The parameter β represents the time constant of the difference equation, and a plot of time responses for several β's is in Figure 4.4. The time constant determines how rapidly γ_i approaches γ_{nom} and, therefore, controls the accuracy with which the minimum robustness specification that admits a causal solution is found. The choice of β involves a fundamental tradeoff between speed and accuracy. In any case, the outer loop ultimately terminates with a finite-dimensional, rational transfer function Q such that $\| \Gamma_Q \| \leq \varepsilon_1$.

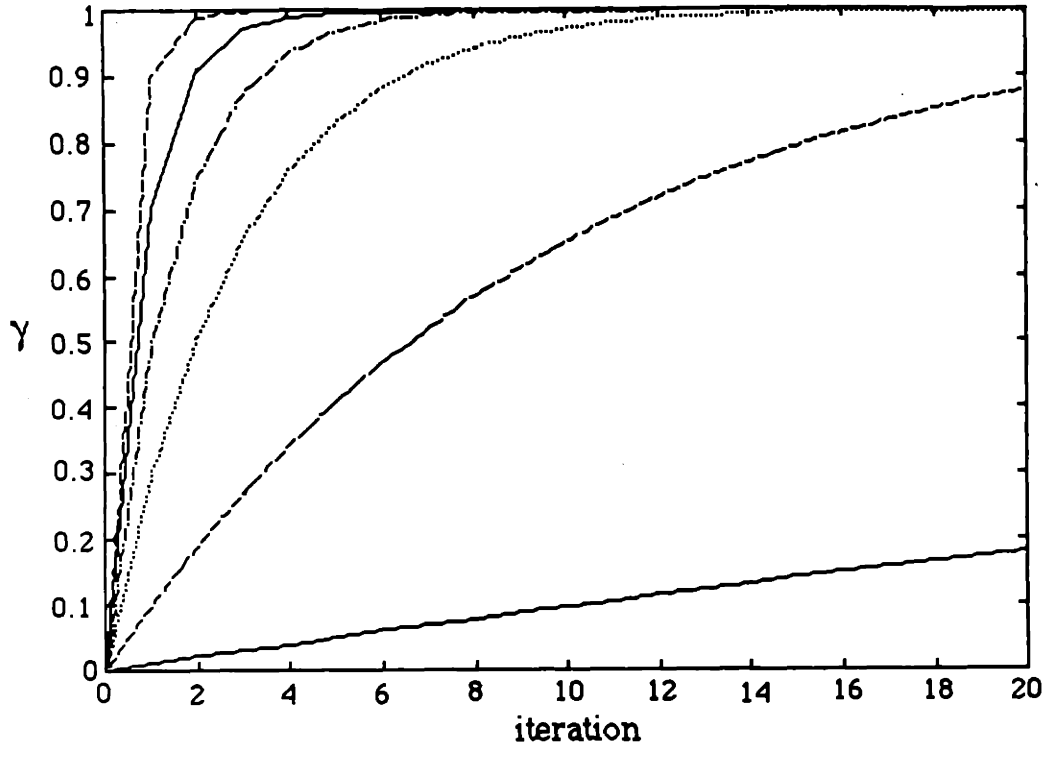

Figure 4.4 Relaxation of robustness specification γ for different time constants β.

Recall that the set of stabilizing controllers is parameterized in terms of a function in H_∞, i.e. a function whose Hankel norm is *identically zero*. The causality recovery algorithm only guarantees producing a Q whose Hankel norm is less than or equal to ε_1. At this point

the best H_∞ approximation Q_H of the L_∞ function Q must be computed (see section 2.3.3). This motivates the following theorem.

Theorem 4.11 Given a function $Q \in L_\infty$ such that

(1) $\| \Gamma_Q \| \leq \varepsilon_1$

(2) $\| D_{nom}(T_{11} + T_{12}QT_{21})D_{nom}^{-1} \|_\infty \leq \gamma$

Then, there exists a $Q_H \in H_\infty$ such that

$\| D_{nom}(T_{11} + T_{12}Q_HT_{21})D_{nom}^{-1} \|_\infty \leq \gamma + k\varepsilon_1$

for a $k > 0$.

Proof: Since $\| \Gamma_Q \| \leq \varepsilon_1$, Nehari's Theorem (see Section 2.3.2) states there exists a Q_H in H_∞ such that $\| Q_H - Q \|_\infty \leq \varepsilon_1$.

Let $Q_H = Q + (Q_H - Q)$

$$\| D_{nom}(T_{11}+T_{12}Q_HT_{21})D_{nom}^{-1} \|_\infty \leq \| D_{nom}(T_{11}+T_{12}QT_{21})D_{nom}^{-1} \|_\infty + \| D_{nom}[T_{12}(Q_H - Q)T_{21}]D_{nom}^{-1} \|_\infty$$

$$\leq \gamma + \| D_{nom}T_{12} \|_\infty \varepsilon_1 \| T_{21}D_{nom}^{-1} \|_\infty$$

$$\leq \gamma + k\varepsilon_1$$

Remark According to Theorem 4.11, ε_1 must be chosen to be sufficiently small. Then, the best H_∞ approximation of the function generated by the causality recovery process results in closed-loop performance-robustness that is arbitrarily close to that achieved by causality recovery.

In this section, an algorithm that is amenable to computer implementation has been developed to find a stable, causal transfer function Q. The resulting closed-loop map exhibits a level of performance-robustness that is better than or equal to the nominal design.

4.7 Concluding Remarks

This chapter has presented the Causality Recovery Methodology in detail. The CRM computes a causal compensator that guarantees the resulting closed-loop system will exhibit performance-robustness that is no worse than, and hopefully superior to, the robustness of a given nominal design. The a priori information required is just the plant P (which includes the control plant G, sensors, actuators, and weighting functions) and the initial stabilizing compensator K_{nom}.

The function yielding optimal robustness (in the scaled singular value sense) is noncausal, in general. The causal compensator is found by γ-iteration and the solving of a series of infinite-dimensional convex optimization programs. Several theorems establish the foundation for a finite-dimensional implementation of the CRM. This causality recovery algorithm will guarantee the finding of a stable, causal transfer function that is finite-dimensional; however, the global minimum in terms of robustness may not be achieved. The CRM is summarized below.

Causality Recovery Methodology

Step 0 (A priori Information)

FDLTI model of the design plant P.

Step 1 (Nominal Compensator Design)

Design the stabilizing compensator K_{nom} using an existing synthesis methodology.

$S_{nom} = F_l(P, K_{nom})$ is the nominal closed-loop transfer function. Compute the performance-robustness properties of S_{nom} via

$$D_{nom}(\omega) = \arg \inf_{D \in \mathbb{D}} \bar{\sigma} [D S_{nom}(j\omega) D^{-1}]$$

$$\mathbb{D} = \{ \text{diag}(d_1 I, d_2 I, \ldots, d_n I) \mid d_j \in \mathbf{R}_+ \}$$

$$\gamma_{nom} = \| D_{nom} S_{nom} D_{nom}^{-1} \|_\infty$$

Note that D_{nom} is just a scaling frequency response function. A finite-dimensional realization of D_{nom} is not required.

Step 2 (Youla Parameterization)

Compute the coprime factorizations of the plant transfer function matrix P_{22} (Eqns. 4.28 and 4.29), and the Bezout factors U_{nom} and V_{nom} (Eqns. 4.49 and 4.50). Then, the parameterization of all stabilizing compensators yields the set of stable closed-loop transfer function matrices described by

$$S = T_{11} + T_{12} Q T_{21}$$

where $T_{11} = S_{nom}$ and $Q \in H_\infty$.

Step 3 (Optimal Noncausal Design)

Compute the function in L_∞ that maximizes performance-robustness by solving

$$Q^*(j\omega) = \arg\min_{Q \in C^{mxp}} \bar{\sigma} \{ D_{nom}(j\omega)[T_{11}(j\omega) + T_{12}(j\omega)\, Q\, T_{21}(j\omega)]D_{nom}(j\omega)^{-1} \}$$

at each frequency. Fit an n^{th} order transfer function $\overline{Q^*}$ to Q^*.

$$\overline{\gamma^*} = \| D_{nom}(T_{11} + T_{12}\overline{Q^*}T_{21})D_{nom}^{-1} \|_\infty$$

Step 4 (Causality Recovery)

Use the algorithm in Section 4.6 to find a $Q \in RH_\infty(n)$ such that

$$\| D_{nom} (T_{11}+T_{12}QT_{21}) D_{nom}^{-1} \|_\infty \leq \gamma_{nom}$$

Step 5 (Construction of Compensator and Closed-loop)

$$K = (U_{nom} + MQ)(V_{nom} + NQ)^{-1}$$

$$S = T_{11}+T_{12}QT_{21}$$

where M, N, U_{nom}, and V_{nom} are the factorizations from the Youla parameterization.

CHAPTER 5. DESIGN EXAMPLES

5.1 Introduction

This chapter presents numerical examples to demonstrate feedback system synthesis via the Causality Recovery Methodology. More specifically, we show how the CRM improves the performance-robustness of a feedback system. The causality recovery process is examined, and the resulting (causal) compensator and closed-loop system analyzed in the time and frequency domains. Two designs, one SISO and one MIMO, illustrate the usefulness, as well as the drawbacks, of the CRM.

The feedback problem to be considered here is the conventional one discussed in Section 1.2.6. That is, we will be given a nominal plant model and a description of (i.e. norm-bound on) the multiplicative uncertainty at the plant input. The performance specification is a frequency-domain bound on the (output) sensitivity function. The standard problem is formulated in terms of the design framework in Figure 1.7 so that the CRM may be applied. The results are then interpreted in terms of the conventional feedback structure (Figure 1.9).

5.2 SISO Case: The Adaptive Benchmark

This typical aerospace problem was proposed by Franklin and Stein [47] to serve as a benchmark example for robustness studies of adaptive control. It is a satellite control problem with known rigid body dynamics, an uncertain bending mode of known structure, and an unstructured, norm-bounded uncertainty. The SISO control plant model is

$$G(s)[\ 1 + L(s)\ ] \qquad (5.1)$$

where

$$G(s) = \frac{9(ds + k)}{s^2(s^2 + 10ds + 10k)} \tag{5.2}$$

$$| L(j\omega) | < | L_o(j\omega) | \tag{5.3}$$

$$L_o(s) = \frac{10s^2}{s^2 + 8s + 64} \tag{5.4}$$

The exact values of the parameters d and k in Eqn. (5.2) are unknown; however, they are known to lie in the ranges

$$0.1 \leq k \leq 0.4 \tag{5.5}$$

$$0.04\sqrt{\frac{k}{10}} \leq d \leq 0.2\sqrt{\frac{k}{10}} \tag{5.6}$$

These parameter ranges cause the natural frequency of the bending mode to vary from 1 to 2 radians/second with a damping ratio between 0.02 and 0.1.

The feedback problem, as has been stated in this thesis (Section 1.2), assumes that the modeling uncertainty is of the unstructured, norm-bounded (complex) type. The real parameter uncertainty in (5.5) and (5.6) is not dealt with directly in μ-synthesis or the CRM, and the variations in (5.5) and (5.6) must be covered by a complex uncertainty block (weighting function). To compute this uncertainty weighting function, a bound must be found on the total modeling error, i.e. the real parameter variations (Eqns. 5.5 and 5.6) and the norm-bounded uncertainty in Eqn (5.4).

Define the plant parameter vector

$$\theta = \begin{bmatrix} k \\ d \end{bmatrix} \tag{5.7}$$

and the associated plant $G(s,\theta)$. θ may take on any value consistent with (5.5) and (5.6). The nominal parameter vector is denoted θ_{nom}. For this example, we arbitrarily chose

$$\theta_{nom} = \begin{bmatrix} 0.25 \\ 0.019 \end{bmatrix} \tag{5.8}$$

The frequency response of $G(s,\theta_{nom})$ is shown in Figure 5.1. The double-integrator response with a lightly damped resonance ($\zeta = 0.06$) at a frequency of 1.6 radians/second is illustrated.

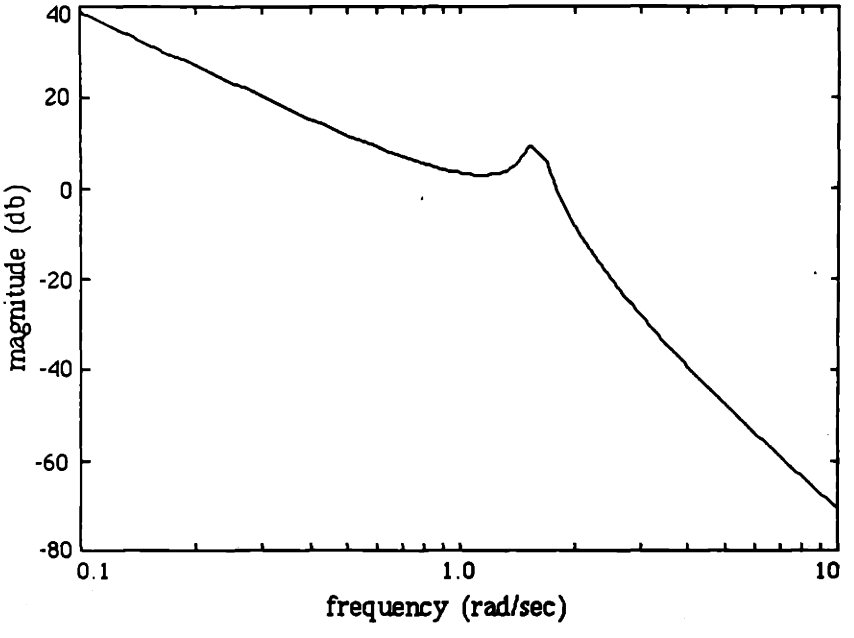

Figure 5.1 Frequency response of the nominal plant $G(s,\theta_{nom})$ for the SISO example.

The plant model is now described as

$$G(s,\theta_{nom})[\ 1 + l(s,\theta)\ ][\ 1 + L(s)\ ] \tag{5.9}$$

where $l(s,\theta)$ denotes the multiplicative error due to the parameter uncertainty.

$$l(s,\theta) = \frac{G(s,\theta)}{G(s,\theta_{nom})} - 1 \tag{5.10}$$

Define a new multiplicative error L' that incorporates the effect of both forms of uncertainty. The plant model becomes

$$G(s,\theta_{nom})[1 + L'(s,\theta)] \tag{5.11}$$

where
$$L'(s,\theta) = l(s,\theta) + [1 + l(s,\theta)]L(s) \tag{5.12}$$

A frequency-dependent magnitude bound $L'_o(\omega)$ on the total multiplicative error (Eqn. 5.12) can be computed at each frequency.

$$L'_o(\omega) = \sup_{\theta} [\ |\ l(j\omega,\theta)\ | + |\ [1 + l(j\omega,\theta)]L_o(j\omega)\ |\ ] \tag{5.13}$$

where θ varies over the ranges in (5.5) and (5.6). A simple grid search was performed to find $L'_o(\omega)$. Then, the uncertainty weighting function $W_z(j\omega)$ is a stable, minimum phase approximation of $L'_o(\omega)$; for this example, the bound on the multiplicative error is

$$W_z(s) = 10L_o(s) \tag{5.14}$$

The Bode plot of $W_z(j\omega)$ is shown in Figure 5.2. The uncertainty weight is flat above 8 radians/second.

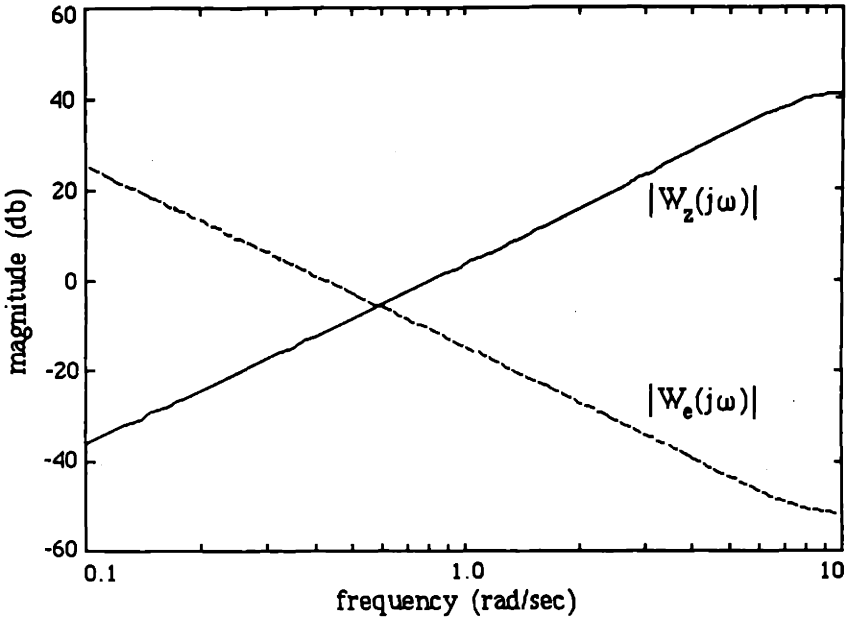

Figure 5.2 Frequency responses of the uncertainty and performance weighting functions for the SISO example.

The performance weight $W_e(s)$ was chosen to provide a "cross-over gap" with respect to the uncertainty weight $W_z(s)$. That is, the cross-over frequency of the performance function must be below that of the uncertainty. Obviously, we cannot expect good performance in frequency ranges where there is a substantial amount of uncertainty. Such a $W_e(s)$ is

$$W_e(s) = \frac{s^2 + 8s + 64}{333s^2} \frac{100}{s + 100} \qquad (5.15)$$

The Bode plot of the performance weight is also shown in Figure 5.2. Note that a high-frequency pole was added to make $W_e(s)$ strictly proper, as required by the Doyle/Glover parameterization in Section 4.2.1. The frequency response flattens out above 8 radians/second, and then rolls off for frequencies above 100 radians/second.

The design plant model P (Eqn 1.27) is defined by Eqns. (5.2), (5.8), (5.14), and (5.15). The H_∞ design procedure in section 4.2.1 was used to compute the nominal compensator for P. The structure of P (i.e. a multiplicative uncertainty at the plant input and a performance specification at the plant output) defines a four-block H_∞ problem [20]. The γ-iteration produced a minimum γ of 10.2, and a nominal compensator with the transfer function

$$K_{nom}(s) = \frac{44.6s^7 + 388s^6 + 3229s^5 + 3053s^4 + 8368s^3 + 3973s^2 + 1177s + 176}{s^8 + 441s^7 + 1820s^6 + 4861s^5 + 8985s^4 + 11592s^3 + 9559s^2 + 188s + 0.93} \tag{5.16}$$

The Bode plot of K_{nom} is shown in Figure 5.3. The response indicates two low frequency poles and very lightly damped poles and zeros at approximately 2 radians/second (see Table 5.1). Note that the order of K_{nom} is eight, not nine as expected, because the H_∞ design produced a pole/zero cancellation.

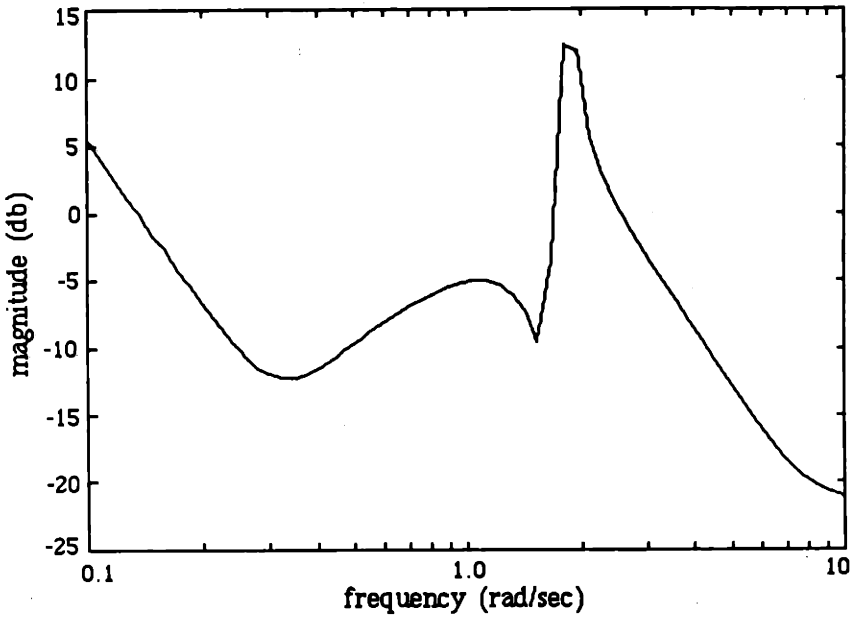

Figure 5.3 Frequency response of the nominal compensator K_{nom} designed by the H_∞ methodology.

Table 5.1: Poles and zeros of the H_∞ compensator K_{nom} for the SISO example.

Poles	Zeros
-0.01	-0.26
-0.01	-0.13 ± 0.28j
0.01 ± 1.85j	-0.09 ± 1.58j
-1.16 ± 1.44j	-4.0 ± 6.93j
-1.82	
-437	

The singular value and structured singular value frequency response of the nominal closed-loop system $S_{nom} = F_l(P, K_{nom})$ is displayed in Figure 5.4. The $\bar{\sigma}$ plot has the "all-pass" response characteristic of an H_∞ design. In this case, the largest singular value $\bar{\sigma}$ is a tight upper bound on μ. This design does not exhibit robust performance with respect to the weighting functions in Figure 5.2 because γ is larger than 1 ($\gamma_{nom} = 10.2$). The nominal robustness margin $\rho_{nom} = 0.098$. Figure 5.5 contains the frequency response of the D scaling associated with the μ computation (i.e. D_{nom}).

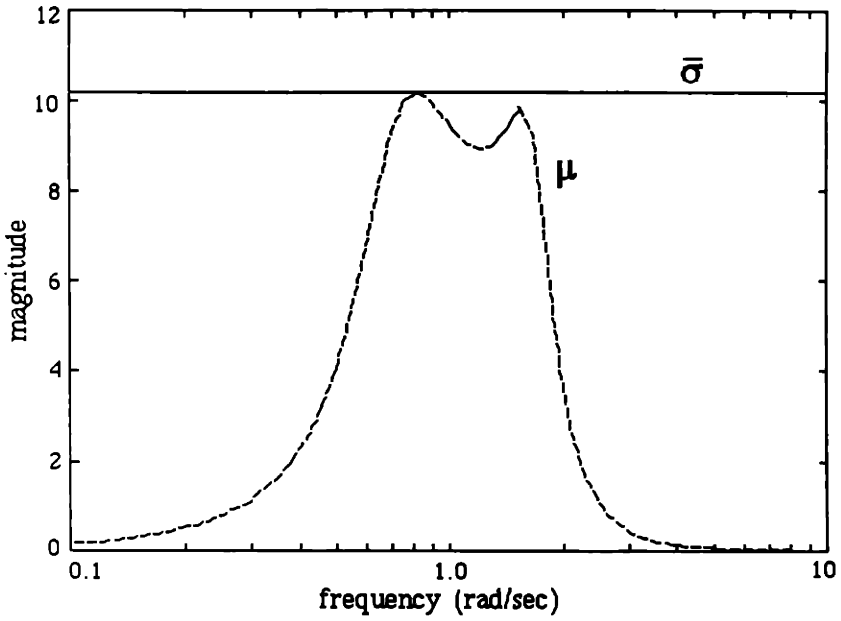

Figure 5.4 Frequency response of the nominal closed-loop transfer function S_{nom}.

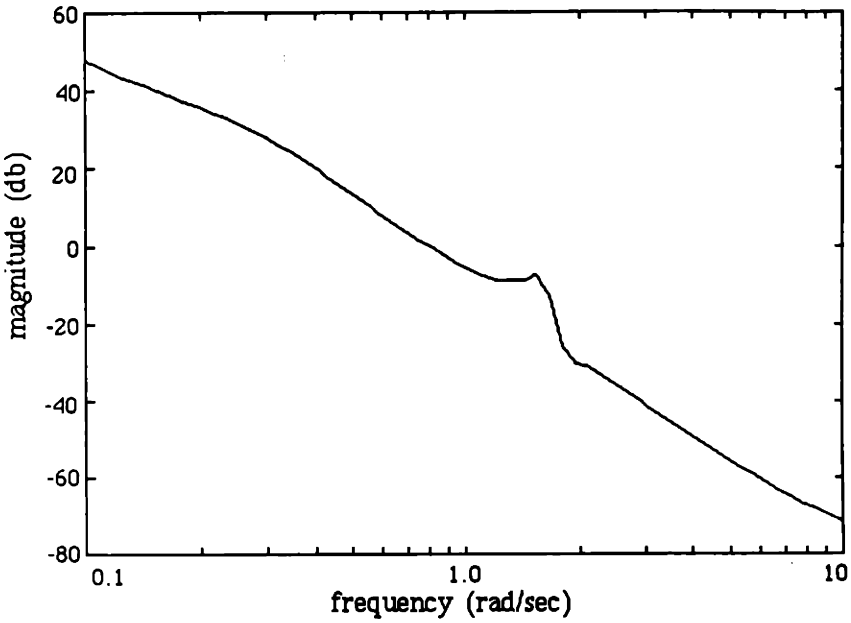

Figure 5.5 Frequency response of the scaling D_{nom}.

Now that the nominal system has been computed, the CRM may proceed. All stable closed-loop transfer function matrices S are parameterized in terms of a transfer function matrix Q.

$$S = T_{11} + T_{12}\, Q\, T_{21} \tag{5.17}$$

where $T_{11} = S_{nom}$ and $Q \in H_\infty$.

The optimal noncausal parameter Q^* was computed, at 60 points over the frequency range from 0.1 through 10 radians/second, by maximizing the closed-loop robustness according to Eqn. (4.55). A seventh-order rational approximation $\overline{Q^*}$ was found using a least-squares fit.

$$\overline{Q^*} = \frac{-0.51s^6 - 6.18s^5 - 1.08s^4 - 15.71s^3 + 8.21s^2 - 0.37s + 0.0011}{s^7 + 0.15s^6 + 2.88s^5 - 0.063s^4 + 1.03s^3 - 0.090s^2 + 0.24s + 0.15} \quad (5.18)$$

The frequency responses of Q^* and its rational approximation $\overline{Q^*}$ are in Figures 5.6 and 5.7. The Hankel norm of $\overline{Q^*}$ is 3.64; $\overline{Q^*}$ is not in H_∞ because of the right half plane poles (see Table 5.2).

Recall that the optimization problem in Eqn. (4.55) is convex at each frequency and all local minima are global. The real and imaginary parts of Q^*, at each frequency, were the parameters in the optimization, and the pattern search algorithm in [43] was used to compute Q^*.

Table 5.2: Poles and zeros of $\overline{Q^*}$ for the SISO example.

Poles	Zeros
-0.09 ± 1.58j	0.0032
-0.21 ± 0.67j	0.047
0.40 ± 0.44j	0.42
-0.34	-0.22 ± 1.67j
	-12.15

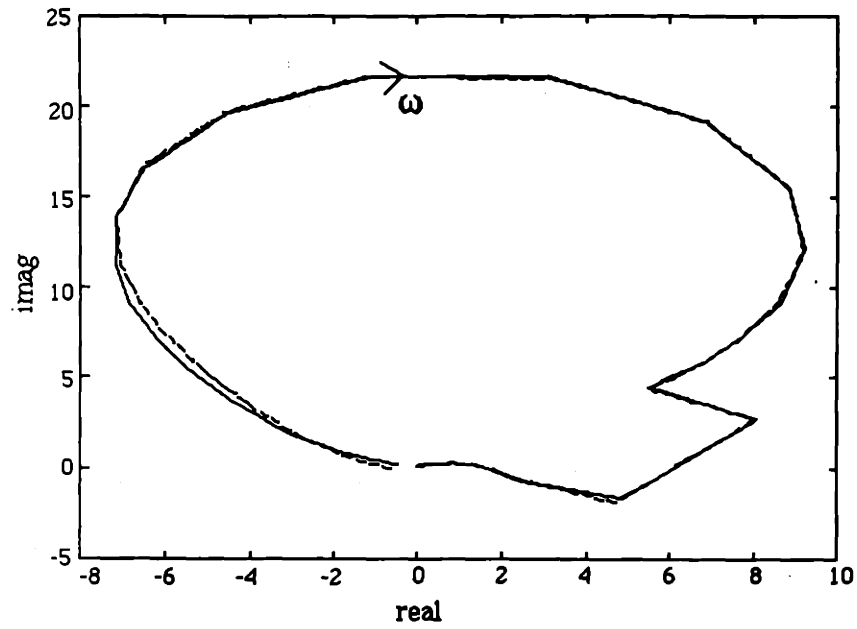

Figure 5.6 Nyquist plot of Q^* (solid) and its rational approximation $\overline{Q}^*$ (dashed).

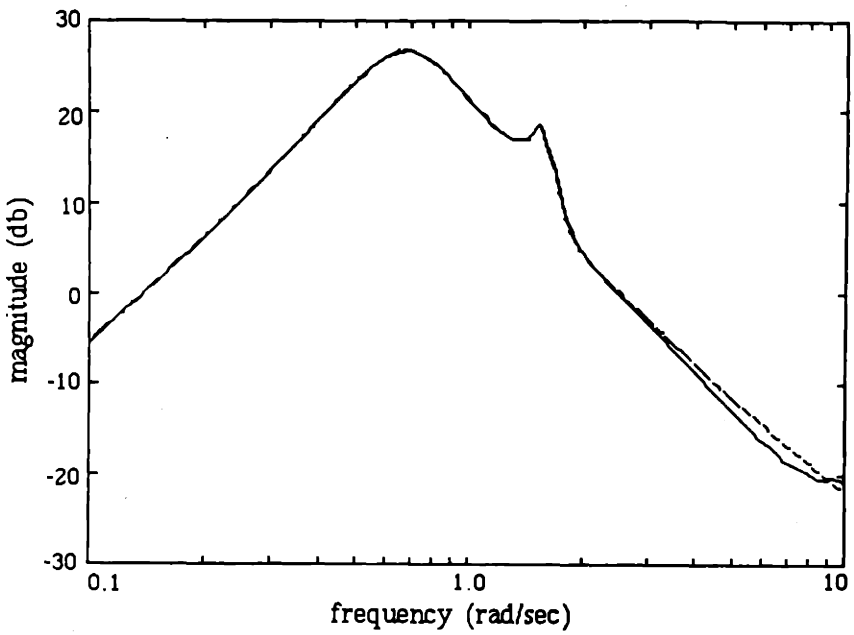

Figure 5.7 Bode plot of Q^* (solid) and its rational approximation $\overline{Q}^*$ (dashed).

The scaled frequency response of the optimal noncausal closed-loop transfer function matrix, $T_{11}+T_{12}\overline{Q}^*T_{21}$, is shown in Figure 5.8, along with the nominal response $S_{nom}= T_{11}$. The robustness margin of the noncausal design is $\overline{\rho}^* = 1.12$, an order of magnitude improvement over the nominal design ($\rho_{nom} = 0.098$). The robustness bound $\overline{\gamma}^* = 0.89$. Although no real significance can be attached to the compensator associated with $\overline{Q}^*$, because it does not yield nominal closed-loop stability, its frequency response is contained in Figure 5.9.

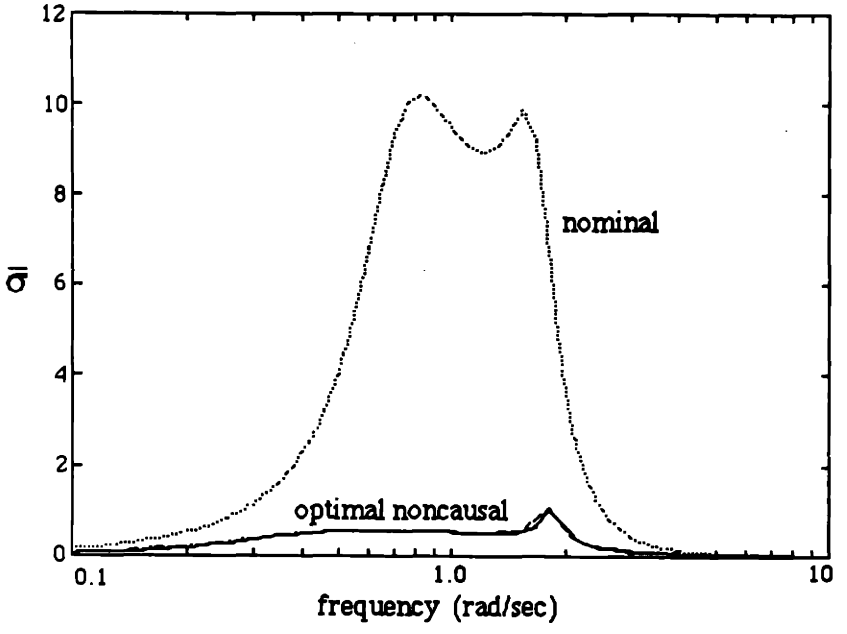

Figure 5.8 Frequency response of the scaled closed-loop transfer function matrix, $D_{nom}(T_{11}+T_{12}QT_{21})D_{nom}^{-1}$, for $Q = 0$ (nominal), $Q = Q^*$ (optimal noncausal), and $Q = \overline{Q}^*$ (rational approximation).

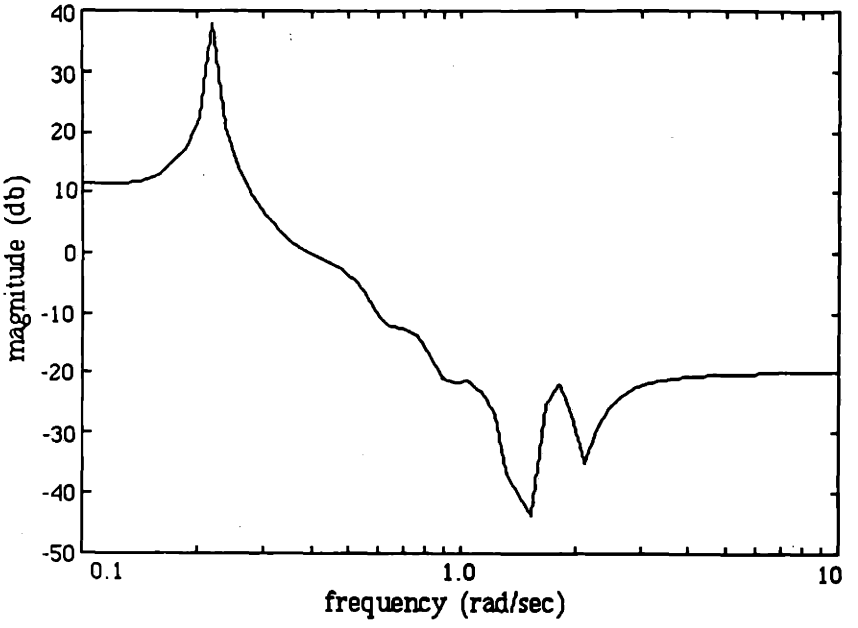

Figure 5.9 Bode plot of the noncausal compensator resulting from $\overline{Q}^*$.

The next step in the CRM is the causality recovery process. The parameters ε_1 and ε_2 (from the causality recovery algorithm in Section 4.6) were chosen to be 0.01 and 0.1, respectively. The time constant $\beta = 0.1$. Given the relatively large Hankel norm of $\overline{Q}^*$ (= 3.64), the initial robustness specification $\gamma_0 = 2$ (vs. $\overline{\gamma}^* = 0.89$). This choice of γ_0 gives the causality recovery algorithm "room" to reduce the Hankel norm, while γ is still significantly less than $\gamma_{nom} = 10.2$.

The CRM algorithm produced the sequence of Hankel norms shown in Figure 5.10. Each element represents the minimum Hankel norm over some feasible set Φ defined by the order n of Q and the robustness specification γ. Table 5.3 summarizes the CRM for this SISO example.

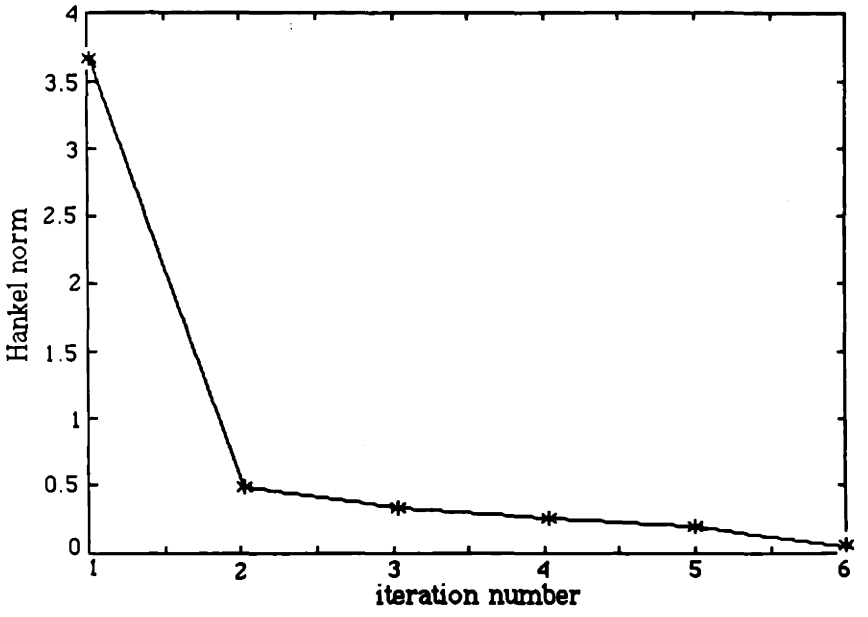

Figure 5.10 Hankel norm sequence generated by the CRM algorithm.

Table 5.3: The causality recovery process for the SISO example.

			Hankel norm	
Iteration Number	n	γ	Initial	Final
1	7	2.0	3.64	0.48
2	8	2.0	0.48	0.37
3	9	2.0	0.37	0.26
4	10	2.0	0.26	0.20
5	10	2.8	0.20	0.004
6	---	---	0.004	0

The order of the Q parameter is increased each time an improvement in the Hankel norm of greater than ε_2 (= 0.1) occurs. When this degree of improvement is no longer achieved (iteration 4), the specification γ is increased to 2.8 according to the difference equation in Section 4.6 ($\beta = 0.1$). Iteration 5 produces a Q whose Hankel norm is less than ε_1 (= 0.01). This terminates the causality recovery process, and iteration 6 consists of simply finding the best H_∞ approximation of the function from iteration 5 (see Section 2.2.3). The result is a stable, causal function Q (Eqn. 5.19 and Table 5.4). The order of Q is less than 10 because of unstable pole/zero cancellations that occur as part of the causality recovery process.

$$Q = \frac{0.29s^6 - 4.44s^5 - 13.52s^4 - 27.97s^3 - 39.58s^2 - 25.31s - 4.91}{s^7 + 3.08s^6 + 6.41s^5 + 10.39s^4 + 10.06s^3 + 6.41s^2 + 2.77s + 0.47} \qquad (5.19)$$

Table 5.4: Poles and zeros of the $Q \in H_\infty$ for the SISO example.

Poles	Zeros
-0.08 ± 1.59j	-0.33
-0.20 ± 0.68j	-0.98
-0.32	-1.03
-0.88	-0.27 ± 1.65j
-1.31	18.37

The evolution of the Q parameter in the causality recovery process is shown in Figures 5.11 and 5.12. Each frequency response represents a Q parameter that minimizes the Hankel norm over a feasible set. Figure 5.11 and 5.12 demonstrate how the frequency response of Q is adjusted, subject to the constraint imposed by the feasible set, to reduce its noncausality.

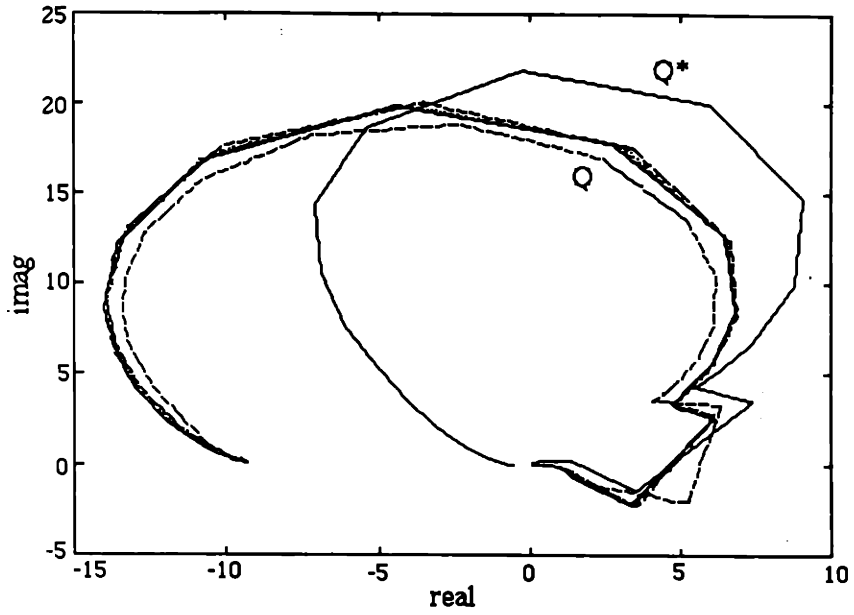

Figure 5.11 Nyquist plot of the Q parameter evolution from causality recovery.

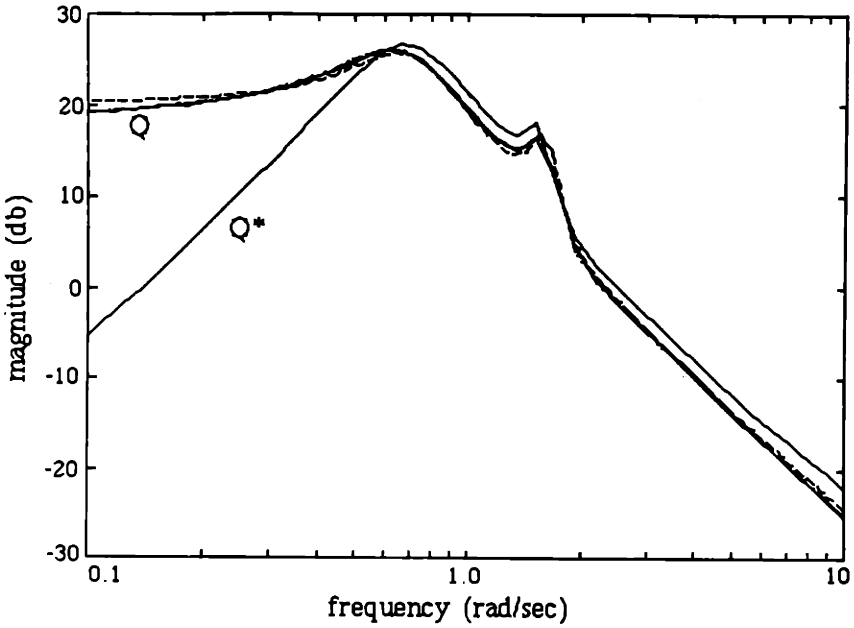

Figure 5.12 Bode plot of the Q parameter evolution from causality recovery.

Figure 5.13 contains the scaled frequency response of the closed-loop transfer function, $D_{nom}(T_{11}+T_{12}QT_{21})D_{nom}^{-1}$, as the Q parameter goes from the optimal noncausal $\overline{Q^*}$ to the causal solution. For $\gamma = 2$, the Hankel norm is reduced by increasing the order of the Q parameter. Finally, a causal Q is found by increasing the robustness bound to 2.8. The robustness margin is $\rho = 0.38$ for the final, causal design. This is less than the optimal $\overline{\rho^*} = 1.12$, as expected, but is much larger than the nominal robustness margin of ρ_{nom}= 0.098. A comparison of the closed-loop structured singular values, $\mu(T_{11}+T_{12}QT_{21})$, is contained in Figure 5.14. Notice that performance-robustness in the low frequency region is sacrificed to improve robustness in the $\| \cdot \|_\infty$ sense.

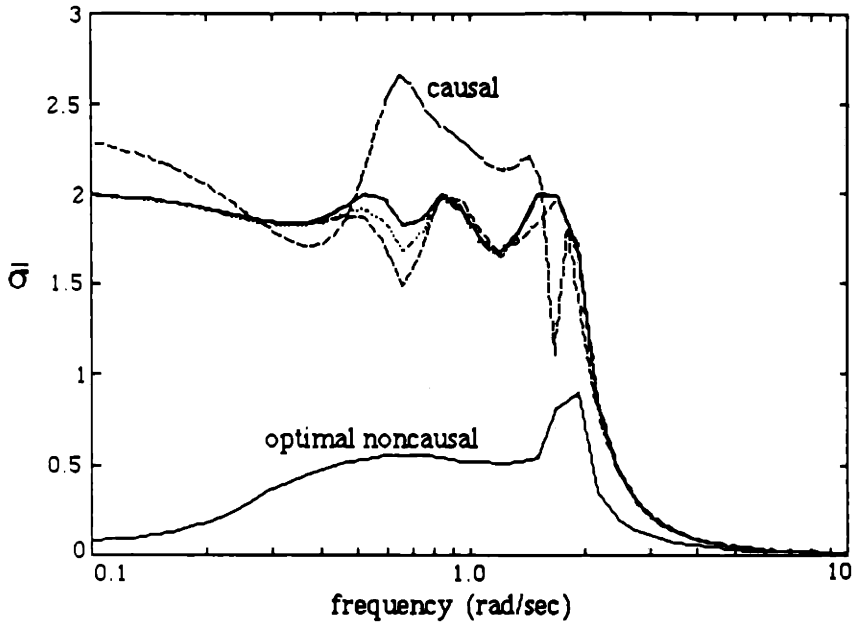

Figure 5.13 Evolution of the scaled closed-loop transfer function, $D_{nom}(T_{11}+T_{12}QT_{21})D_{nom}^{-1}$, as Q becomes causal.

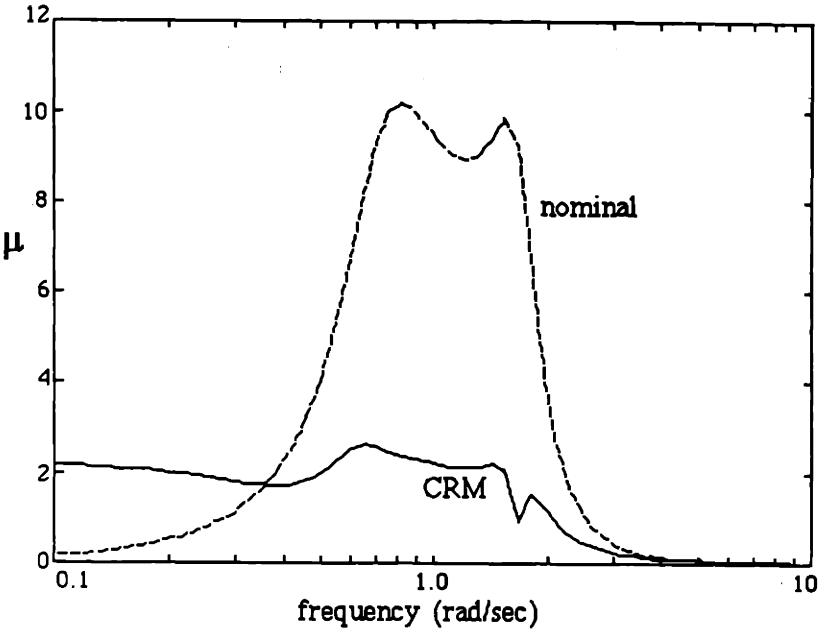

Figure 5.14 Comparison of the structured singular value frequency responses of the nominal and CRM closed-loop transfer functions.

The frequency response of the final compensator from the CRM is in Figure 5.15. The CRM response is precisely what one would have expected from a classical design method. The plant G is characterized by high gain and large phase lag due to the double integrator. This suggests a low gain lead-lag compensator. The CRM compensator is of this type with a sharp notch at the bending mode frequency.

Although the nominal compensator K_{nom} (Eqn. 5.16) has degree 8 and the stable, causal Q (Eqn. 5.19) has degree 7, the frequency response in Figure 5.15 can be approximated closely by a sixth order transfer function (see Table 5.5).

$$K = \frac{1.43s^5 + 0.89s^4 + 4.24s^3 + 2.43s^2 + 1.28s + 0.18}{s^6 + 3.83s^5 + 8.35s^4 + 13.53s^3 + 13.09s^2 + 5.41s + 1.91} \tag{5.20}$$

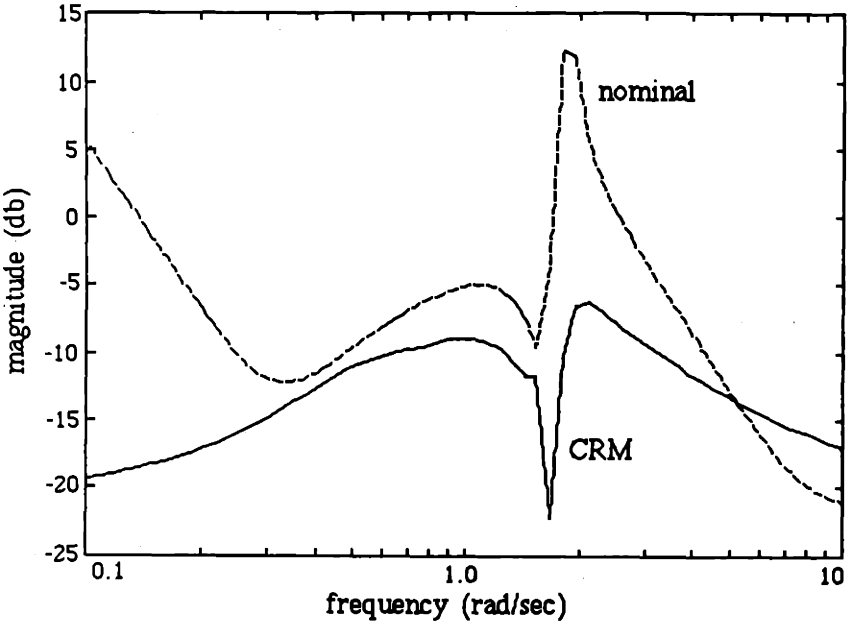

Figure 5.15 A comparison of the frequency responses of the nominal and CRM compensators.

Table 5.5: Poles and zeros of the CRM compensator for the SISO example.

Poles	Zeros
-0.19 ± 0.47j	0.0035 ± 1.62j
-0.21 ± 1.71j	-0.22 ± 0.46j
-1.51 ± 0.49j	-0.19

Several interesting comparisons can be made with K_{nom}. The CRM K is stable, whereas the nominal H_∞ compensator is unstable. In addition, K does not have any very low or very high frequency poles; however, K does have a pair of lightly damped, non-minimum phase zeros. These zeros form a notch filter, to reduce the influence of the lightly-damped bending mode, at a frequency of 1.62 radians per second. Since these zeros are so close to the imaginary axis, it is conjectured that a minimum phase compensator may also satisfy the same robust performance specification. The transfer function in Table 5.5 is the first robust, causal compensator that the CRM found; it certainly is not unique. Thus, the CRM has improved the performance-robustness of the closed-loop system by substantially lowering the compensator gain at low frequencies and adding a sharp notch at the nominal bending mode frequency.

In order to assess the merits of the CRM in familiar terms, we will interpret the above results in the context of the standard feedback configuration in Figure 5.16. The (output) sensitivity R(s) and the (input) complementary sensitivity C(s), as defined in Section 1.2.6, will be examined. In addition, the response to a step command r and a sinusoidal disturbance d will be evaluated.

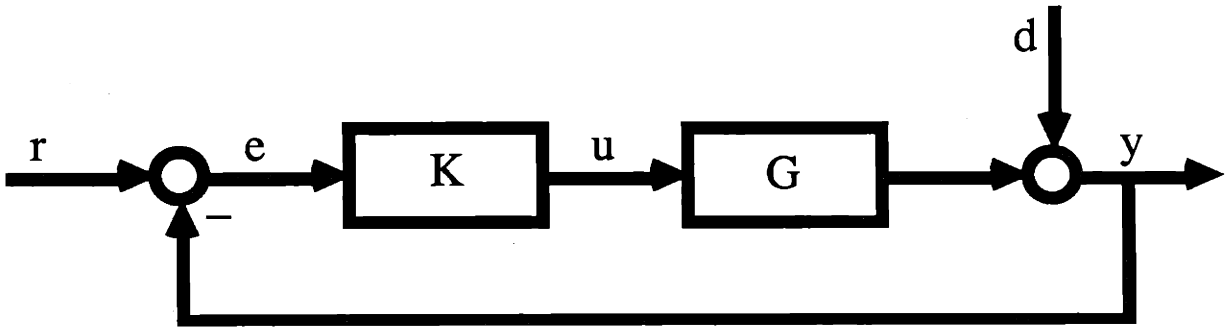

Figure 5.16 Standard feedback loop for evaluation of the compensator designs.

The primary goal of the CRM is to design a compensator and closed-loop system that exhibits robust stability and performance with respect to some given modeling error and performance specification. Therefore in order to clearly demonstrate the benefits of the CRM, the response of the closed-loop system must be evaluated with respect to not only the nominal plant G, but some *legal* perturbed plant $\tilde{G}$. $\tilde{G}$ is a member of the set of possible plants defined by the nominal plant G and the uncertainty weighting function.

To define a legal perturbation, we must first recall the condition for robust stability and performance of the closed-loop system S (see Section 3.4).

$$\| \mu(S) \|_\infty \leq 1 \tag{5.21}$$

From Figure 5.14, we see that the CRM design does not meet the condition in (5.21), with respect to the weighting functions in Eqns (5.14) and (5.15). However, the CRM design is robust (i.e. $\| \mu(S) \|_\infty \leq 1$) with respect to the original weighting functions scaled by the CRM robustness margin ($\rho = 0.38$). That is, let $W_z = 0.38W_z$ and $W_e = 0.38W_e$. This rescaling merely shifts the y-axis of Figure 5.14. Note that the nominal H_∞ design still does not exhibit performance-robustness with respect to the scaled weights. For the remainder of this example, it will be assumed that the weighting functions have been scaled such that the CRM design satisfies the condition in Eqn. (5.21).

The set of possible plants $\tilde{G}$ is

$$\tilde{G} = G[I + L'] \tag{5.22}$$

where G is defined by Eqns. (5.2) and (5.8), and $| L'(j\omega) |$ is bounded by the new (scaled) uncertainty weighting function $W_z(s)$. Then, a legal perturbation is simply

$$L' = kW_z \tag{5.23}$$

where k < 1. For this example k was chosen to be 0.8, and a plot of the frequency responses of the uncertainty weight and the selected perturbation is shown in Figure 5.17. The perturbed plant $\tilde{G}$ Bode plot is shown in Figure 5.18. Compare this Bode plot to that in Figure 5.1. Note the dynamics around 1.5 radians/second and the increased gain in the high frequency region.

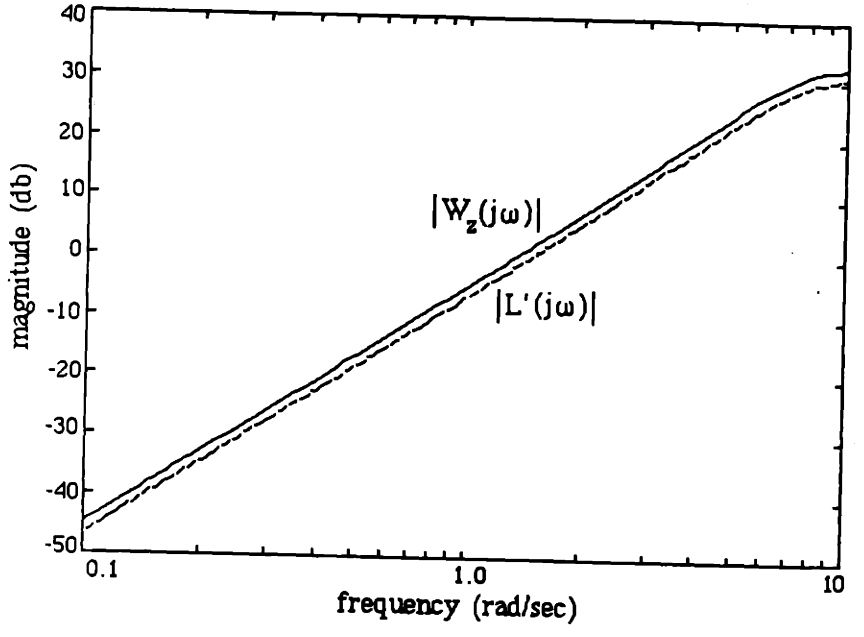

Figure 5.17 Frequency responses of the uncertainty weighting function and the multiplicative perturbation.

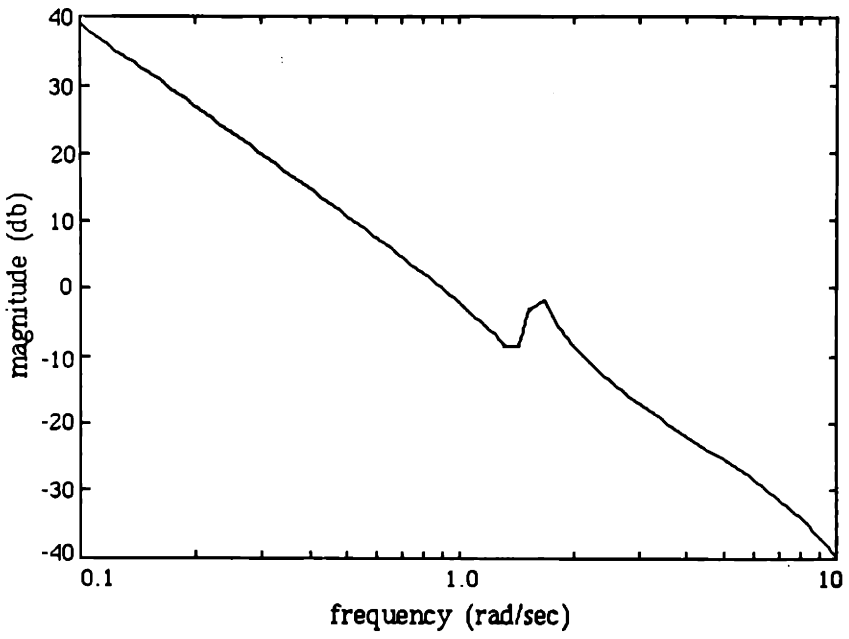

Figure 5.18 Frequency response of the perturbed plant $\tilde{G}$.

Figures 5.19 and 5.20 show the complementary sensitivity frequency responses for the plant G. The complementary sensitivity associated with the nominal (H_∞) compensator is quite poor. In fact, it does not satisfy the stability-robustness condition in Eqn. (1.20). We will see that the perturbation in Eqn. (5.23) will drive the closed-loop system, with the nominal compensator, unstable. Of course, the complementary sensitivity of the CRM design is well-behaved and satisfies the stability-robustness condition.

The complementary sensitivity responses for the perturbed plant $\tilde{G}$ are in Figures 5.21 and 5.22. As expected, the nominal (H_∞) compensator produces a terrible frequency response. The CRM design is still acceptable, and is almost insensitive to the rather large perturbation defined by Eqn. (5.23). Note that the frequency response of the uncertainty weight has been plotted for reference purposes only, and there is no significance to the fact that the response in Figure 5.21 violates the stability-robustness condition.

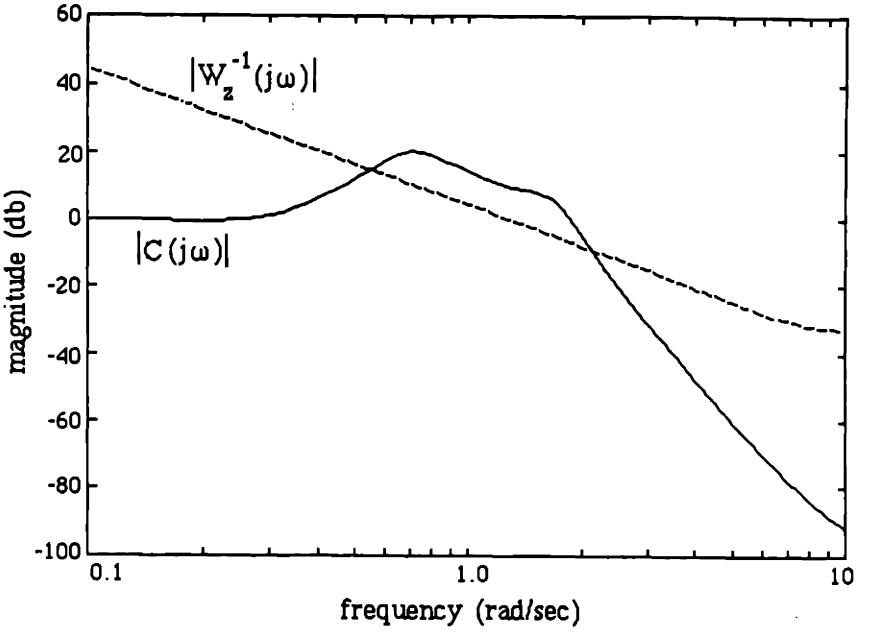

Figure 5.19 The frequency response of the complementary sensitivity function with plant G and the nominal compensator.

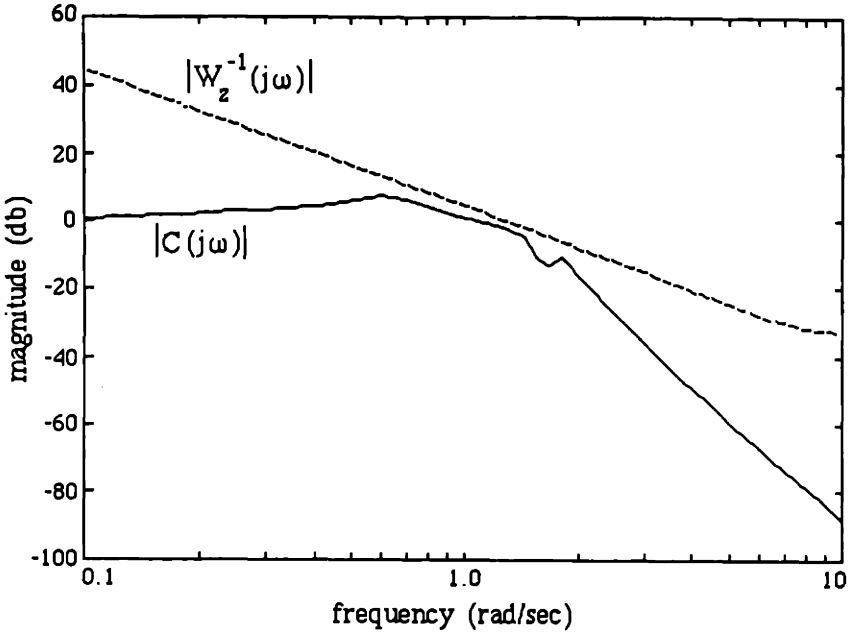

Figure 5.20 The frequency response of the complementary sensitivity function with plant G and the CRM compensator.

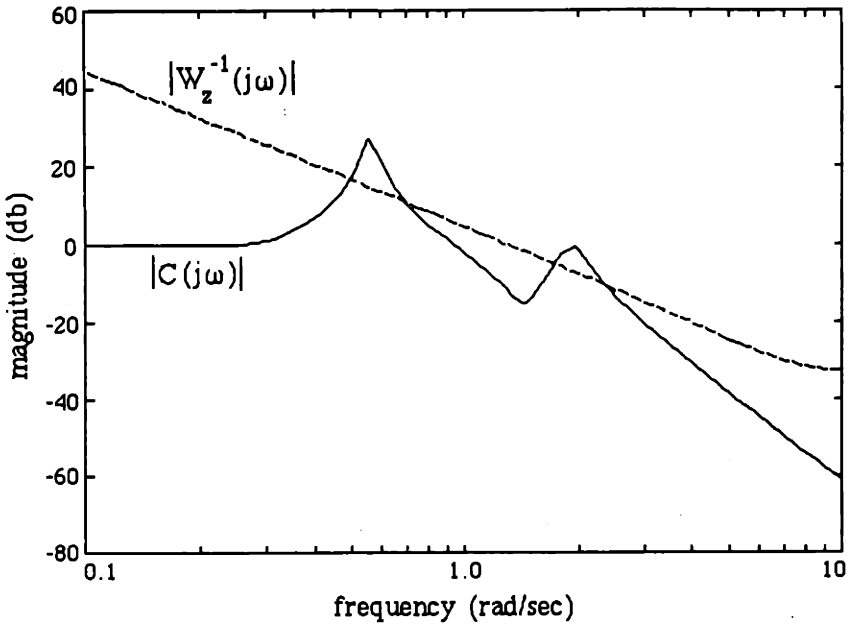

Figure 5.21 The frequency response of the complementary sensitivity function with perturbed plant $\tilde{G}$ and the nominal compensator.

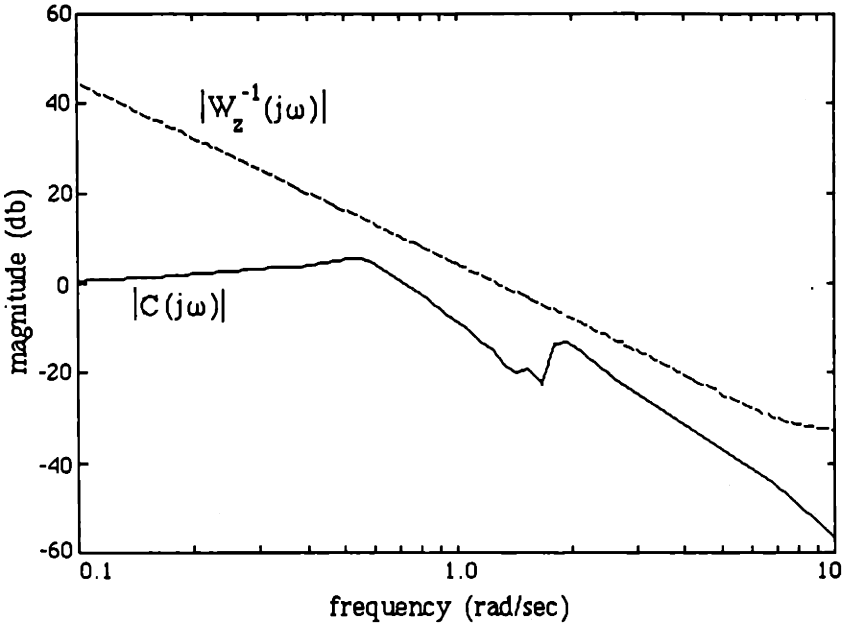

Figure 5.22 The frequency response of the complementary sensitivity function with perturbed plant $\tilde{G}$ and the CRM compensator.

Figures 5.23 through 5.26 show the frequency response of the sensitivity function and the inverse of the performance weight. The nominal compensator violates the performance specification (Eqn. 1.21) in both cases (i.e. for plants G and $\tilde{G}$). The CRM design, on the other hand, meets the specification for either plant, and the sensitivity is almost unaffected by the perturbation. Note that the H_∞ design does exhibit better sensitivity at low frequencies.

The output (y) responses to a unit step reference command (r) are shown in Figures 5.27 through 5.30. The step response of the closed-loop system with plant G and the nominal compensator is highly oscillatory. While the step response of the CRM design with the nominal plant G is oscillatory (Figure 5.28), it is far better than the H_∞ design. When the perturbed plant is in the feedback loop with the nominal compensator, an unstable system results (Figure 5.29). On the other hand, the step response of the CRM compensator with the perturbed plant $\tilde{G}$ (Figure 5.30) appears to be slightly better than that with the nominal plant G (i.e. there is slightly less overshoot). It is clear that the large amount of modeling error, as defined by W_z, severely limits the performance of the H_∞ design. This suggests that the (unscaled) four-block H_∞ problem is not particularly well-suited for solving the robust performance problem, at least in this case.

For completeness, the output (y) response to an additive output disturbance (d) at a frequency of 0.1 radians/second is included in Figures 5.31 through 5.34. As the sensitivity function indicated (Figure 5.23), the disturbance-rejection of the H_∞ design with the nominal plant is quite good, and better than that of the CRM design at a frequency of 0.1 radians/second (Figure 5.32). Figure 5.33 dramatically illustrates the effect of a legal perturbation on the nominal design. Again, the response of the CRM design in Figure 5.34 is insensitive to the perturbation.

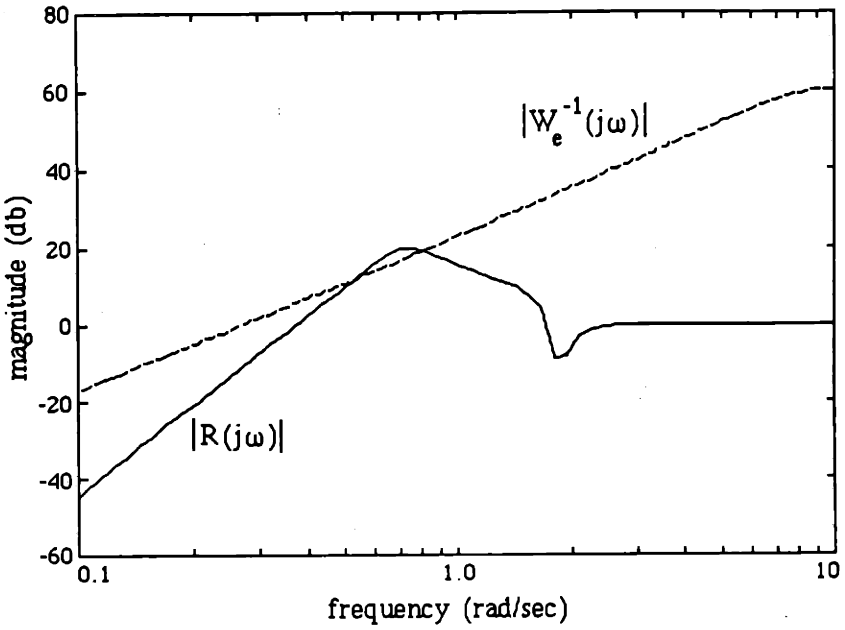

Figure 5.23 The frequency response of the sensitivity function with plant G and the nominal compensator.

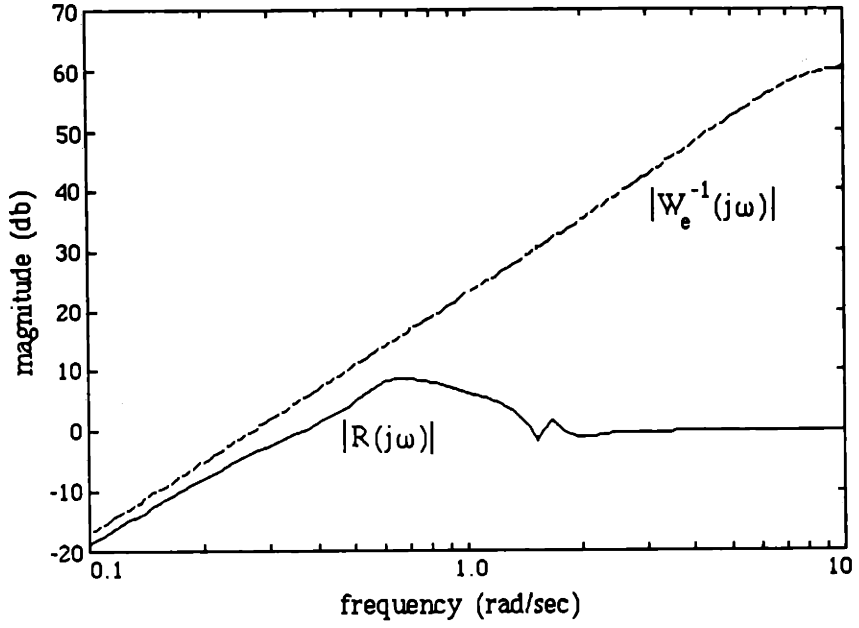

Figure 5.24 The frequency response of the sensitivity function with plant G and the CRM compensator.

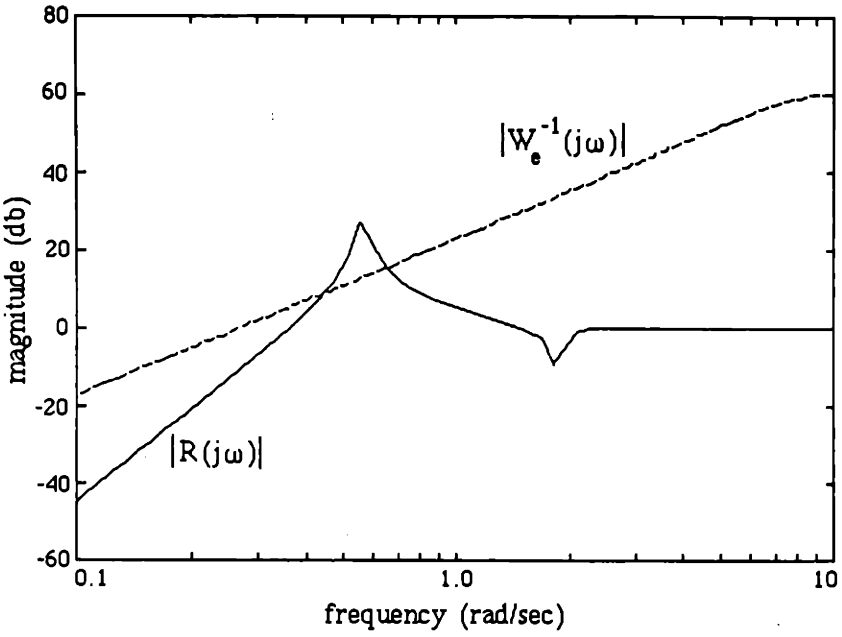

Figure 5.25 The frequency response of the sensitivity function with perturbed plant $\tilde{G}$ and the nominal compensator.

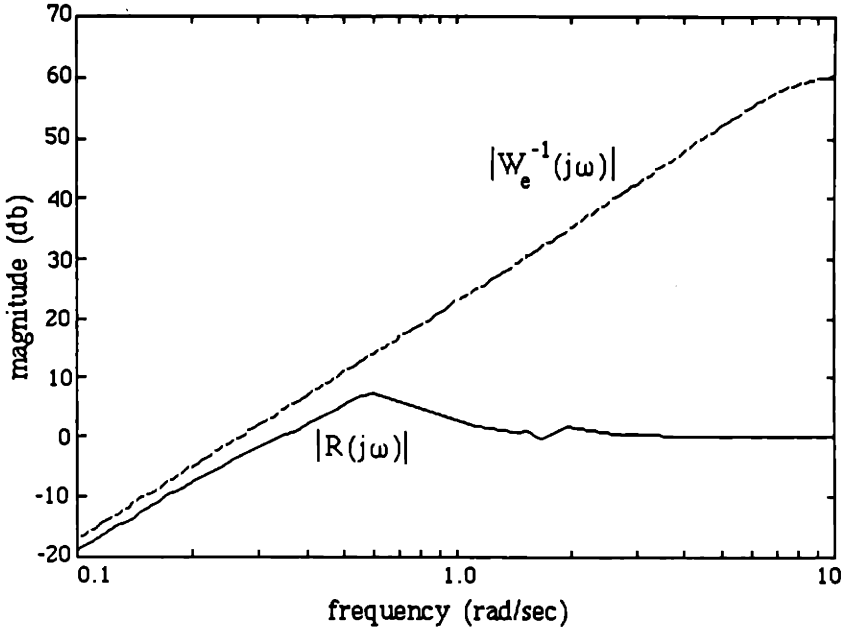

Figure 5.26 The frequency response of the sensitivity function with perturbed plant $\tilde{G}$ and the CRM compensator.

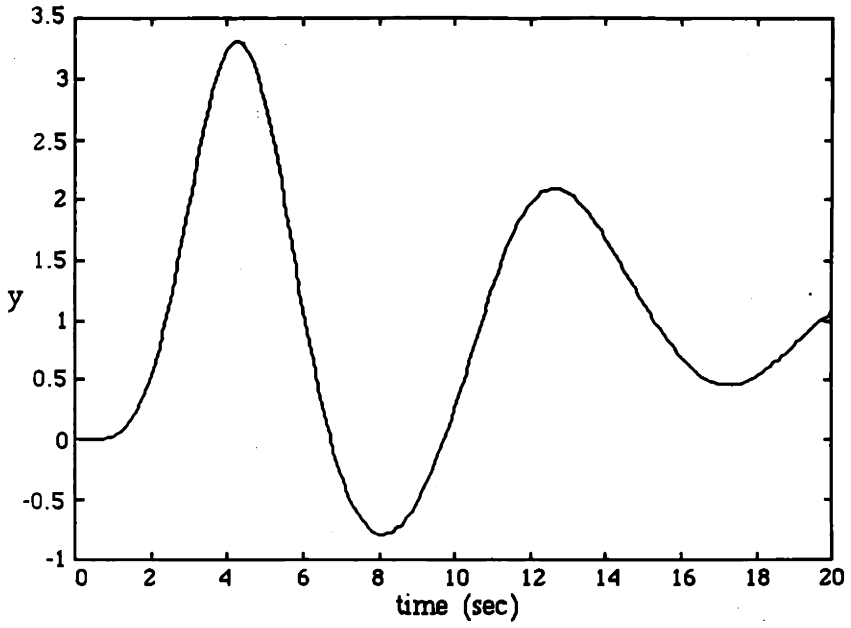

Figure 5.27 The step response of the closed-loop system with plant G and the nominal compensator.

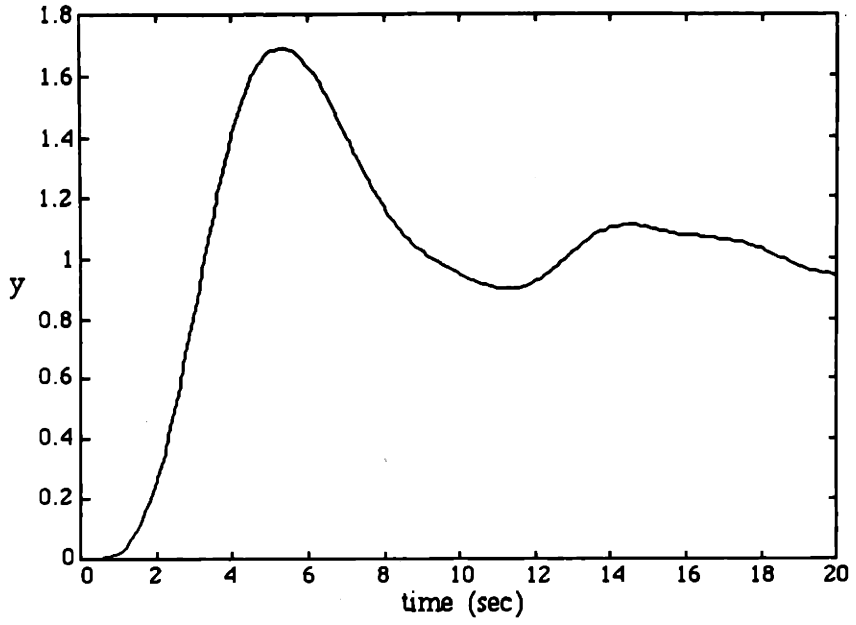

Figure 5.28 The step response of the closed-loop system with plant G and the CRM compensator.

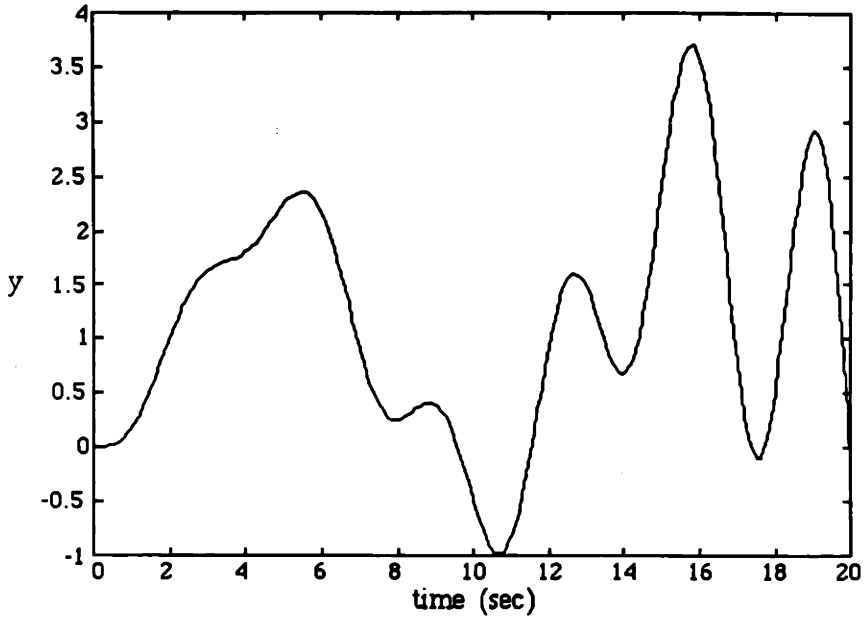

Figure 5.29 The step response of the closed-loop system with perturbed plant $\tilde{G}$ and the nominal compensator.

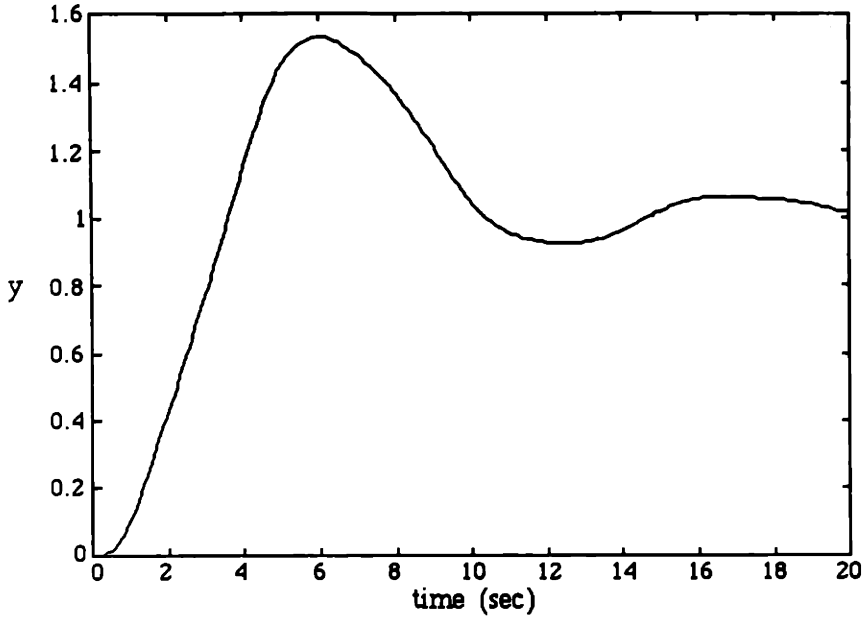

Figure 5.30 The step response of the closed-loop system with perturbed plant $\tilde{G}$ and the CRM compensator.

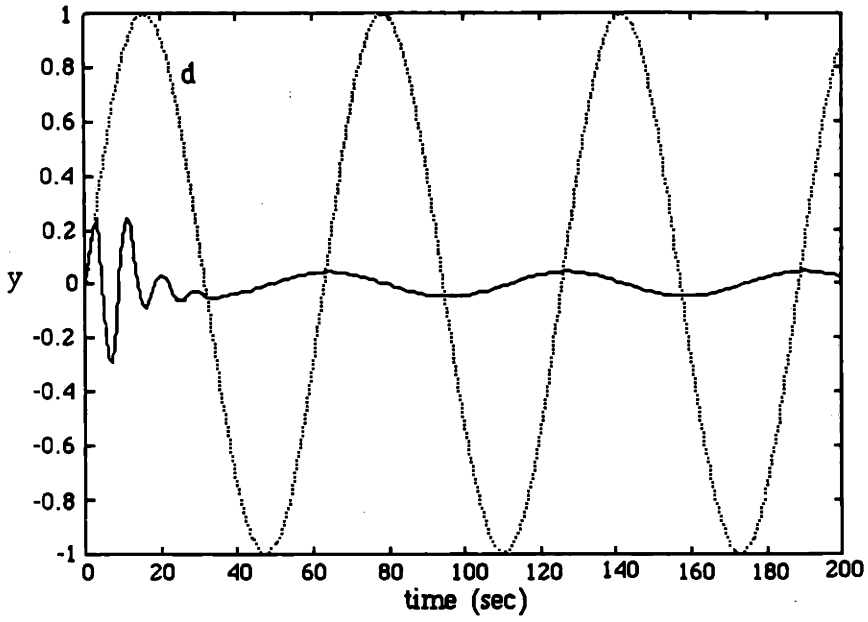

Figure 5.31 The output response to a disturbance d = sin(0.1t) of the closed-loop system with plant G and the nominal compensator.

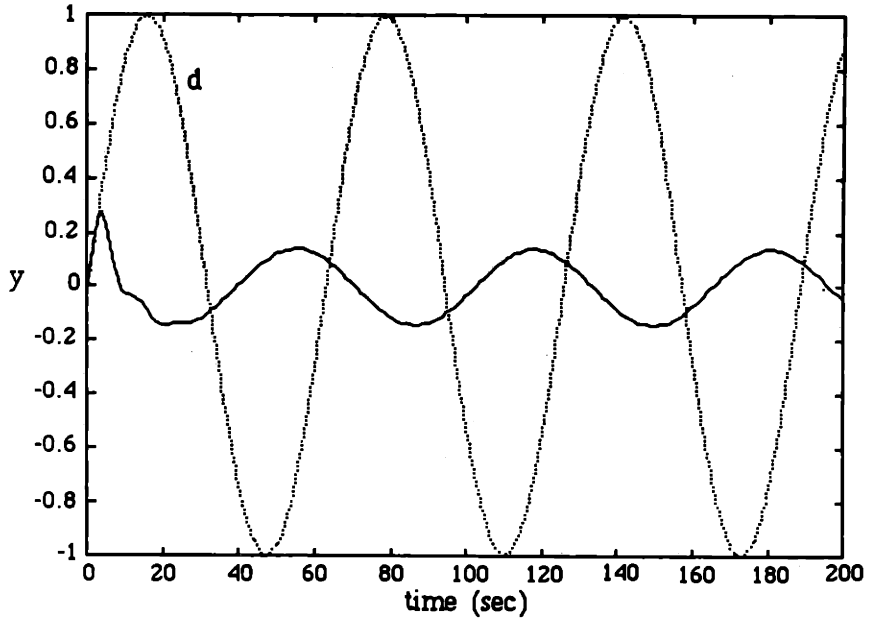

Figure 5.32 The output response to a disturbance d = sin(0.1t) of the closed-loop system with plant G and the CRM compensator.

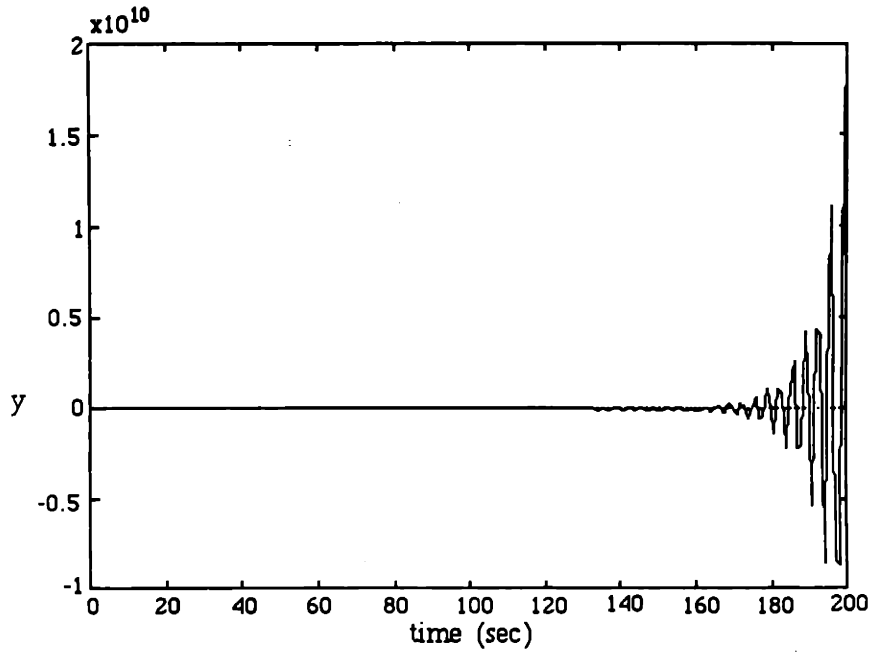

Figure 5.33 The output response to a disturbance d = sin(0.1t) of the closed-loop system with perturbed plant $\tilde{G}$ and the nominal compensator.

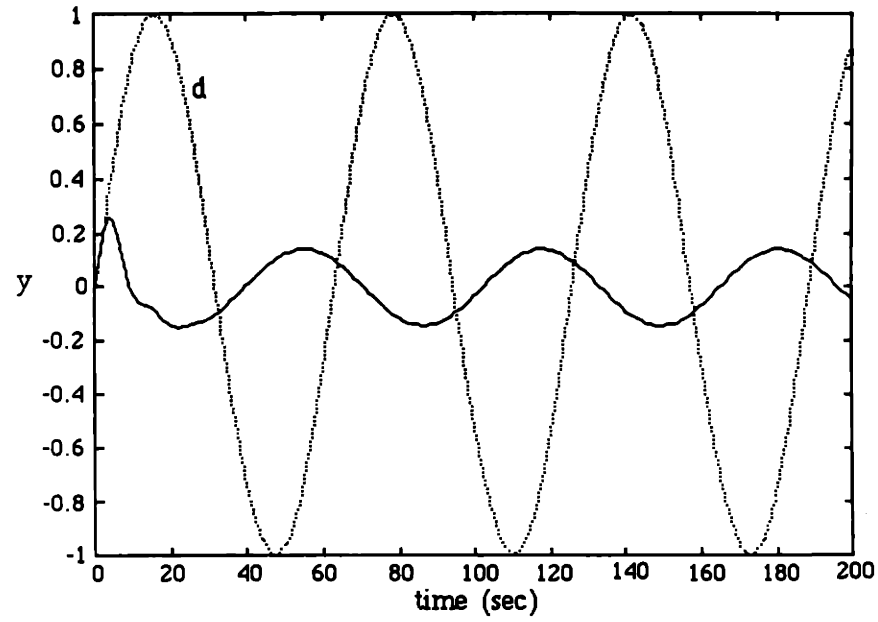

Figure 5.34 The output response to a disturbance d = sin(0.1t) of the closed-loop system with perturbed plant $\tilde{G}$ and the CRM compensator.

This example demonstrates how the CRM starts with a nominally stabilizing design and improves the performance-robustness of the closed-loop system. In fact, the CRM design was fairly insenstive to the large perturbation used in the example. That is, the closed-loop response did not vary significantly even with substantially different plants in the feedback loop.

There are significant costs associated with the performance improvement, however. Running on a MicroVAX II workstation, the causality recovery process took approximately 8 hours (in batch mode). Six hundred million floating point operations were performed, as computed by the software package PRO-MATLAB. An issue that will not be discussed further is whether the performance benefits of the CRM outweigh the computational costs.

5.3 MIMO Case: A Benchmark for μ-Synthesis

The example discussed in this section is a multivariable system created by G. Stein [48]. It is an academic problem of very simple structure; however, it turns out to be a challenge for μ-synthesis, and local minima have been achieved. Thus, this simple example is quite rich and may serve as a useful benchmark for the robust performance problem. Again, this example should be thought of in terms of the conventional feedback framework in Section 1.2.6.

The nominal plant is

$$G(s) = \frac{1}{s}\begin{bmatrix} a & 0 \\ 0 & a^{-1} \end{bmatrix} \tag{5.24}$$

The condition number of G is a^2. A poorly conditioned plant may limit the performance of a feedback system, and some type of μ-synthesis method should prove useful in achieving

adequate performance and robustness. For a = 5 the singular values of G are shown in Figure 5.35.

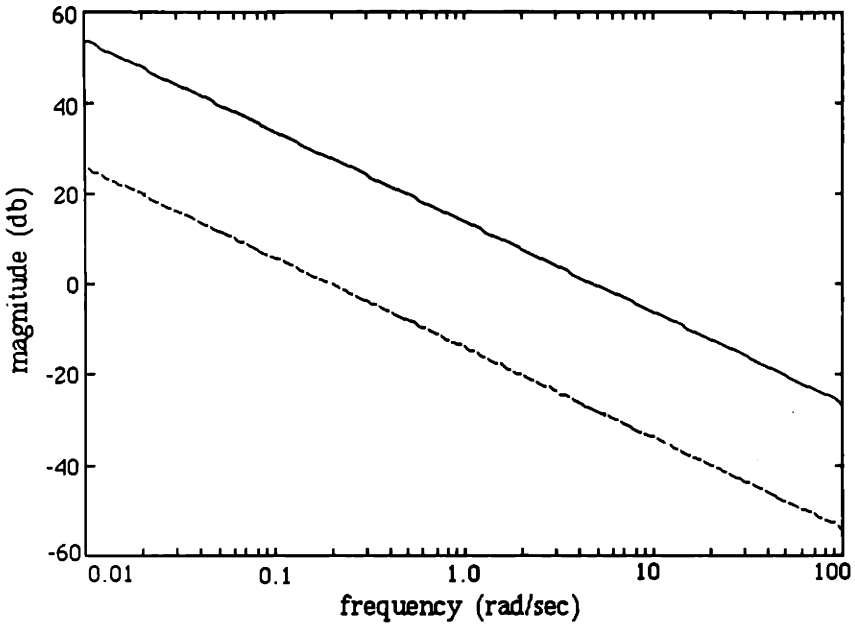

Figure 5.35 The frequency response of the singular values of the plant G for the MIMO example.

There are modeling errors associated with the nominal plant in Eqn. (5.24) This uncertainty will be described by a multiplicative perturbation at the plant input. The perturbed plant is then

$$\tilde{G} = G[I + L] \tag{5.25}$$

The bound on the multiplicative error L is given in the problem statement as

$$W_z(s) = 0.5(s+1)\frac{1000}{s+1000}\begin{bmatrix}1 & 0\\ 0 & 1\end{bmatrix} \qquad (5.26)$$

The singular values of W_z are shown in Figure 5.36. The two singular values are equal because of the simple structure of the transfer function matrix. The modeling error is relatively small at low frequencies and rises with increasing frequency. The high-frequency pole in Eqn. (5.26) was added to make the transfer function matrix proper.

After examining Eqns. (5.24) and (5.26), one may conclude that the system is decoupled and can be treated as two SISO problems. This is not the case, however. The diagonal uncertainty weight merely provides a bound on the *singular values* of the multiplicative perturbation; a legal perturbation may be a full transfer function matrix. In such a case, the perturbed plant $\tilde{G}$ would be coupled. *Thus, this problem is truly multivariable in nature and may not be treated as two SISO designs.* In the sequel, we will evaluate the performance of the CRM design with one of these coupled plants.

The weighting function on performance was chosen to provide a cross-over gap with respect to the uncertainty weight in Eqn. (5.26).

$$W_e(s) = \frac{0.5(s+1)}{s}\frac{1000}{s+1000}\begin{bmatrix}1 & 0\\ 0 & 1\end{bmatrix} \qquad (5.27)$$

The high-frequency pole was added to make the transfer function matrix strictly proper, as required by the H_∞ design procedure in Section 4.2.1. The singular values of the performance weighting function are shown in Figure 5.36. Again, the two singular values

are equal because of the structure in Eqn. (5.27).

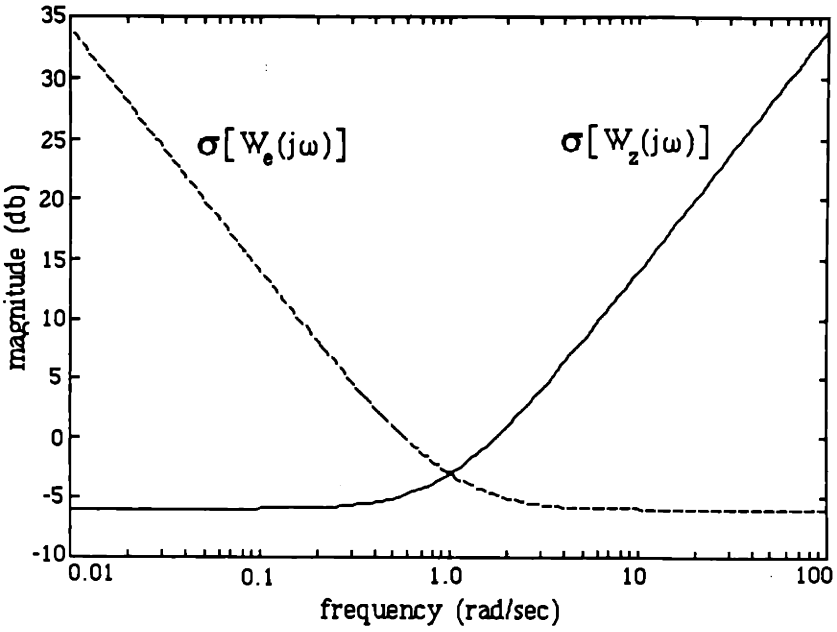

Figure 5.36 The singular values of the uncertainty and performance weighting functions for the MIMO example.

The plant G and the weighting functions W_e and W_z define the design plant model P, according to Eqn. (1.27). Two preliminary designs were performed for this example: an H_∞ and a nonconverged DK iteration. The Doyle/Glover γ-iteration in Section 4.2.1 was used to compute the H_∞ compensator. This produced a minimum $\gamma = 1.91$, and the diagonal compensator (Eqn. 5.28 and Table 5.6) shown in Figure 5.37. The frequency responses of the largest singular value and the structured singular value of the closed-loop transfer function $S = F_l(P, K)$ are plotted in Figure 5.38. The robustness margin of this design is $\rho = 0.52$.

$$K = \begin{bmatrix} \dfrac{6s^3 + 2760s^2 + 388660s + 235242}{s^4 + 654s^3 + 110577s^2 + 864864s + 865} & 0 \\ 0 & \dfrac{1.2s^3 + 1193s^2 + 387134s + 47217}{s^4 + 647s^3 + 106338s^2 + 173677s + 174} \end{bmatrix} \quad (5.28)$$

Table 5.6: Poles and zeros of the H_∞ compensator for the MIMO example.

	Poles	Zeros
K_{11}	-0.001	-0.61
	-8.21	-230 ± 108j
	-323 ± 33.1j	
K_{22}	-0.001	-0.12
	-1.65	-478 ± 286j
	-323 ± 33.1j	

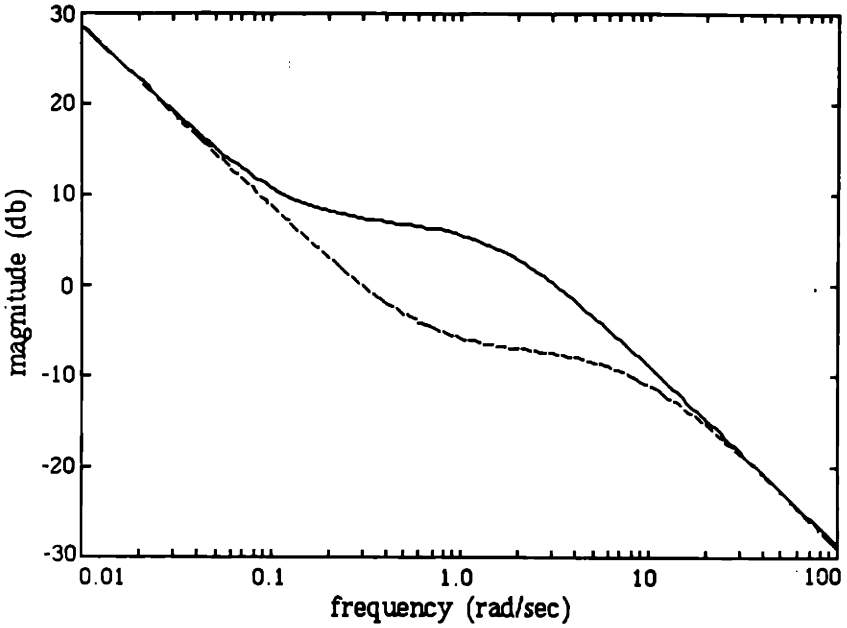

Figure 5.37 The singular values of the H_∞ compensator for the MIMO example.

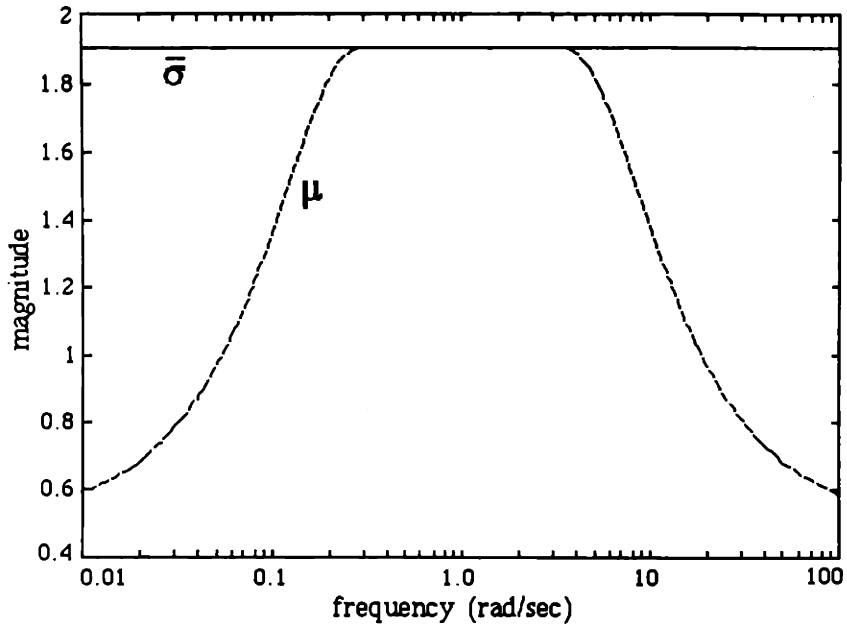

Figure 5.38 Characteristics of the closed-loop transfer function for the H_∞ design.

The second compensator was computed by Stein [48]. The design, which represents the best compensator available in June 1987, is an intermediate result of the DK iteration. The singular values of this diagonal compensator are shown in Figure 5.39, and the characteristics of the associated closed-loop transfer function $S = F_l(P, K)$ are shown in the following figure. The structured singular value response is all-pass with a robustness bound $\gamma = 1.64$ and a robustness margin $\rho = 0.61$. Comparing Figures 5.38 and 5.40 we see that the second design ($\rho = 0.61$) is superior to the H_∞ design ($\rho = 0.52$) in terms of performance-robustness.

The (nonconverged) DK iteration compensator was chosen to be the nominal design for the reason just cited. It is a diagonal, proper system whose singular values are matched at high and low frequencies.

$$K_{nom} = \begin{bmatrix} \dfrac{0.45s^2 + 0.70s + 0.54}{s^2 + 0.70s + 0.25} & 0 \\ 0 & \dfrac{0.45s^2 + 1.30s + 1.85}{s^2 + 1.30s + 0.84} \end{bmatrix} \tag{5.29}$$

The poles and zeros of each element of K_{nom} are listed in Table 5.7. The D scaling associated with this design is given in Figure 5.41.

Table 5.7: Poles and zeros of the nominal compensator K_{nom} for the MIMO example.

	Poles	Zeros
K_{11}	$-0.35 \pm 0.35j$	$-0.77 \pm 0.77j$
K_{22}	$-0.65 \pm 0.65j$	$-1.43 \pm 1.43j$

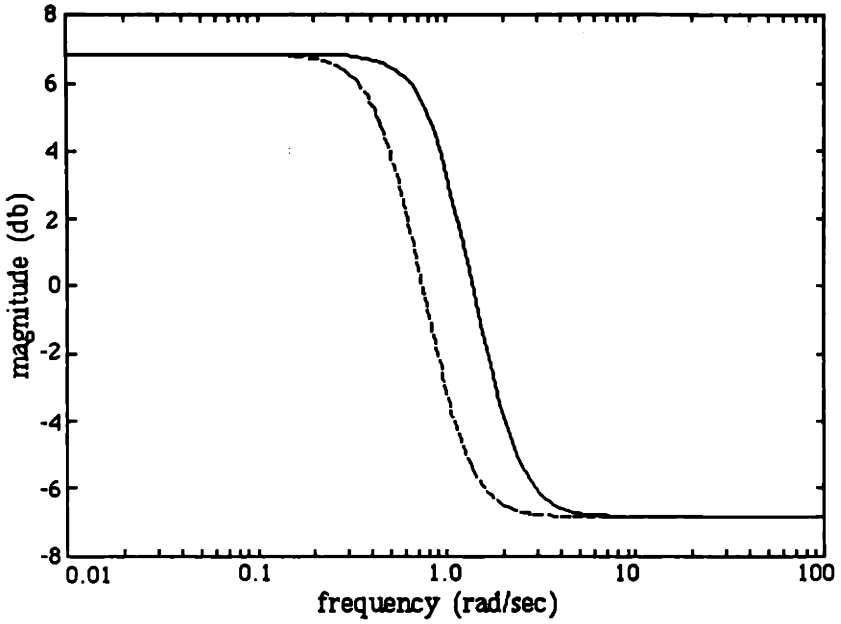

Figure 5.39 The frequency response of the singular values of the (nonconverged) DK compensator.

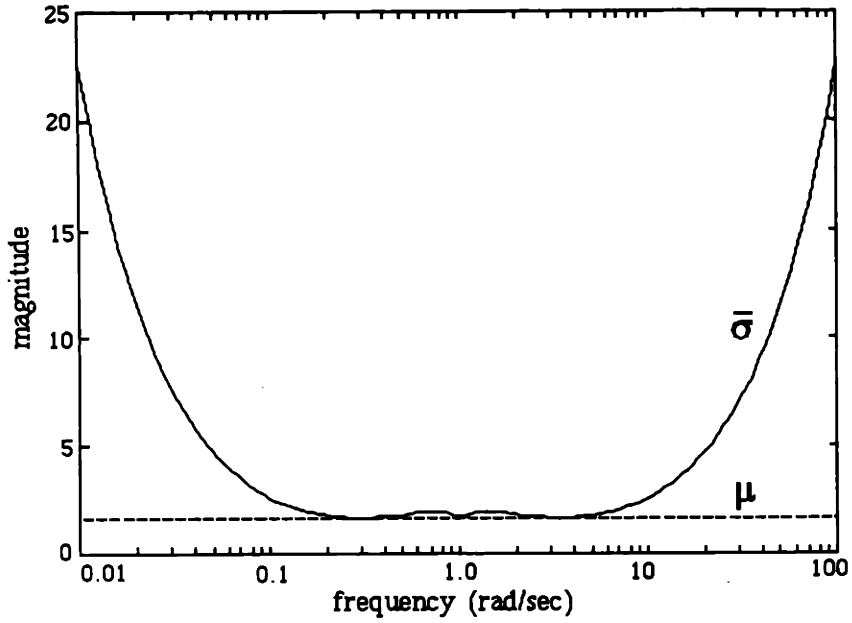

Figure 5.40 Characteristics of the closed-loop transfer function matrix for the (nonconverged) DK design.

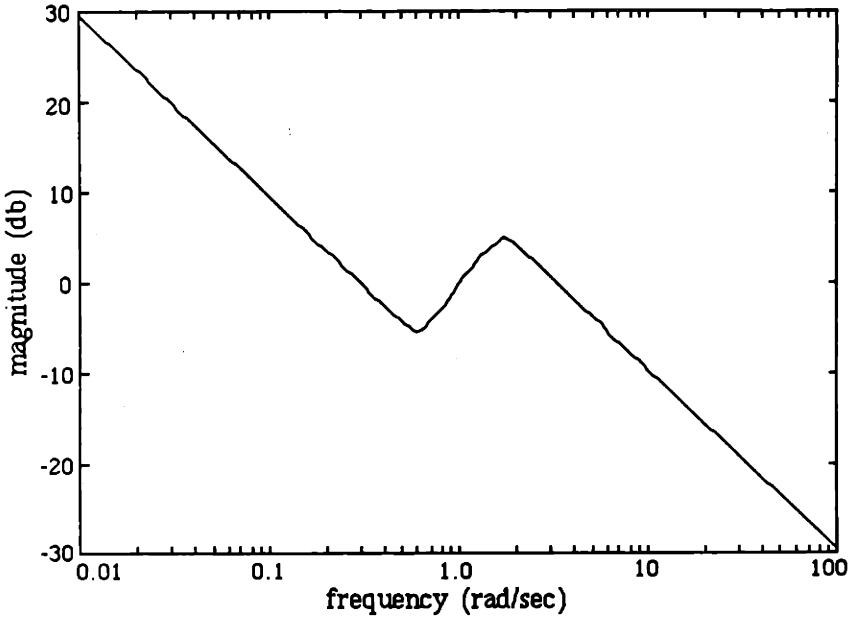

Figure 5.41 The frequency response of the scaling D_{nom}.

With the nominal system defined by Eqn. (5.29), the CRM is started. The Youla parameterization produces the set of internally stable transfer function matrices S that are affine in the free parameter Q (Eqn 5.17).

The optimal parameter Q^* was computed, according to Eqn. (4.55), at 80 frequency points over the range from 0.01 to 100 radians/second. Not surprisingly, Q^* is diagonal. An eleventh-order least-squares fit was performed to find a rational approximation $\overline{Q^*}$. The result is

$$\overline{Q^*_{11}} = \frac{-0.45s^6 - 4.24s^5 - 9.40s^4 + 2.32s^3 - 3.38s^2 - 1.08s - 0.26}{s^6 - 0.025s^5 - 0.52s^4 - 1.51s^3 + 0.96s^2 - 0.98s - 1.90} \qquad (5.30)$$

$$\overline{Q^*_{22}} = \frac{-0.005s^5 - 0.21s^4 + 1.11s^3 + 1.62s^2 + 0.29s + 0.017}{s^5 - 0.55s^4 + 0.35s^3 - 0.34s^2 + 0.31s + 0.037} \tag{5.31}$$

The frequency responses of the diagonal elements of Q^* and $\overline{Q}^*$ are shown in Figures 5.42 through 5.45. The "x's" represent the complex value of Q_{ii}^* at a specific frequency. Note that there is "numerical noise" at low gains (see Figures 5.43 and 5.45). The poles and zeros of $\overline{Q}^*$ are listed in Table 5.8. The Hankel norm of $\overline{Q}^*_{11}$ is 1.27, and the Hankel norm of $\overline{Q}^*_{22}$ is 1.20. The singular values of the diagonal, noncausal compensator associated with $\overline{Q}^*$ are shown in Figure 5.46.

Table 5.8: Poles and zeros of $\overline{Q}^*$ for the MIMO example.

	Poles	Zeros
$\overline{Q}^*_{11}$	-0.86 ± 1.03j	-0.15 ± 0.19j
	0.54 ± 0.85j	0.32 ± 0.56j
	-0.74	-4.86 ± 0.39j
	1.41	
$\overline{Q}^*_{22}$	-0.30 ± 0.71j	-0.10 ± 0.05j
	0.63 ± 0.45j	-1.02
	-0.11	5.82
		-48.3

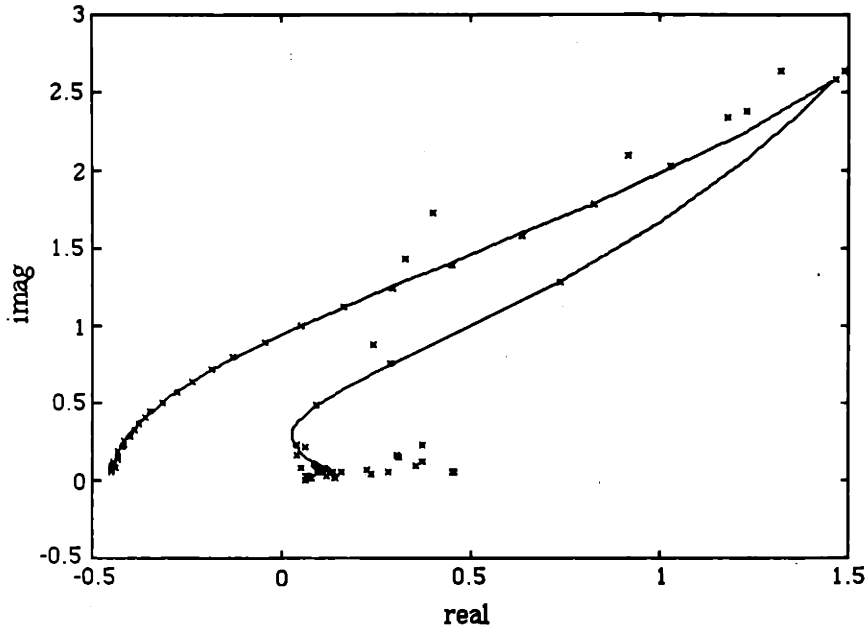

Figure 5.42 Nyquist plot of Q_{11}^* and its rational approximation $\overline{Q}_{11}^*$.

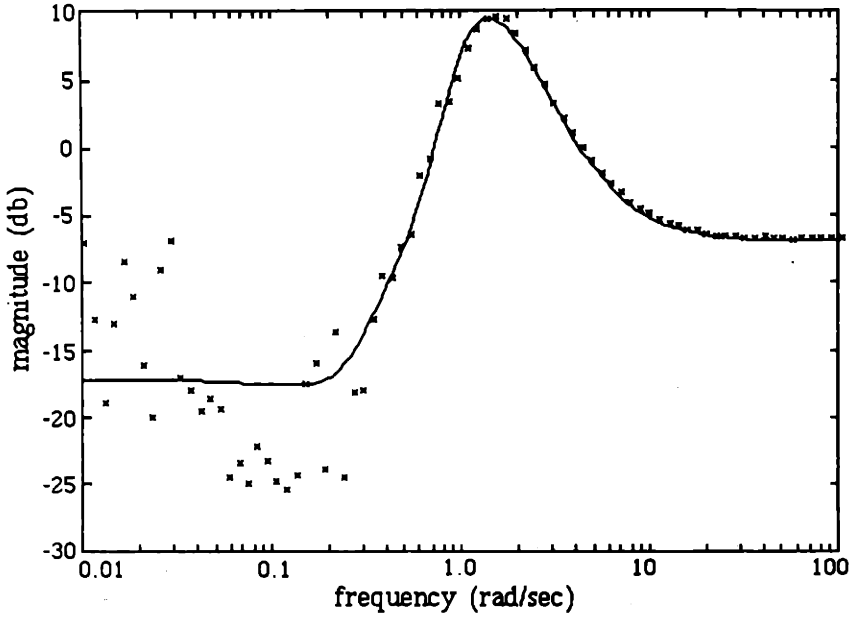

Figure 5.43 Bode plot of Q_{11}^* and its rational approximation $\overline{Q}_{11}^*$.

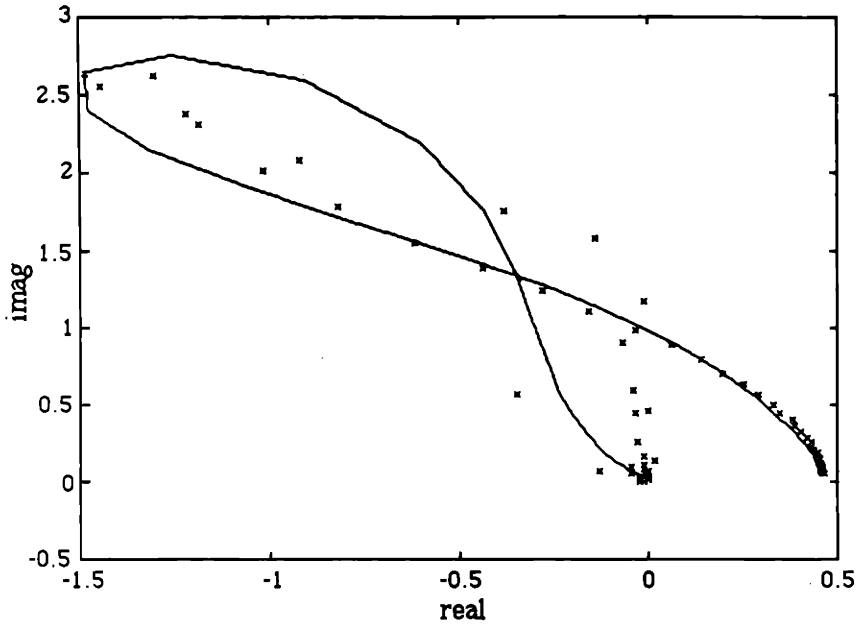

Figure 5.44 Nyquist plot of Q_{22}^* and its rational approximation $\overline{Q}_{22}^*$.

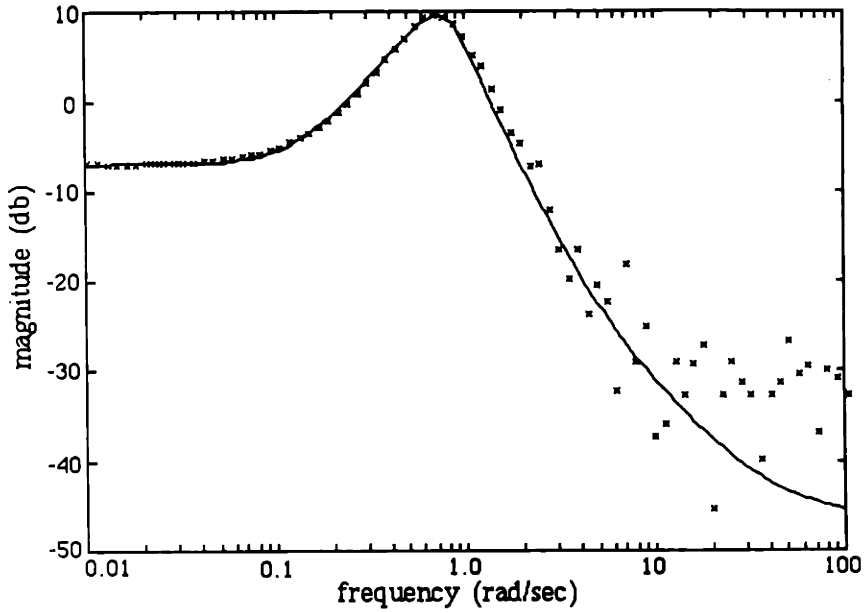

Figure 5.45 Bode plot of Q_{22}^* and its rational approximation $\overline{Q}_{22}^*$.

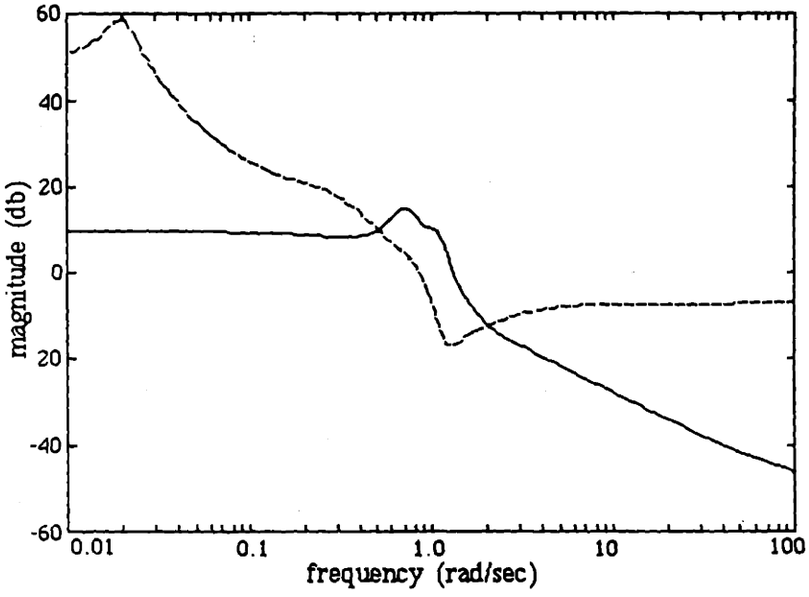

Figure 5.46 The frequency response of the singular values of the noncausal compensator resulting from $\overline{Q}^*$.

The largest singular value responses of the optimal noncausal closed-loop function and its rational approximation, $T_{11}+T_{12}\overline{Q}^*T_{21}$, are plotted in Figure 5.47. The robustness bound is $\overline{\gamma}^* = 0.91$, and the robustness margin is $\overline{\rho}^* = 1.10$.

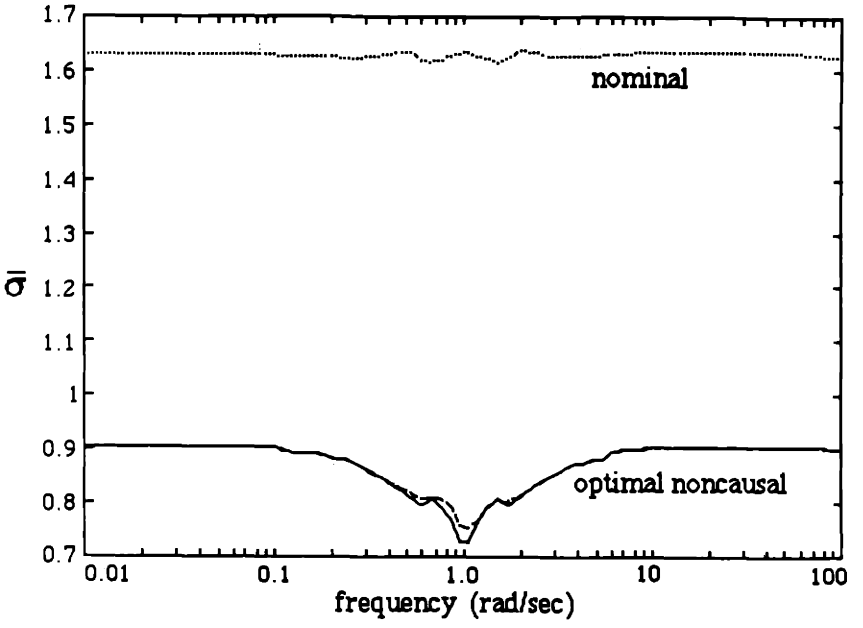

Figure 5.47 Frequency response of the scaled closed-loop transfer function matrix, $D_{nom}(T_{11}+T_{12}QT_{21})D_{nom}^{-1}$, for $Q = 0$ (nominal), $Q = Q^*$ (optimal noncausal), and $Q = \overline{Q}^*$ (rational approximation).

The next step is to find a stable, causal Q, using the causality recovery algorithm in Section 4.6, that improves the robustness of the nominal system ($\rho_{nom} = 0.61$). For computational reasons (speed and numerical), the parameter ε_2 was set to a large value. This effectively removed the inner loop from the algorithm, i.e. the loop that increases the order of the Q parameter. Thus, the order of the Q parameter remained fixed at the order of $\overline{Q}^*$ throughout the causality recovery process, and the only way to reduce the Hankel norm was to relax the robustness specification γ.

Remark The large value of ε_2 will not affect the ability of the algorithm to find a stable, causal solution. According to Theorem 4.9, we can always construct a sequence of functions of fixed McMillan degree such that the associated Hankel norm sequence approaches zero and the *nominal* performance specification is satisfied. However, the amount of performance improvement (over the nominal design) may be reduced.

It should be mentioned that this example was also run with ε_2 set to a small value (0.1). The resulting increase in the order of the Q parameter produced a tremendous computaional burden (i.e. the program ran for approximately 6 days on the MicroVAX and still had not found a causal solution). In addition, it appeared that no noticeable improvement in performance was going to be obtained.

For $\varepsilon_1 = 0.01$ and $\beta = 0.4$, the causality recovery algorithm produced the sequence of Hankel norms shown in Figure 5.48. Figure 5.49 contains the relaxation of the robustness specification γ that was needed to reduce the Hankel norm. The frequency response of the Q parameter evolution, as γ was increased, is documented in Figures 5.50 through 5.53. Each frequency response function represents a Q parameter that minimizes the Hankel norm over a feasible set defined by γ (the order of Q is fixed at 11). Figures 5.50 through 5.53 illustrate how the frequency response of the Q parameter is adjusted to reduce its Hankel norm, subject to the constraint imposed by the feasible set.

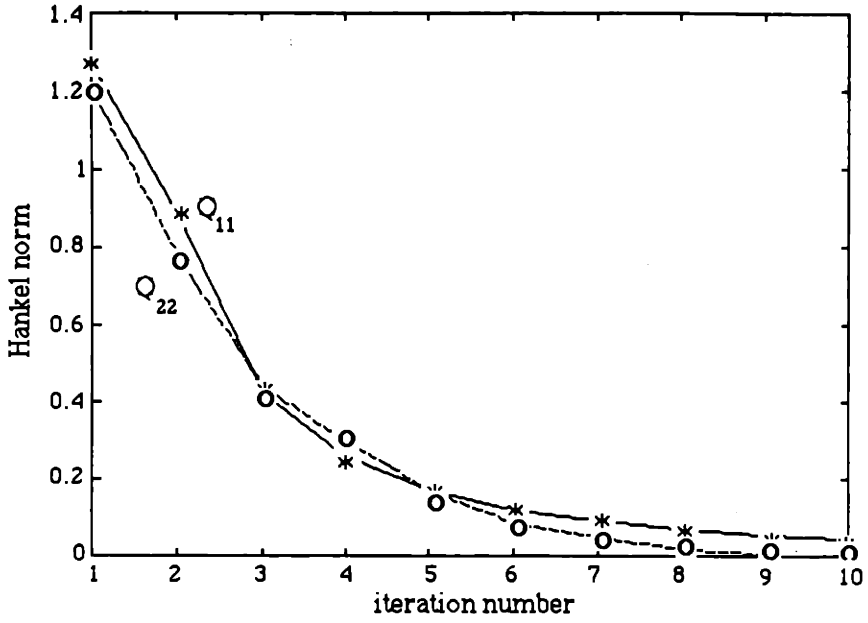

Figure 5.48 Hankel norm sequence generated by the causality recovery process.

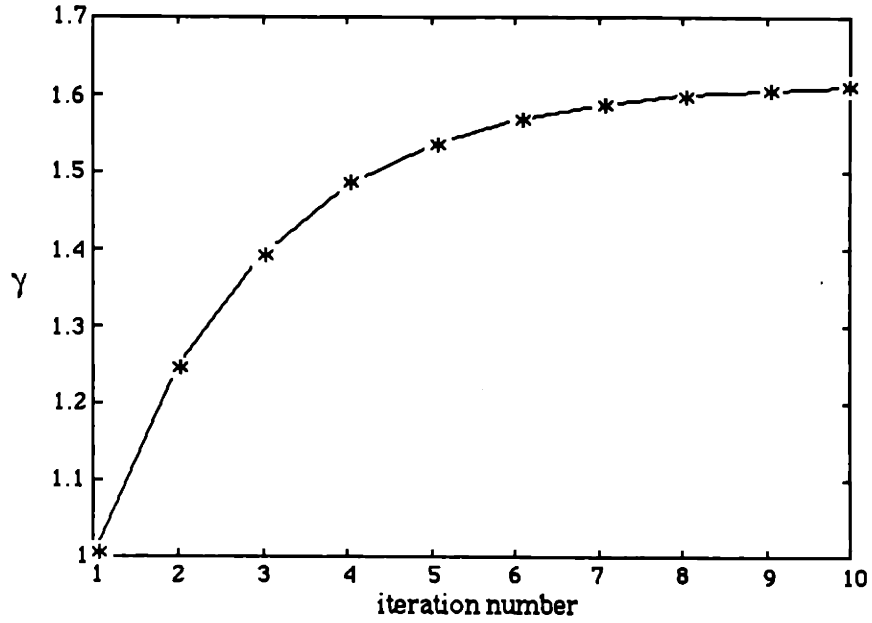

Figure 5.49 Robustness specification sequence for the causality recovery process.

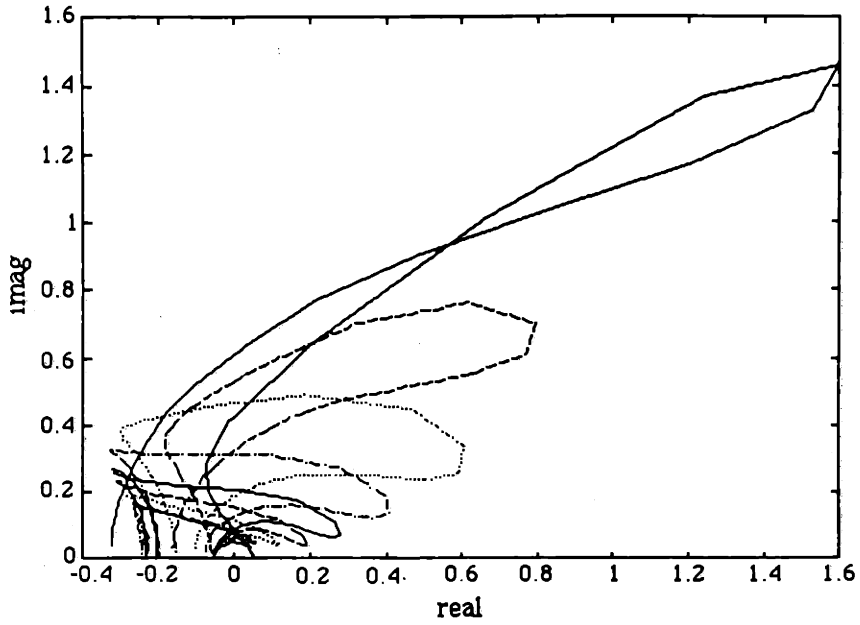

Figure 5.50 Nyquist plot of the Q_{11} parameter evolution from causality recovery.

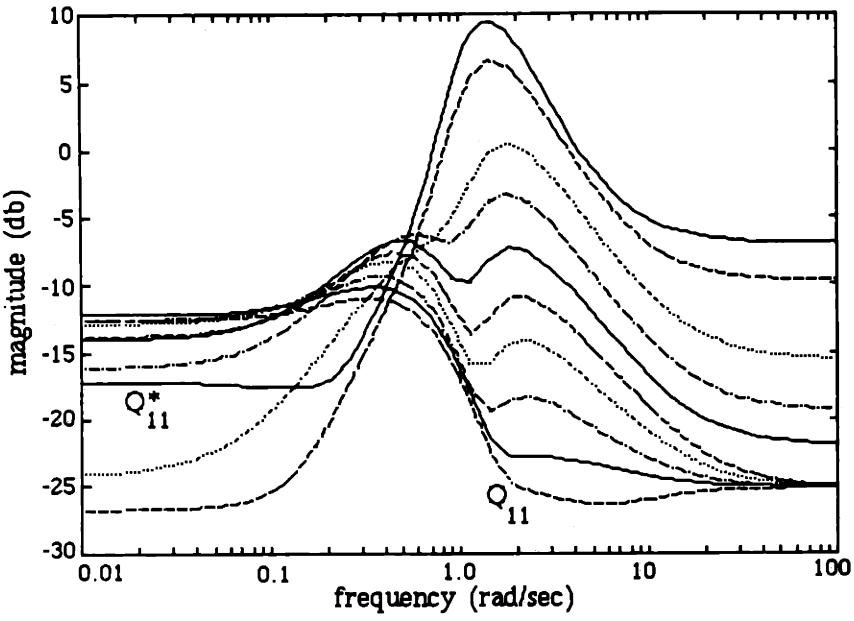

Figure 5.51 Bode plot of the Q_{11} parameter evolution from causality recovery.

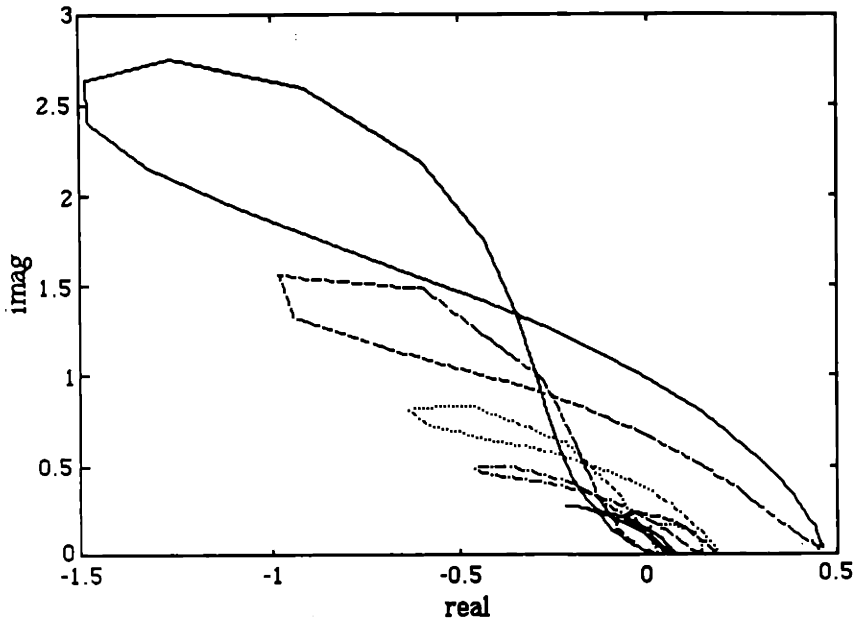

Figure 5.52 Nyquist plot of the Q_{22} parameter evolution from causality recovery.

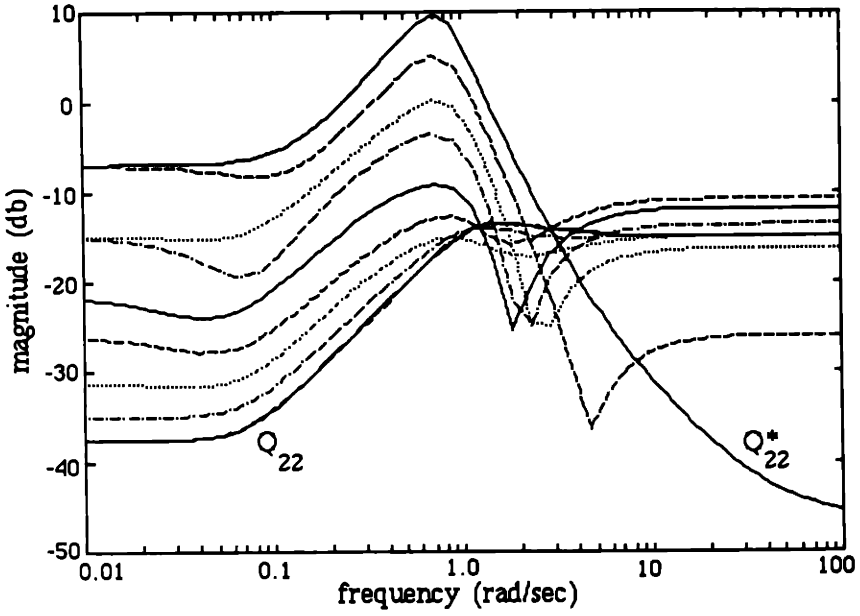

Figure 5.53 Bode plot of the Q_{22} parameter evolution from causality recovery.

The progress of the scaled closed-loop transfer function matrix, $D_{nom}(T_{11}+T_{12}QT_{21})D_{nom}^{-1}$, is shown in Figure 5.54 as the Q parameter goes from $\overline{Q}^*$ to the causal solution. Each closed-loop frequency response represents the noncausal function associated with the Q that minimizes the Hankel norm over the feasible set. As the robustness specification γ is increased, the largest singular value of the closed-loop frequency response rises to the limit imposed by γ. This rise is accompanied by a reduction in the minimum Hankel norm over the feasible set.

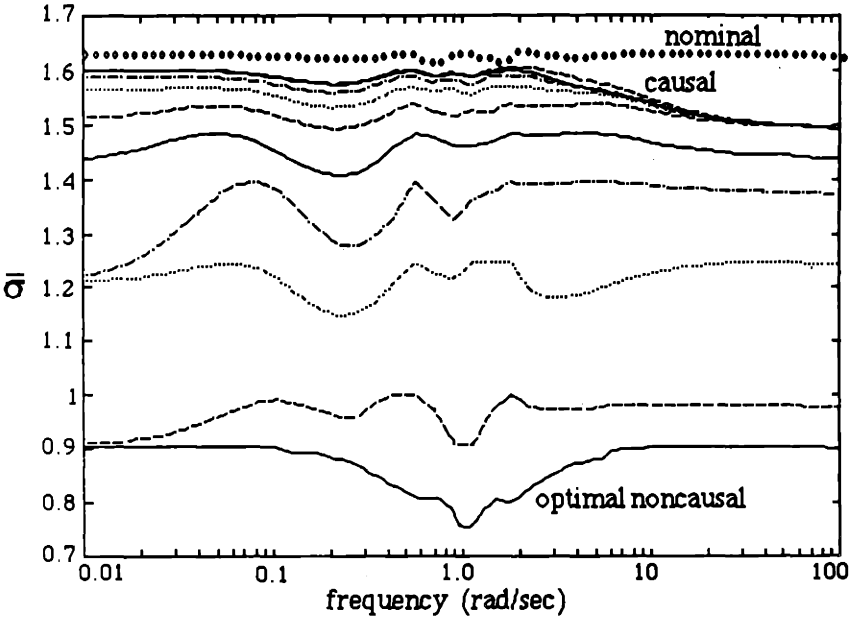

Figure 5.54 Evolution of the scaled closed-loop transfer function matrix, $D_{nom}(T_{11}+T_{12}QT_{21})D_{nom}^{-1}$, as Q becomes causal.

The robustness margin of the final, causal design is $\rho = 0.63$ (vs. $\rho_{nom} = 0.61$). There are several possible explanations for this very slight improvement. First, the decision to keep the order of the Q parameter fixed is suspect. This conclusion is discounted because of the

remark made earlier that increasing the order of Q appeared to have no benefit. A second possibility is that the nominal compensator is a good design (i.e. very close to an optimal solution). Additional DK iterations suggest that this is the case.

The $Q \in H_\infty$ produced by the CRM follows.

$$Q_{11} = \frac{-(0.014s^3 + 0.11s^2 + 0.37s + 0.29)}{s^3 + 2.53s^2 + 2.94s + 1.05} \tag{5.32}$$

$$Q_{22} = \frac{0.18s^4 + 0.29s^3 + 0.044s^2 + 0.0027s + 0.0001}{s^4 + 1.75s^3 + 1.56s^2 + 0.16s + 0.0045} \tag{5.33}$$

Table 5.9: Poles and zeros of the $Q \in H_\infty$ for the MIMO example.

	Poles	Zeros
Q_{11}	-0.58	-1.06
	-0.97 ± 0.93j	-3.37 ± 2.87j
Q_{22}	-0.047	-0.051
	-0.070	-0.054 ± 0.042j
	-0.82 ± 0.83j	-1.44

The singular values of the CRM compensator are shown in Figure 5.55. The response is no longer round at low and high frequencies; however, the CRM and nominal designs are

virtually identical in the mid-frequency range (compare with Figure 5.39). The CRM compensator frequency response can be very closely approximated by a fifth-order, diagonal transfer function (see Table 5.10).

$$K = \begin{bmatrix} \dfrac{0.44s^3 + 0.87s^2 + 0.82s + 0.25}{s^3 + 1.16s^2 + 0.66s + 0.18} & 0 \\ 0 & \dfrac{0.64s^2 + 1.38s + 1.67}{s^2 + 1.17s + 0.73} \end{bmatrix} \tag{5.34}$$

Table 5.10: Poles and zeros of the CRM compensator for the MIMO example.

	Poles	Zeros
K_{11}	$-0.30 \pm 0.48j$	$-0.74 \pm 0.76j$
	-0.56	-0.50
K_{22}	$-0.58 \pm 0.63j$	$-1.09 \pm 1.20j$

A close-up comparison of the structured singular values of the CRM and nominal closed-loop transfer functions is shown in Figure 5.56. The responses are of similar shape, while the CRM design exhibits a (slight) robustness improvement ($\rho = 0.63$ vs. $\rho_{nom} = 0.61$).

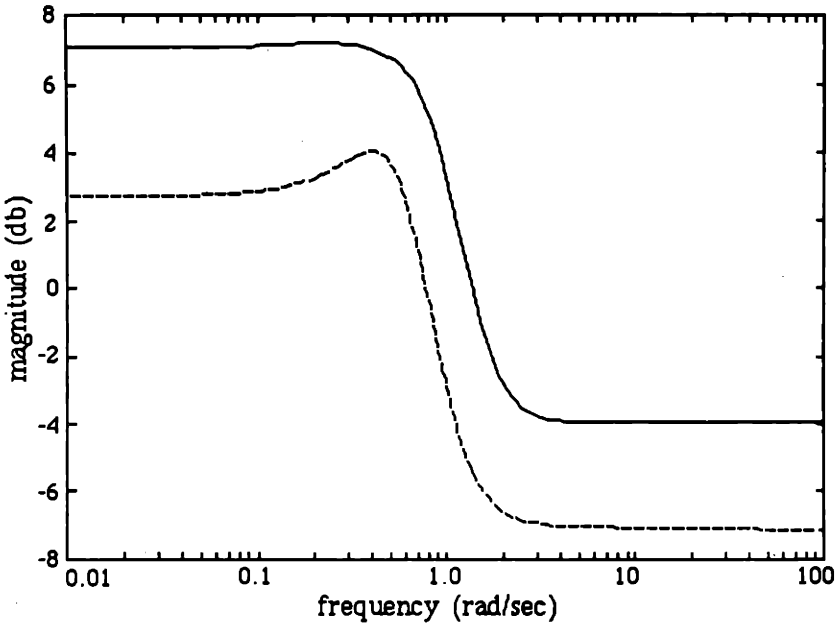

Figure 5.55 The frequency response of the singular values of the CRM compensator.

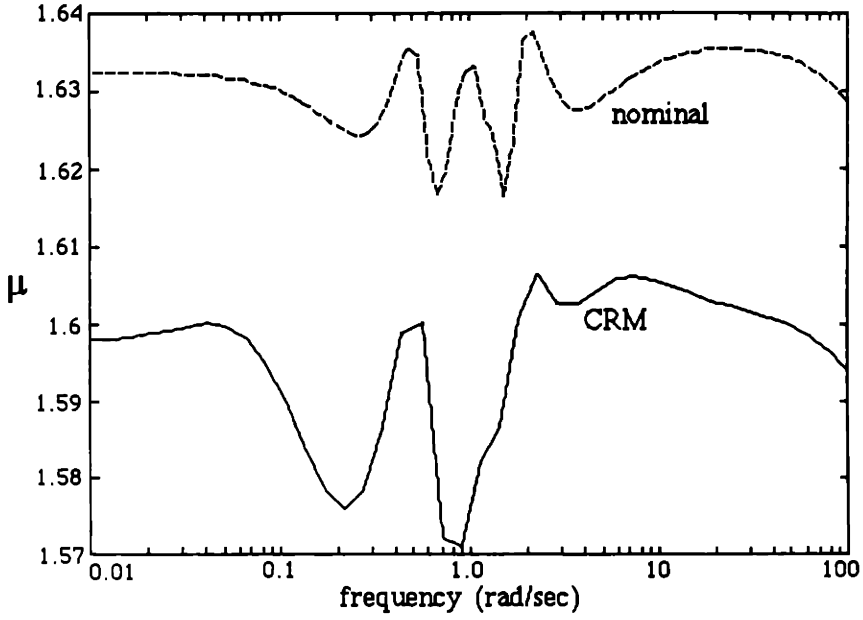

Figure 5.56 Comparison of nominal and CRM closed-loop transfer function matrices.

Once again, these results must be interpreted in terms of the conventional feedback loop in Figure 5.16. It is clear from Figure 5.56 that the nominal and CRM compensators result in very similar closed-loop maps. Other than the very slight improvement in robustness, we would not expect the responses of these two systems to be significantly different. Therefore, the primary comparison will be between the H_∞ design in Figure 5.37 and the CRM design. Recall that the robustness margin of the H_∞ design is 0.52 and that of the CRM is 0.63.

Since the robustness margin of the CRM design is less than one, we will have to scale the uncertainty and performance weighting functions by $\rho = 0.63$, i.e. $W_z = 0.63W_z$ and $W_e = 0.63W_e$. The CRM design now satisfies the condition in Eqn. (5.21) with respect to the scaled weights. In the remainder of this section we will deal only with the scaled weighting functions.

The response of the closed-loop system in Figure 5.16 will be examined for some legal, perturbed plant $\tilde{G}$. $\tilde{G}$ is a product of the nominal plant G and some multiplicative input uncertainty (Eqn. 5.27). In this case, the perturbation L will have the structure

$$L = \begin{bmatrix} l_{11} & l_{12} \\ l_{21} & l_{22} \end{bmatrix} \tag{5.35}$$

where l_{ij} are SISO transfer functions.

Since the plant G is nominally diagonal (Eqn. 5.24), we would like the perturbation L to introduce coupling in the plant. For this purpose, l_{11} and l_{22} are taken to be identically zero, and let $l_{12} = l_{21}$. Then, the two singular values of L at a particular frequency ω are equal and equal to

$$\sigma\,[L(j\omega)] = |\, l_{12}(j\omega)\,| \tag{5.36}$$

For this example, a legal perturbation is

$$l_{12}(s) = \frac{ks}{s+5} \tag{5.37}$$

where k = 1.75. The singular values of the uncertainty weight and the perturbation L are shown in Figure 5.57. Note that L is a legal perturbation because it is bounded by W_z over all frequencies. Then,

$$\tilde{G} = \begin{bmatrix} \frac{a}{s} & \frac{ka}{s+5} \\ \frac{ka^{-1}}{s+5} & \frac{a^{-1}}{s} \end{bmatrix} \tag{5.38}$$

where a = 5 and k = 1.75. Figure 5.58 contains the singular values of $\tilde{G}$.

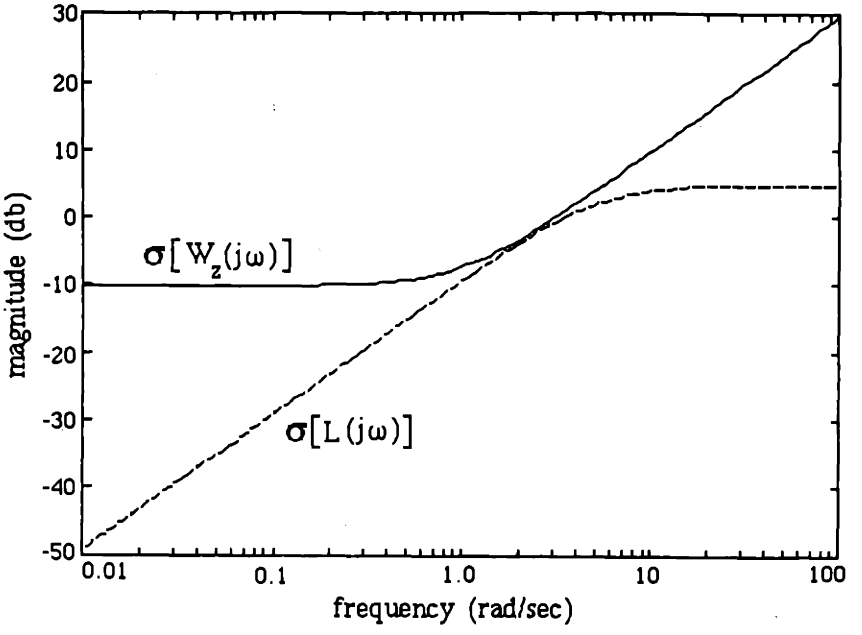

Figure 5.57 The frequency responses of the uncertainty weighting function and the multiplicative perturbation.

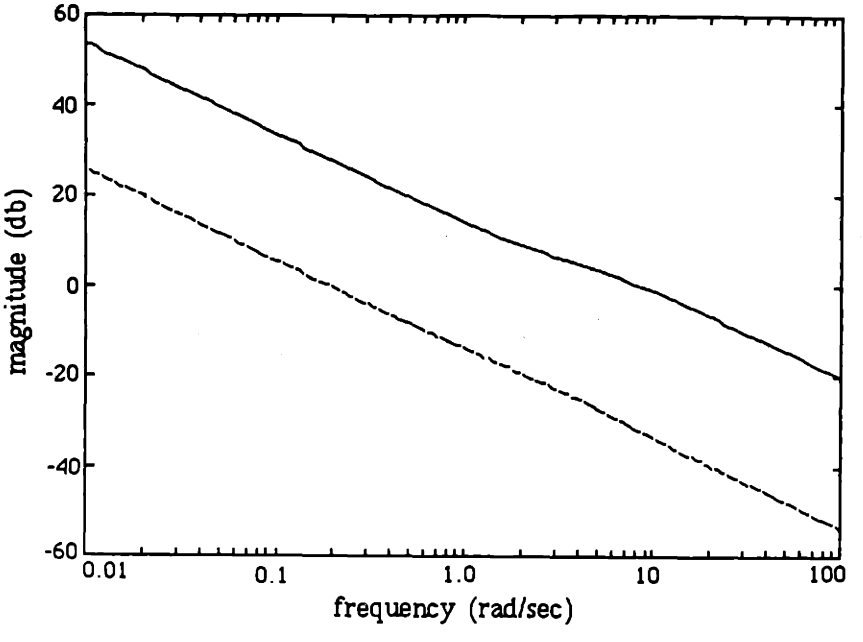

Figure 5.58 The frequency response of the singular values of the perturbed plant $\tilde{G}$.

The singular values of the complementary sensitivity and the sensitivity transfer functions will be presented for six cases: three compensators and two plants. The compensators are the H_∞, the nominal (i.e. nonconverged DK iteration), and the CRM designs. The closed-loop system with the nominal plant G and the perturbed plant $\tilde{G}$ is examined.

Figures 5.59 through 5.64 contain the frequency responses of the complementary sensitivity function for the six feedback loops. All three designs with the nominal plant G have "nice shapes" and satisfy the stability-robustness condition in Eqn. (1.20). Therefore, legal perturbations will not drive the system unstable. With the perturbed plant $\tilde{G}$ in the loop, the H_∞ design exhibits the most performance deterioration. The complementary sensitivity develops a large, broad peak around 2 radians/second (Figure 5.62). The responses of the nominal and CRM designs are similar.

The singular values of the sensitivity function for each case are plotted in Figures 5.65 through 5.70. The performance specification is met by all three compensators when the nominal plant G is in the loop. The H_∞ design is characterized by a significantly lower sensitivity at low frequencies (Figure 5.65), when compared to the nominal and CRM designs. For the perturbed plant $\tilde{G}$, the H_∞ design no longer meets the performance specification (Figure 5.68). The violation occurs in the frequency range of 1 to 2 radians/second. The nominal and CRM designs meet the specification with the perturbed plant in the loop (Figures 5.69 and 5.70). However the frequency responses are no longer round above 5 radians/second, as they were with the nominal plant.

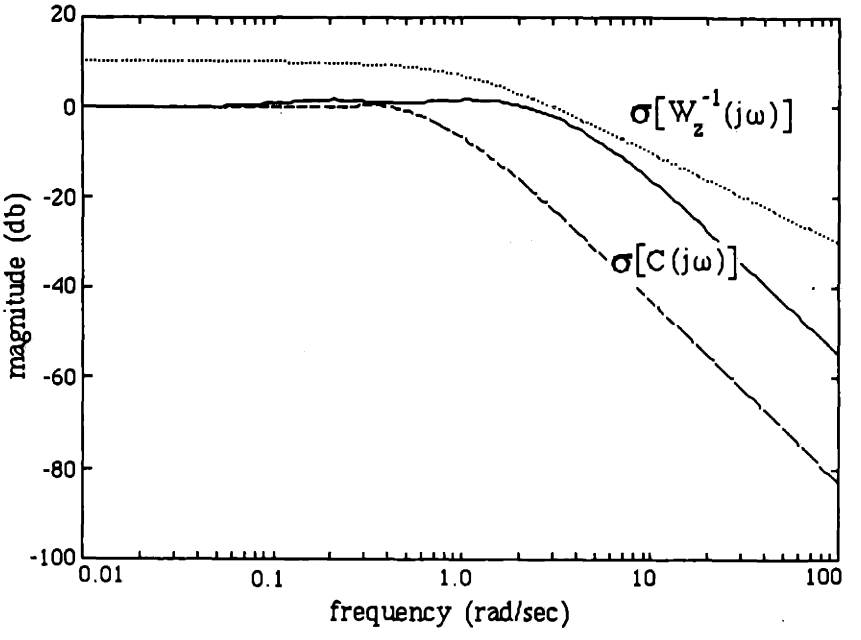

Figure 5.59 The singular values of the complementary sensitivity function with plant G and the H_∞ compensator.

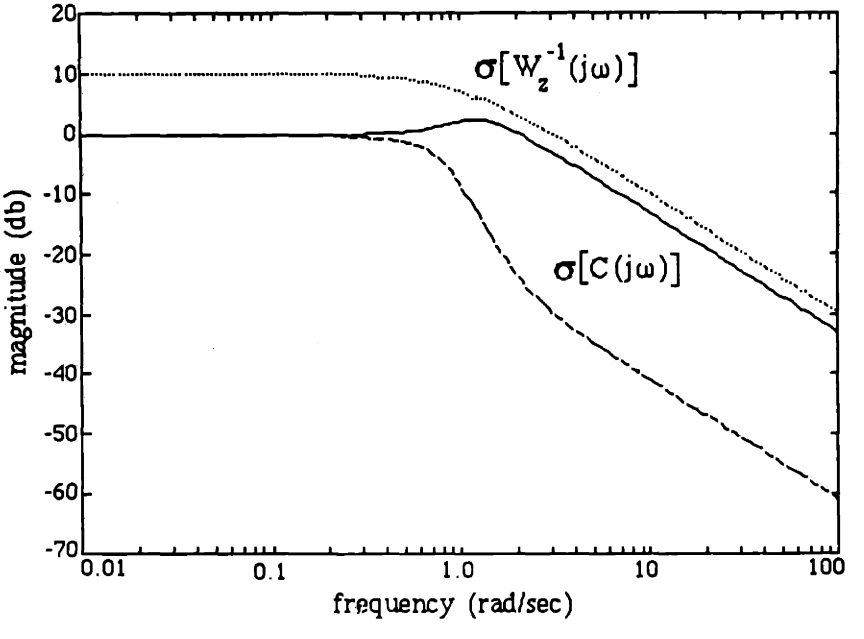

Figure 5.60 The singular values of the complementary sensitivity function with plant G and the nominal compensator.

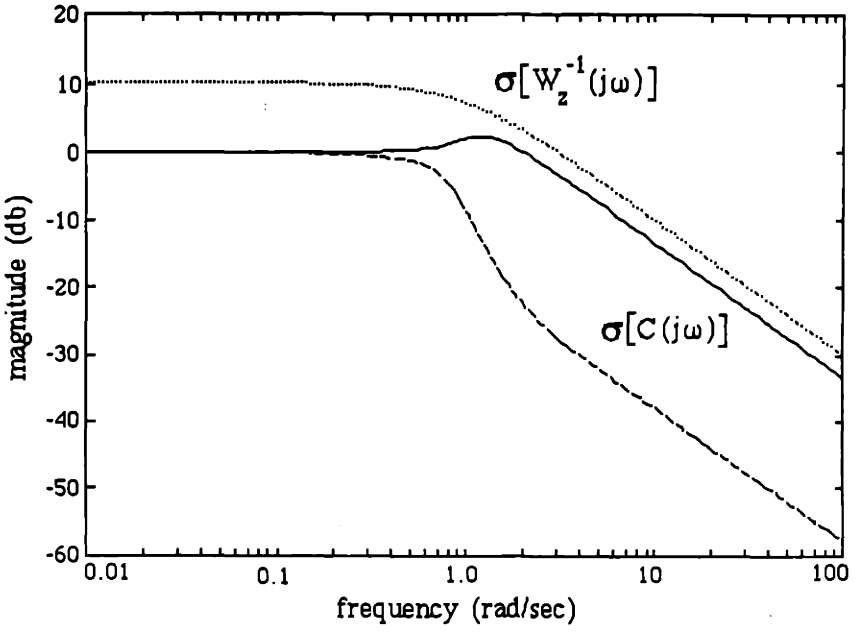

Figure 5.61 The singular values of the complementary sensitivity function with plant G and the CRM compensator.

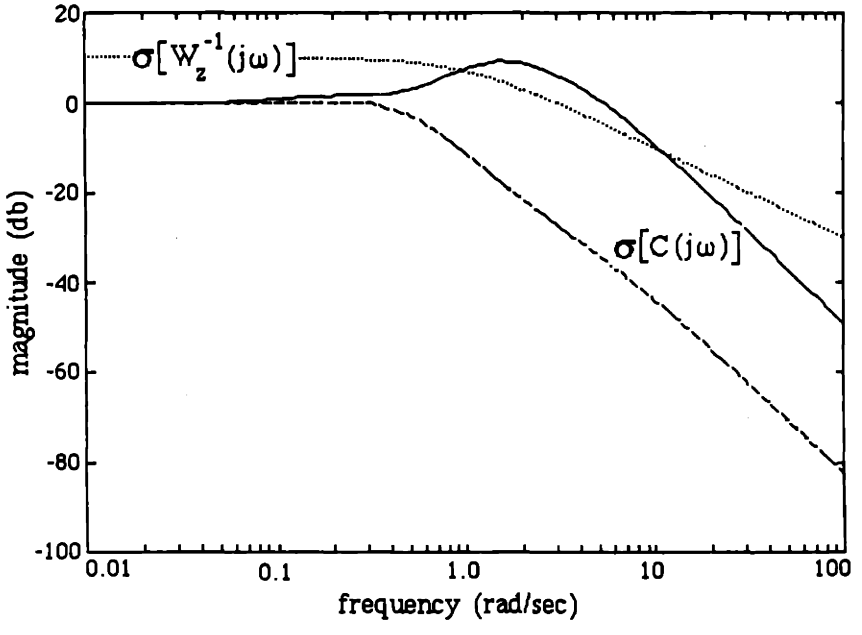

Figure 5.62 The frequency response of the complementary sensitivity function with perturbed plant $\tilde{G}$ and the H_∞ compensator.

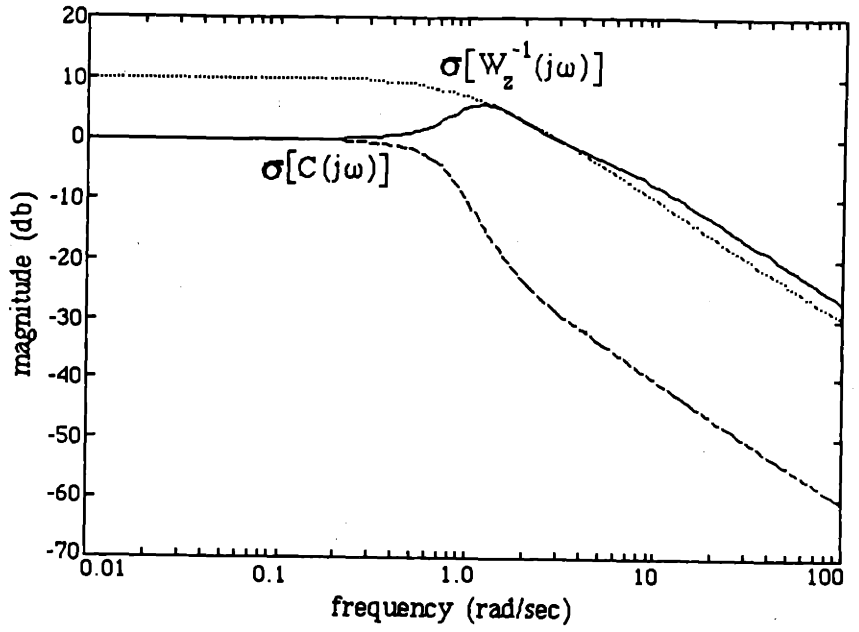

Figure 5.63 The singular values of the complementary sensitivity function with perturbed plant $\tilde{G}$ and the nominal compensator.

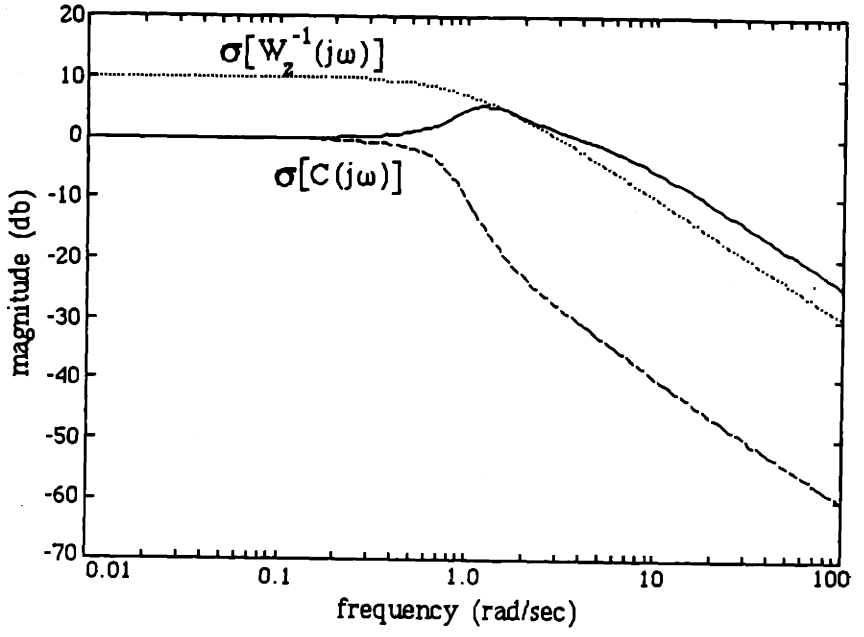

Figure 5.64 The singular values of the complementary sensitivity function with perturbed plant $\tilde{G}$ and the CRM compensator.

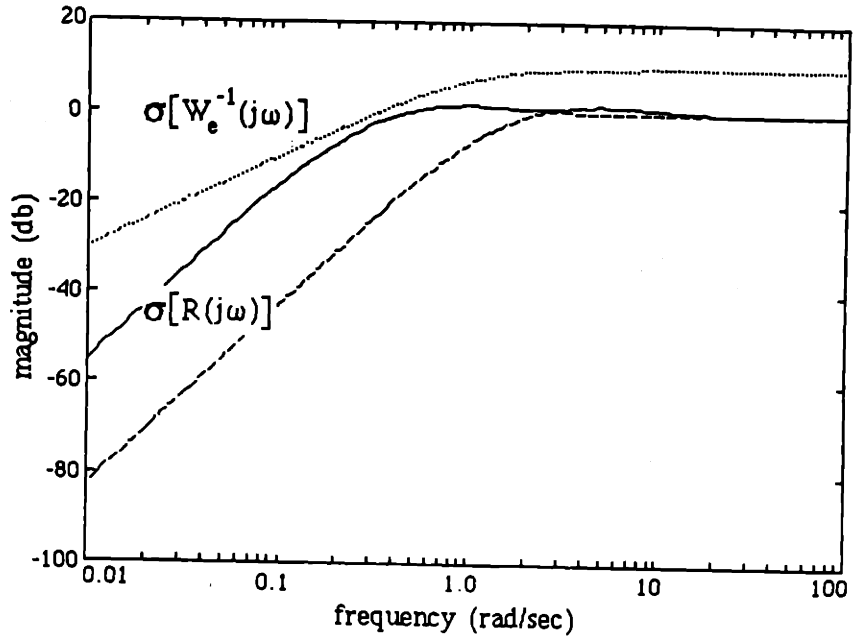

Figure 5.65 The singular values of the sensitivity function with plant G and the H_∞ compensator.

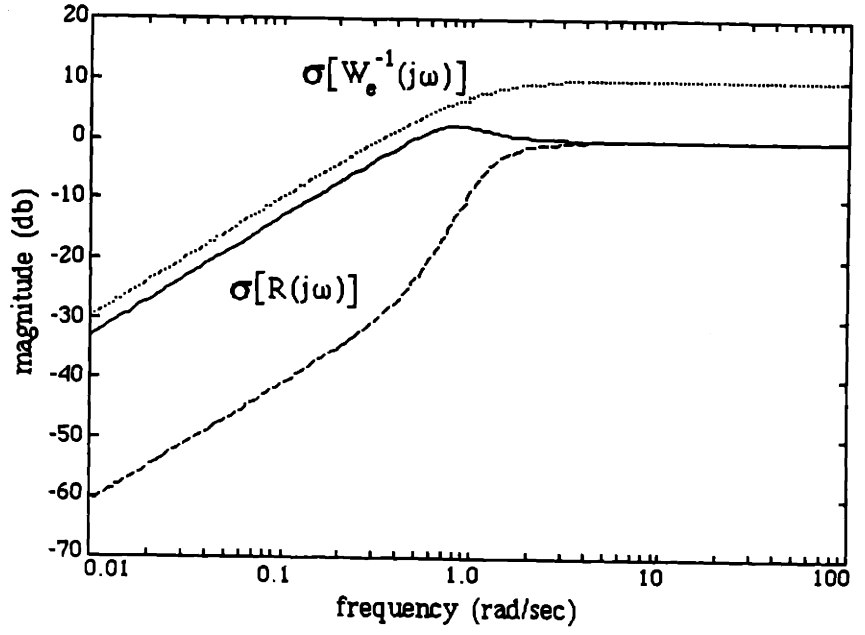

Figure 5.66 The singular values of the sensitivity function with plant G and the nominal compensator.

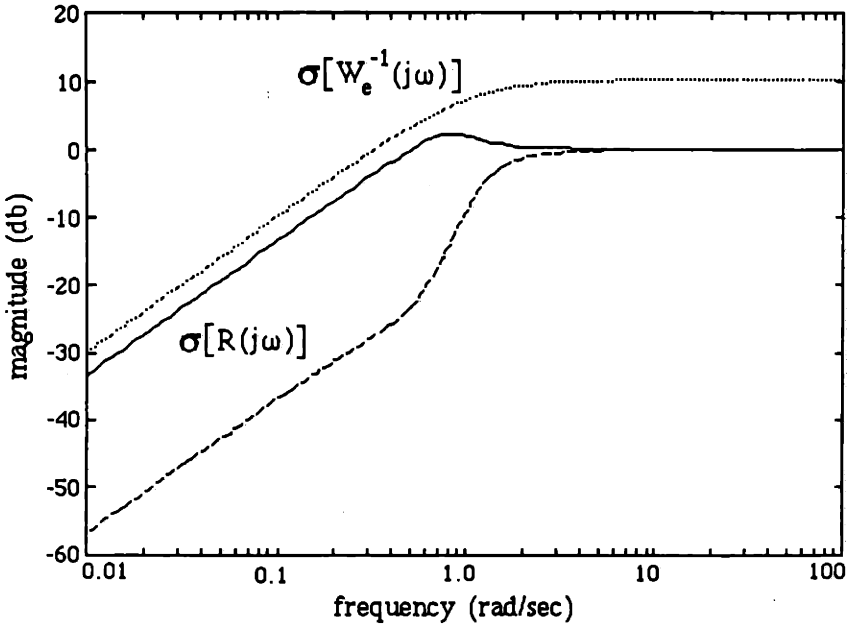

Figure 5.67 The singular values of the sensitivity function with plant G and the CRM compensator.

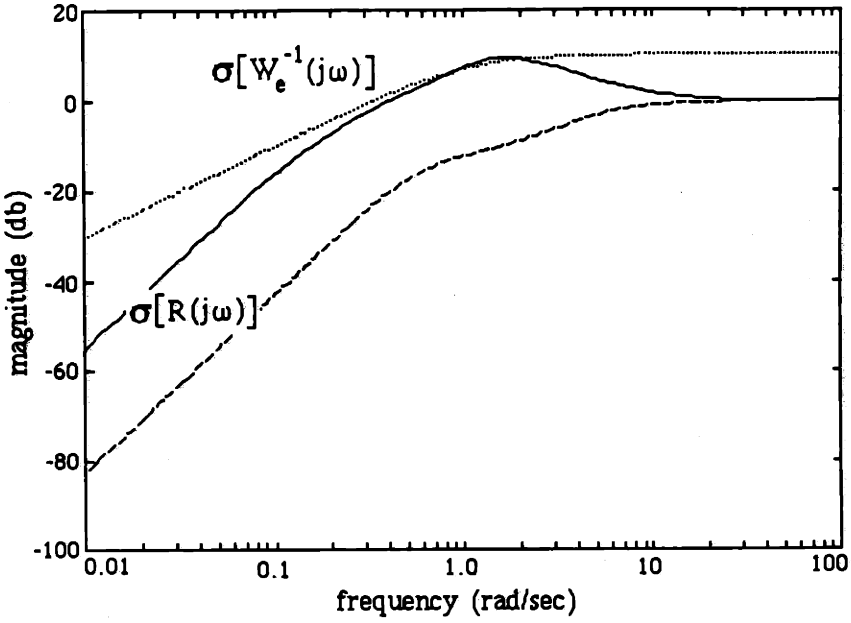

Figure 5.68 The singular values of the sensitivity function with perturbed plant $\tilde{G}$ and the H_∞ compensator.

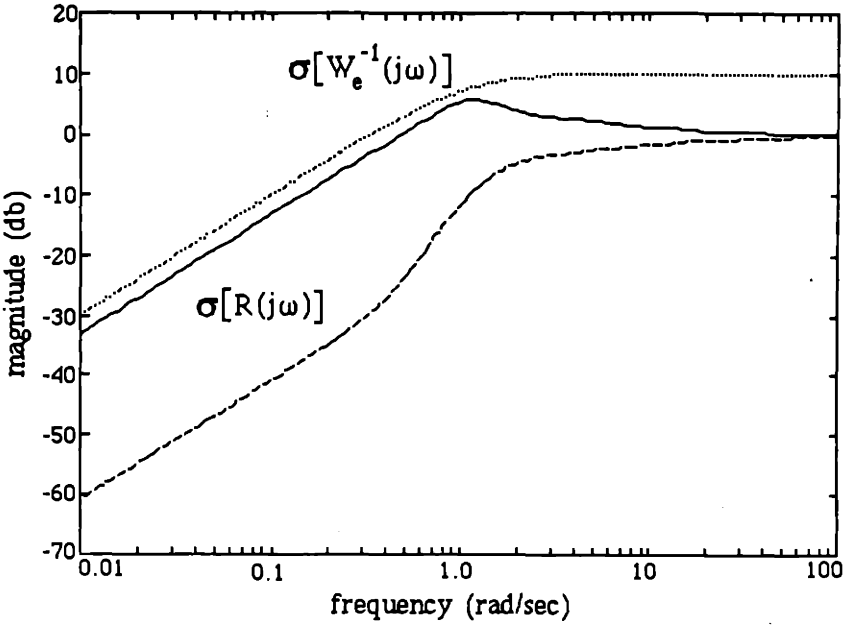

Figure 5.69 The singular values of the sensitivity function with perturbed plant $\tilde{G}$ and the nominal compensator.

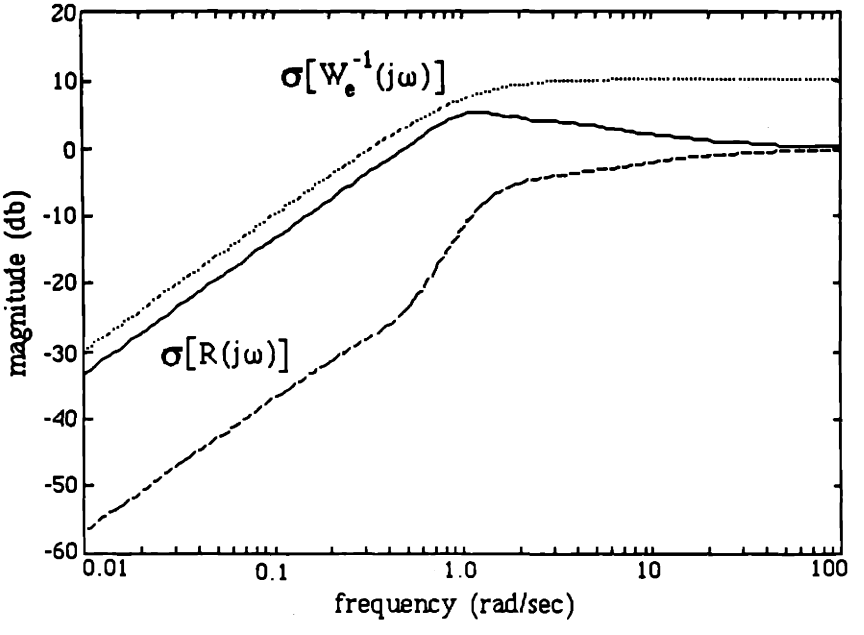

Figure 5.70 The singular values of the sensitivity function with perturbed plant $\tilde{G}$ and the CRM compensator.

The output (y) responses to a reference command r = [1 1]' are in Figures 5.71 through 5.75. The step responses with the nominal plant G are quite good. Note that the response of the closed-loop with the nominal compensator and the nominal plant G is not included because it is very similar to the CRM response. The y_1 response of the H_∞ design exhibits 18% overshoot and no undershoot (Figure 5.71). The y_1 response of the CRM design has the same overshoot, and a little undershoot (Figure 5.72). However, the settling times of the two designs are about the same (6 seconds). The y_2 CRM response has much less overshoot and a significantly faster settling time than the H_∞ design.

The H_∞ compensator and the perturbed plant produce a poor y_1 step response, shown in Figure 5.73. However, the y_2 response is unaffected by the perturbation. The step responses of the nominal and CRM designs, with $\tilde{G}$, are in Figures 5.74 and 5.75. The y_1 response exhibits over twice as much overshoot, when compared to the response with G in the loop, but this is significantly better than the H_∞ design. Although it is difficult to see from Figures 5.74 and 5.75, the CRM design results in less undershoot and overshoot (at 3.5 and 6 seconds) as compared to the nominal design. The y_2 responses are virtually identical, and the same as the closed-loop with the nominal plant G. Note that the y_2 response is largely unaffected by the perturbation because of the factor of a^{-1} (0.2) in the $\tilde{G}_{21}$ transfer function (Eqn. 5.38).

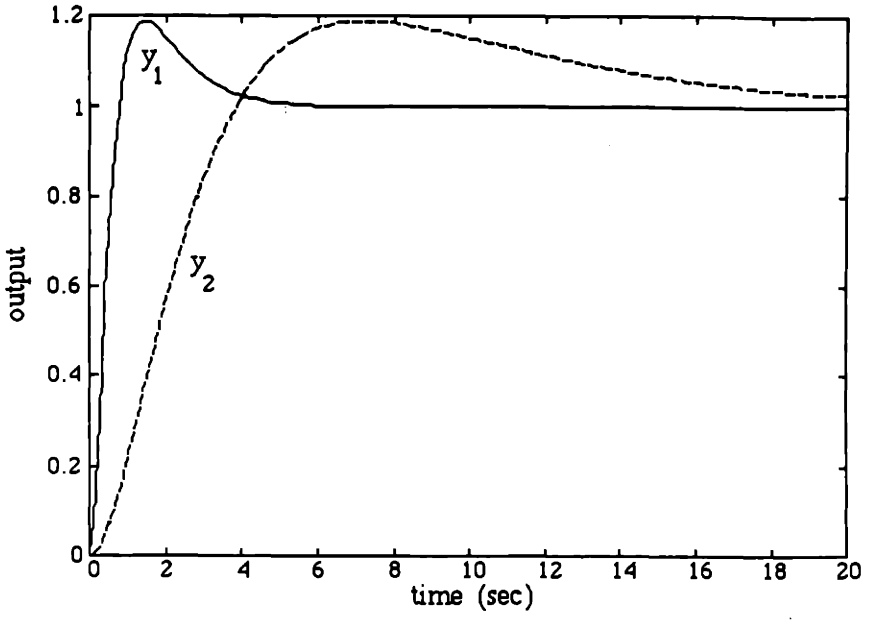

Figure 5.71 The closed-loop output response to an input command r = [1 1]' with plant G and the H_∞ compensator.

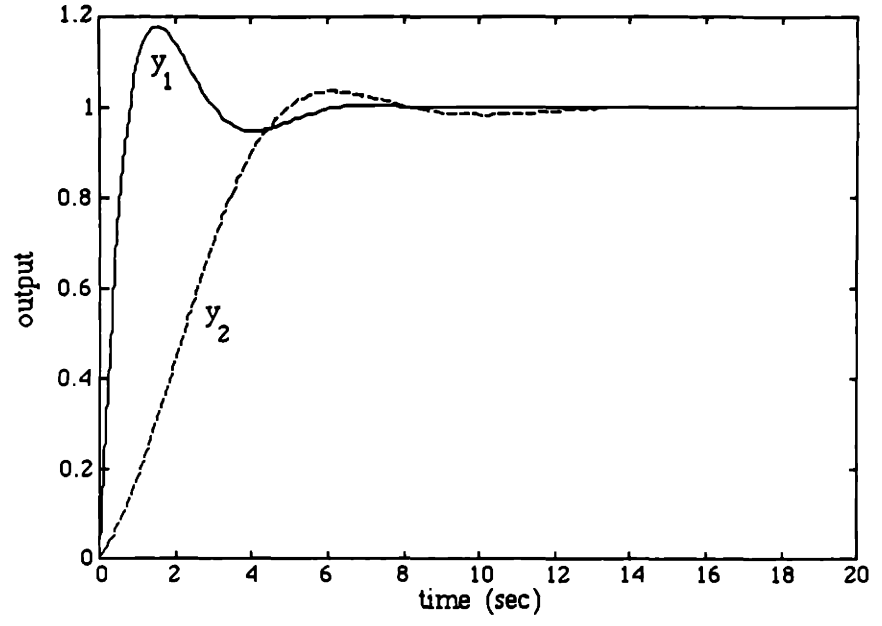

Figure 5.72 The closed-loop output response to an input command r = [1 1]' with plant G and the CRM compensator.

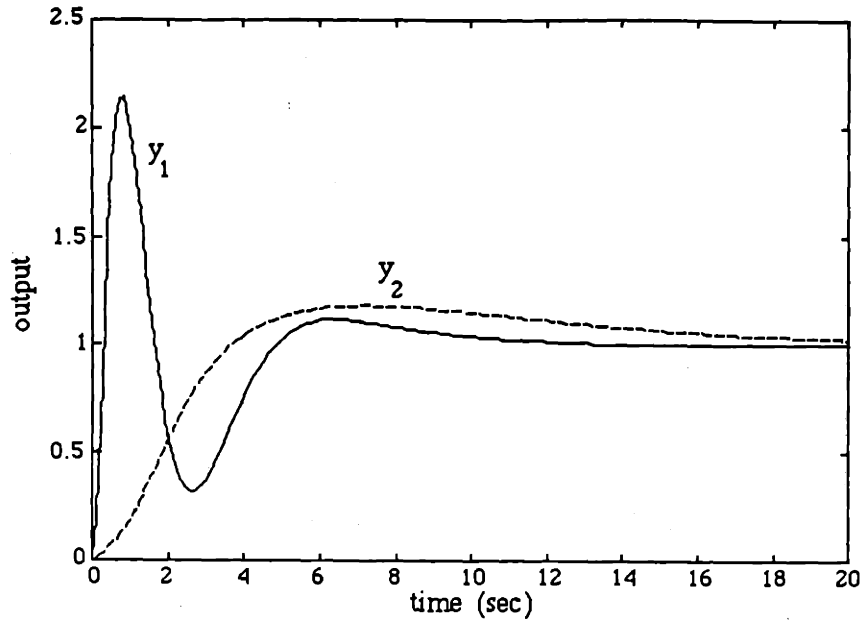

Figure 5.73 The closed-loop output response to an input command r = [1 1]' with perturbed plant $\tilde{G}$ and the H_∞ compensator.

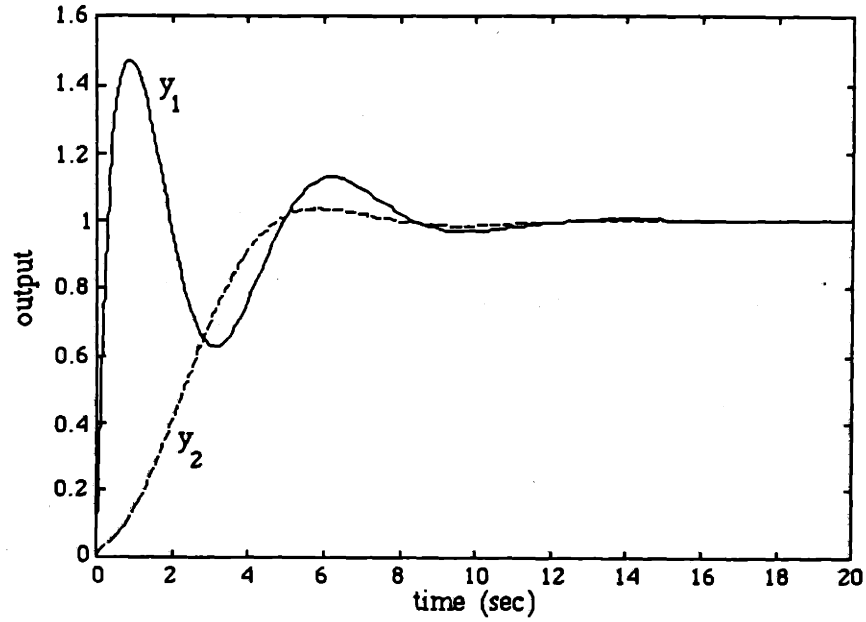

Figure 5.74 The closed-loop output response to an input command r = [1 1]' with perturbed plant $\tilde{G}$ and the nominal compensator.

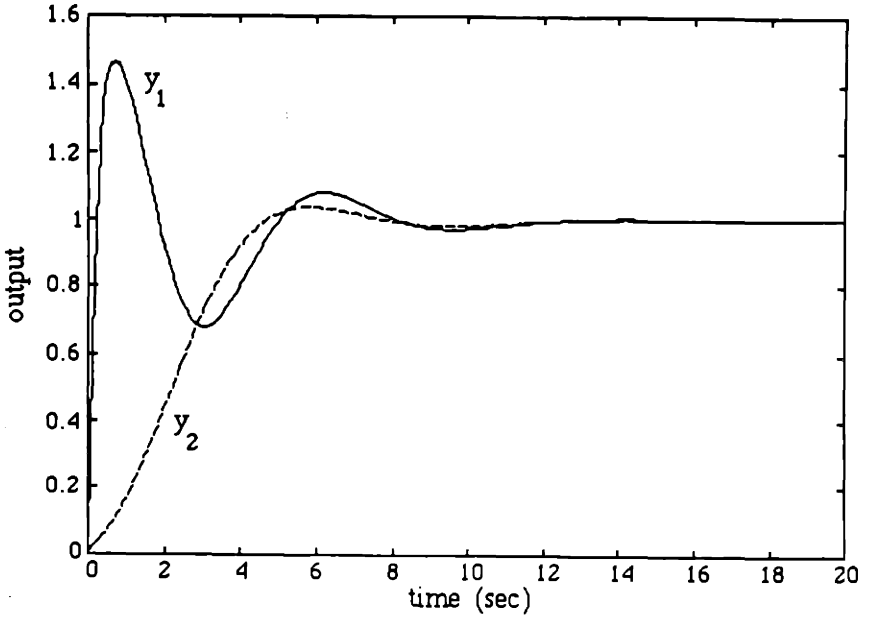

Figure 5.75 The closed-loop output response to an input command r = [1 1]' with perturbed plant $\tilde{G}$ and the CRM compensator.

Figures 5.76 and 5.77 contain the closed-loop output response to a disturbance d = [1 1]'sin(0.1t) for the H_∞ and CRM designs with the nominal plant G. The H_∞ design has better disturbance-rejection at this frequency, and the multiplicative perturbation does not affect the performance at this frequency. Although not plotted, the CRM and nominal closed-loop responses are virtually identical. Note that while the H_∞ design does produce better disturbance-rejection, the CRM performance meets the specification (see Figure 5.67).

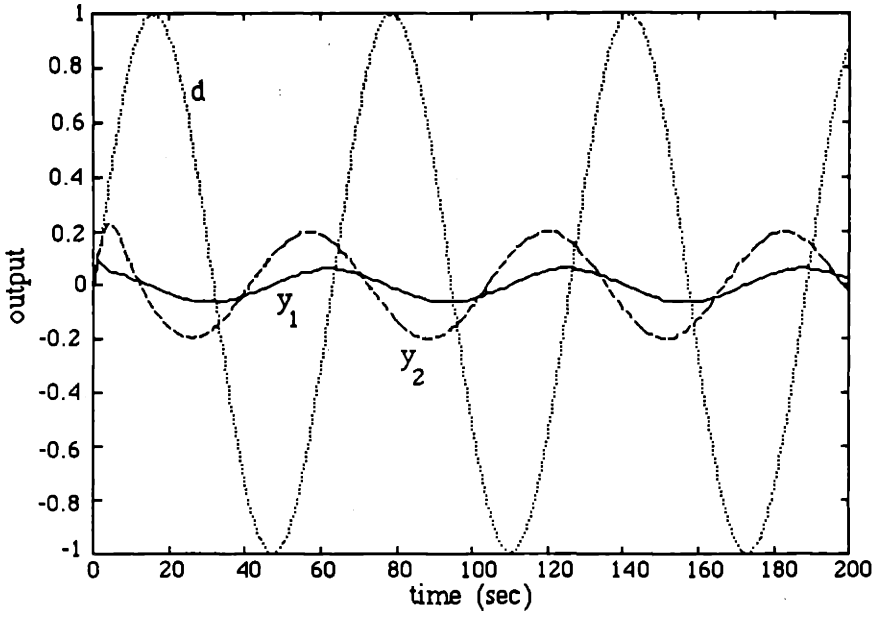

Figure 5.76 The closed-loop output response to a disturbance d = [1 1]'sin(0.1t) with plant G and the H_∞ compensator.

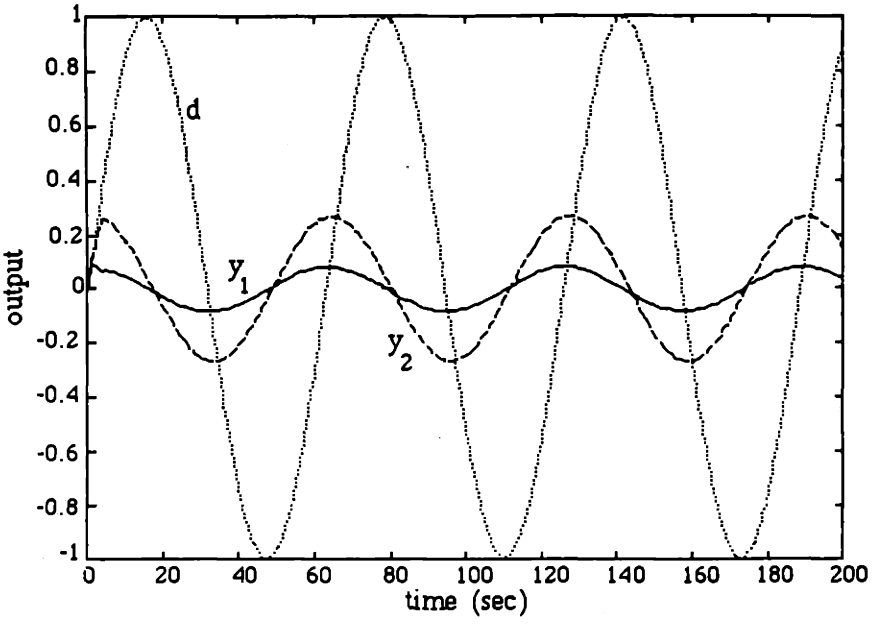

Figure 5.77 The closed-loop output response to a disturbance d = [1 1]'sin(0.1t) with plant G and the CRM compensator.

The disturbance frequency was increased to 1 radian/second, and the responses are plotted in Figures 5.78 through 5.82. Of course, the disturbance rejection is much worse in general at this frequency because the sensitivity function is near unity. For the nominal plant G, the y_1 response of the CRM design (Figure 5.79) is superior to that of the H_∞ design (Figure 5.78), while the y_2 responses are the same. The y_1 response deteriorates significantly in the case of the H_∞ design when the perturbed plant $\tilde{G}$ is in the feedback loop (Figure 5.80). In the case of the nominal and CRM designs, the performance degradation is not as severe. The disturbance rejection of the CRM design is slightly better than that of the nominal design when $\tilde{G}$ is in the loop (compare Figures 5.81 and 5.82).

In this example, the CRM was tested in a multivariable setting. Only a slight improvement in performance-robustness was achieved. The author believes that the marginal improvement is a result of the fact that the nominal design was nearly optimal. The performance and robustness benefits of using the CRM were illustrated vis-a-vis an H_∞ design.

The computational requirements of the multivariable example were quite severe. The CRM performed 1.8 *billion* floating point operations, as computed by PRO-MATLAB, over a period of approximately 4 days (in batch mode).

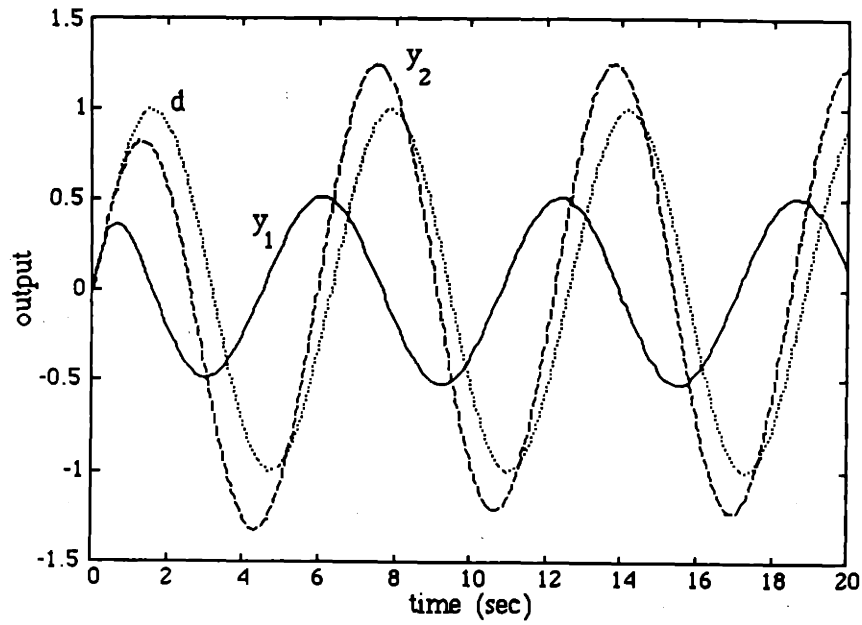

Figure 5.78 The closed-loop output response to a disturbance d = [1 1]'sin(t) with plant G and the H_∞ compensator.

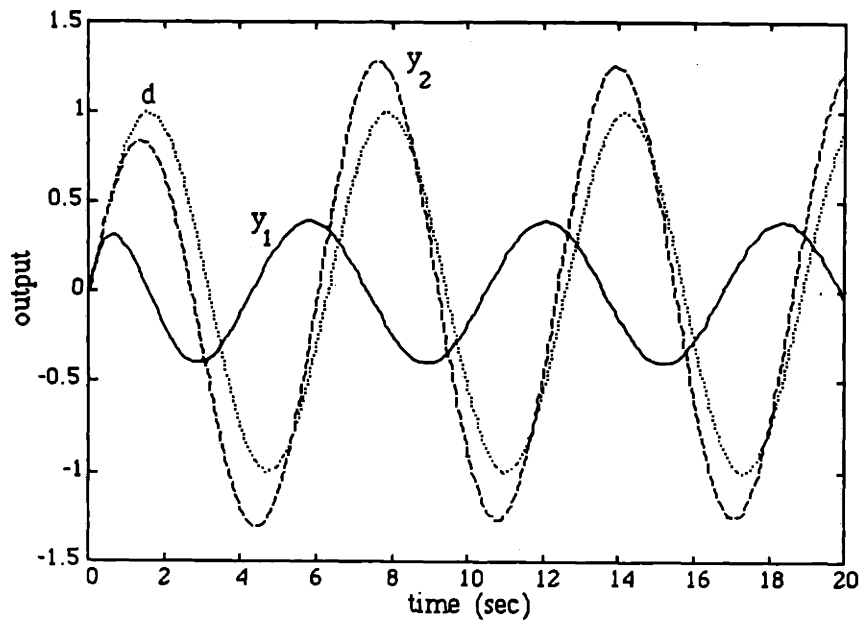

Figure 5.79 The closed-loop output response to a disturbance d = [1 1]'sin(t) with plant G and the CRM compensator.

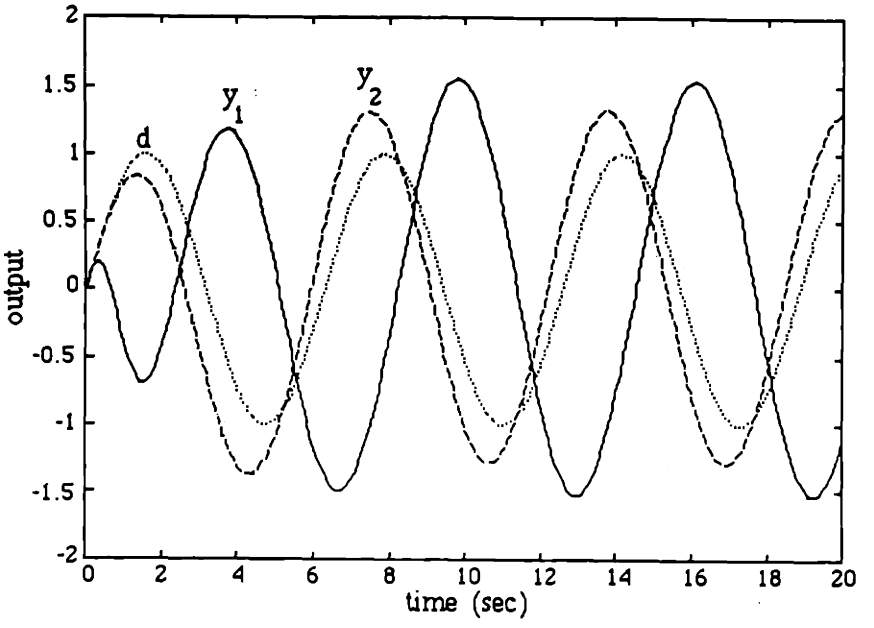

Figure 5.80 The closed-loop output response to a disturbance d = [1 1]'sin(t) with pertubed plant $\tilde{G}$ and the H_∞ compensator.

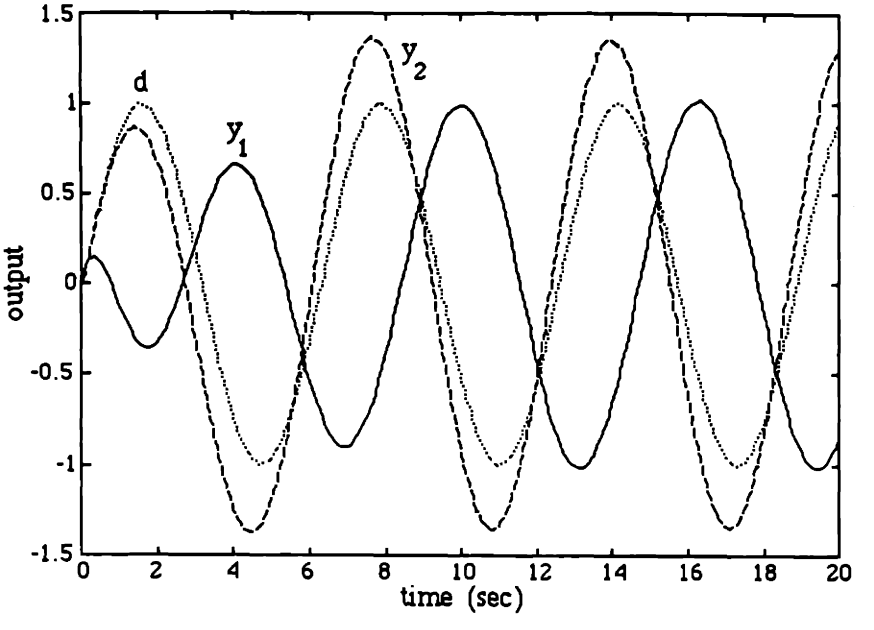

Figure 5.81 The closed-loop output response to a disturbance d = [1 1]'sin(t) with perturbed plant $\tilde{G}$ and the nominal compensator.

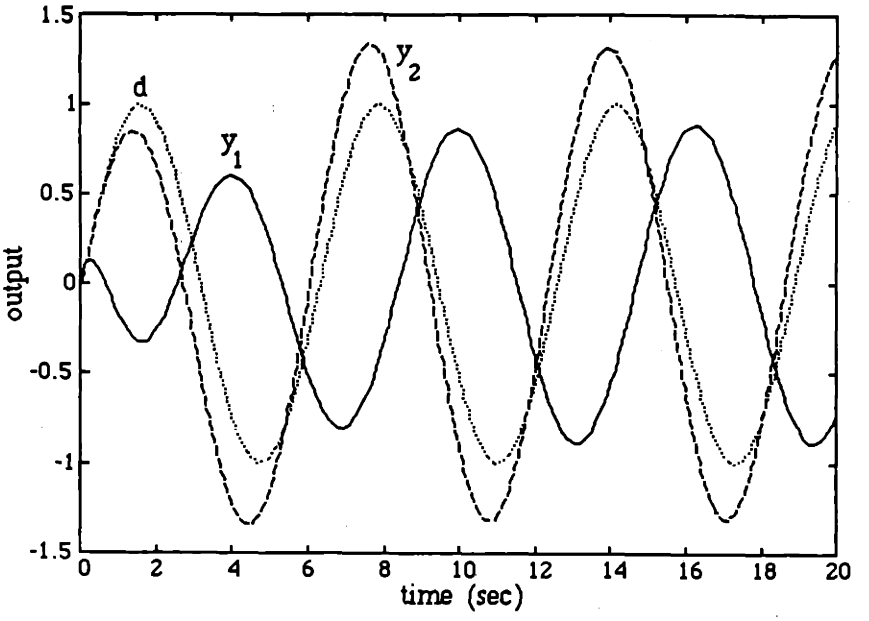

Figure 5.82 The closed-loop output response to a disturbance d = [1 1]'sin(t) with perturbed plant $\tilde{G}$ and the CRM compensator.

5.4 Concluding Remarks

We have seen the CRM successfully applied to two design examples: one SISO and one MIMO. The objective of increasing the robustness margin was achieved in both cases with finite-dimensional Q parameters. The resulting compensators improved robustness and were of relatively low order. In fact, the CRM compensator was of lower order (vs. the nominal design) in the SISO example.

The inefficiency of the causality recovery algorithm is the most significant drawback of the CRM. Clearly, the severe computational burden is sufficient to make the CRM impractical at this time. However, the optimization programs should be parallelizable for super-computer implementation.

CHAPTER 6. CONCLUSIONS AND FUTURE RESEARCH

6.1 Conclusions

Given the Youla parameterization of all stabilizing compensators in terms of a free parameter Q, the feedback synthesis problem may be generally stated as: *Find a Q in H_∞ such that some closed-loop performance objective is satisfied.* Each design methodology is simply a procedure for finding an appropriate Q to satisfy its specific performance criterion.

The role of modeling error in the feedback design process has been stressed throughout the thesis. Clearly, the uncertainty must be explicitly incorporated into the design process if performance is to be optimized and guarantees made concerning robustness. A realistic description of the uncertainty results in a perturbation of known structure. Stability and performance robustness with respect to structured uncertainty is the performance criterion of interest in this thesis. A necessary and sufficient robustness condition leads to a frequency-domain inequality on the closed-loop transfer function involving the structured singular value.

A new design technique, the Causality Recovery Methodology, has been developed for the synthesis of finite-dimensional, linear, time-invariant feedback systems. Stability *and* performance in the presence of multiple, unstructured modeling uncertainties is guaranteed. The concept of a robustness margin was introduced as a quantitative way of measuring performance; it has been proven that the CRM will produce a closed-loop system whose robustness margin is greater than or equal to that of a given (nominal) feedback system. The CRM should be viewed as a technique to fine-tune an already reasonable design by exploiting the degree of freedom available in Q. That is, the method proposed in this thesis should be used *in conjunction*, and not in competition, with existing design methods for the possible improvement of performance-robustness. The CRM requires the solution of a series of

infinite-dimensional convex programs.

The design examples in the previous chapter demonstrate that the CRM is a viable design concept and the finite-dimensional algorithm is useful. The CRM increased the robustness margin of feedback systems designed with the standard H_∞ theory and the (nonconverged) DK iteration. The examples also illustrate the benefits of a μ-synthesis compensator over the H_∞ approach; the performance of the robust designs was fairly insensitive to the actual plant in the feedback loop, provided that it was a legal perturbation. While these preliminary results are encouraging, the tremendous computational cost associated with robustness enhancement makes the method impractical at this time.

6.2 Directions for Future Research

6.2.1 Robust Feedback Design

The synthesis of a feedback system exhibiting robust stability and performance (i.e. satisfying some μ specification) is a fundamentally difficult and nonconvex problem. Nonconvexity implies that a local solution may be encountered. In such a situation, it is always beneficial to have more than one method for attacking the problem. Therefore, any new methods for solving the robust performance problem are welcome, and active research should continue in this area.

The direct handling of real parameter variations, the so-called real-μ problem, is still not possible. Although some progress has been made, the analysis of such systems is not completely understood. Additional work in the analysis area is required before a synthesis methodology can be formulated.

6.2.2 The Causality Recovery Methodology

While the theoretical foundation of the CRM has been laid, additional research is required before it becomes a practical design tool. The major shortcoming of the CRM is the computational burden associated with the design algorithm. Specifically, the most computationally intensive part of the algorithm is the minimization of the Hankel norm over the feasible set.

Part of the problem can be attributed to the particular implementation of the CRM used for the design examples in Chapter 5. The CRM was written as a function within the commercially available software package PRO-MATLAB. The optimization solver that performs the Hankel norm minimization is a basic pattern search algorithm, and was chosen for its simplicity and ease of programming rather than for speed and efficiency. This suggests that a dedicated algorithm, written in a compiled language and capable of taking advantage of the problem structure, may significantly reduce the amount of time required to find a stable, causal solution to the feedback problem. Another possible technique for improving the efficiency of the CRM would involve the exploitation of the parallel nature of the optimization problem.

Regardless of the numerical algorithms used by the CRM, its implementation will be finite-dimensional and nonconvex. Therefore, such issues as starting points and parameterizations in the Hankel norm minimization are significant. The pole/zero parameterization of Q was chosen for its numerical and conceptual properties, as well as its ease of implementation. Other realizations, such as the Jordan form, may prove computationally superior.

The final issue that must be examined before the CRM becomes a useful design technique. That is, what are the properties of the CRM solution (other than satisfying some μ condition)? The CRM is essentially a frequency-domain approach to feedback synthesis,

intimately coupled with the structured singular value as the analysis tool. What are the implications for time-domain signals other than L_2 functions or sinusoids? What pole/zero structure will the compensator possess?

6.2.3 Extensions of the CRM

The CRM proposes a new approach to feedback system design. That is, the two basic constraints on the free parameter Q, i.e. the H_∞ restriction and the performance specification, are treated independently. The performance specification is satisfied at each frequency by complex matrices, and a stable, causal transfer function is recovered from these matrices. This same philosophy could potentially be applied to other feedback problems.

Through appropriate definition of the feasible set Φ a broad class of frequency-domain problems may be handled. Let $f(Q)$ be some closed-loop performance objective that is a function of the free parameter Q in the Youla parameterization. Define acceptable performance as $f(Q) \leq 1$, and the feasible set is simply

$$\Phi = \{ Q \in L_\infty \mid f(Q) \leq 1 \}$$

The familiar optimization problem must then be solved.

$$\min_{Q \in \Phi} \| \Gamma_Q \|$$

The convexity of the above problem will determine the usefulness of this method. However, the framework is quite general, with the H_2 and H_∞ problems as convex special cases.

This framework will admit several other interesting problems, but a great deal of research is needed to determine its feasibility as a design method. Assuming a real-μ analysis

tool is available, this may be one approach to the synthesis problem with real parameter variations. That is, the feasible set would be defined in terms of the real-μ function; and the Hankel norm minimization would be performed over the set of L_∞ frequency responses that satisfy some real-μ performance specification. Besides being a useful design methodology in its own right, the real-μ solution has implications for adaptive control as well. It is believed that such a design would prove to be a useful benchmark for the adaptive control problem. The true performance benefits of a time-varying compensator could be quantitatively evaluated with respect to the best fixed-parameter, real-μ design.

It may also be interesting to investigate the possibility of integrating time and frequency constraints into the definition of the feasible set. This would represent a significant step in the unification of the time and frequency domains in the design of feedback systems. Finally, it seems worthwhile, because of the methodology's infinite-dimensional nature, to explore the extension of the CRM concepts to infinite-dimensional systems (i.e. systems with delays).

CHAPTER 7. REFERENCES

[1] H.W. Bode, *Network Analysis and Feedback Amplifier Design*, Princeton: Van Nostrand, 1945.

[2] I.M. Horowitz, *Synthesis of Feedback Systems*, New York: Academic Press, 1963.

[3] J.C. Doyle and G. Stein, "Multivariable Feedback Design: Concepts for a Classical/ Modern Synthesis", *IEEE Trans. Auto. Control*, Vol. AC-26, Feb. 1981, pp. 4 - 16.

[4] J.C. Doyle, J.E. Wall, and G. Stein, "Performance and Robustness Analysis for Structured Uncertainty", *Proc. IEEE Conf. on Decision and Control*, Orlando, FL, 1982, pp. 629 - 636.

[5] J.C. Doyle, "Analysis of Feedback Systems with Structured Uncertainties", *IEE Proceedings*, Vol. 129, Part D, No. 6, Nov. 1982, pp. 242 - 250.

[6] J.C. Doyle, "Synthesis of Robust Controllers and Filters", *Proc. IEEE Conf. on Decision and Control*, San Antonio, TX, 1983, pp. 109 - 114.

[7] C.E. Rohrs, L. Valavani, M. Athans, and G. Stein, "Robustness of Continuous Time Adaptive Control Algorithms in the Presence of Unmodeled Dynamics", *IEEE Trans. Auto. Control*, Vol. AC-30, Sep. 1985, pp. 881 - 889.

[8] R.O. LaMaire, "Robust Time and Frequency Domain Estimation Methods in Adaptive Control", Ph.D. Thesis, LIDS-TH-1674, MIT, Cambridge, MA, June 1987.

[9] K.J. Astrom, "Analysis of Rohrs' Counterexamples to Adaptive Control", *Proc. IEEE Conf. on Decision and Control*, San Antonio, TX, 1983, pp. 982 - 987.

[10] B. Wittenmark and K.J. Astrom, "Practical Issues in the Implementation of Self-Tuning Control", *Automatica*, Vol. 20, Sep. 1984, pp. 595 - 605.

[11] G.C. Goodwin, D.J. Hill, and M. Palaniswami, "A Perspective on Convergence of Adaptive Control Algorithms", *Automatica*, Vol. 20, Sep. 1984, pp. 519 - 531.

[12] G.C. Goodwin, D.J. Hill, and M. Palaniswami, "Towards an Adaptive Robust Controller", *7th IFAC Symposium on Identification and System Parameter Estimation*, York, UK, 1985, pp. 997 - 1002.

[13] G.C. Goodwin, D.J. Hill, D.Q. Mayne, and R.H. Middleton, "Adaptive Robust Control (Convergence, Stability, and Performance)", Technical Report EE8544, Dept. of Electrical and Computer Engineering, University of Newcastle, Australia, Dec. 1985.

[14] C.E. Rohrs and J. Sisianni, "Examples of Robust Adaptive Control in Sampled Data Systems", *Proc. American Control Conference*, Seattle, WA, 1986.

[15] D.M. Orlicki, "Model Reference Adaptive Control Systems Using a Dead Zone Non-Linearity", Ph.D. Thesis, LIDS-TH-1455, MIT, Cambridge, MA, April 1985.

[16] J.C. Doyle, "Structured Uncertainty in Control System Design", *Proc. IEEE Conf. on Decision and Control*, Fort Lauderdale, FL, 1985, pp. 260 - 265.

[17] B.A. Francis, *A Course in H_∞ Control Theory*, Lecture Notes in Control and Information Sciences, Springer-Verlag, Berlin, 1987.

[18] B.A. Francis and J.C. Doyle, "Linear Control Theory with an H_∞ Optimality Criterion", *SIAM Journal of Control and Optimization*, Vol. 25, No. 4, July 1987, pp. 815 - 844.

[19] C.C. Chu, J.C. Doyle, and E.B. Lee, "The General Distance Problem in H_∞ Optimal Control Theory", *Int. Journal of Control*, Vol. 44, 1986, pp. 565 - 596.

[20] C.C. Chu, "H_∞ Optimization and Robust Multivariable Control", Ph.D. Thesis, Dept. of Electrical Engineering, Univ. of Minnesota, Minn., MN, 1985.

[21] J.C. Doyle, K. Lenz, and A. Packard, "Design Examples Using μ-Synthesis: Space Shuttle Lateral Axis FCS During Reentry", *Proc. IEEE Conf. on Decision and Control*, Athens, Greece, 1986, pp. 2218 - 2223.

[22] G. Stein, "Latest H_∞ Results", unpublished note, Oct. 1987.

[23] J.C. Doyle, *Lectures Notes*, 1984 ONR/Honeywell Workshop on Advances in Multivariable Control, Minn., MN, Oct. 1984.

[24] J.C. Doyle, "A Review of μ for Case Studies in Robust Control", *1987 IFAC Triennial World Congress*, Munich, West Germany, 1987, pp. 395 - 402.

[25] D.C. Youla, H.A. Jabr, and J.J. Bongiorno, Jr., "Modern Weiner-Hopf Design of Optimal Controllers, Part II: The Multivariable Case", *IEEE Trans. Auto. Control*, Vol. AC-21, June 1976, pp. 319 - 338.

[26] C.A. Desoer, R.W. Liu, J. Murray, and R. Saeks, "Feedback System Design: The Fractional Representation Approach to Analysis and Synthesis", *IEEE Trans. Auto. Control*, Vol. AC-25, June 1980, pp. 399 - 412.

[27] G. Zames, "Feedback and Optimal Sensitivity: Model Reference Transformations, Multiplicative Seminorms, and Approximate Inverses", *IEEE Trans. Auto. Control*, Vol. AC-26, April 1981, pp. 301 - 320.

[28] G. Zames and B.A. Francis, "Feedback, Minimax Sensitivity, and Optimal Robustness", *IEEE Trans. Auto. Control*, Vol. AC-28, April 1983, pp. 585 - 601.

[29] B.A. Francis and G. Zames, "On H_∞-Optimal Sensitivity Theory for SISO Feedback Systems", *IEEE Trans. Auto. Control*, Vol. AC-29, Jan. 1984, pp. 9 - 16.

[30] B.A. Francis, J.W. Helton, and G. Zames, "H_∞-Optimal Feedback Controllers for Linear Multivariable Systems", *IEEE Trans. Auto. Control*, Vol. AC-29, Oct. 1984, pp. 888 - 900.

[31] K. Glover, "All Optimal Hankel-Norm Approximations of Linear Multivariable Systems and their L_∞-error Bounds", *Int. Journal of Control*, Vol. 39, 1984, pp. 1115 - 1193.

[32] K. Glover, "Robust Stabilization of Linear Multivariable Systems: Relations to Approximation", *Int. Journal of Control*, Vol. 43, 1986, pp. 741 - 766.

[33] D.G. Luenberger, *Optimization by Vector Space Methods*, New York: John Wiley & Sons, Inc., 1969.

[34] I.M. Horowitz and M. Sidi, "Synthesis of Feedback Systems with Large Plant Ignorance for Prescribed Time-Domain Tolerances", *Int. Journal of Control*, Vol. 16, 1972, pp. 287 - 309.

[35] I.M. Horowitz, "Quantitative Feedback Theory", *IEE Proceedings*, Vol. 129, Part D, No. 6, Nov. 1982, pp. 215 - 226.

[36] A. Sideris and M.G. Safonov, "A Design Algorithm for the Robust Synthesis of SISO Feedback Control Systems Using Conformal Maps and H_∞ Theory", *Proc. American Control Conference*, Seattle, WA, 1986, pp. 1710 - 1715.

[37] P.P. Khargonekar and A. Tannenbaum, "Non-Euclidean Metrics and the Robust Stabilization of Systems with Parameter Uncertainty", *IEEE Trans. Auto. Control*, Vol. AC-30, Oct. 1985, pp. 1005 - 1013.

[38] H. Kimura, "Robust Stabilization for a Class of Transfer Functions", *IEEE Trans. Auto. Control*, Vol. AC-29, Sep. 1984, pp. 788 - 793.

[39] M. Vidyasagar and H. Kimura, "Robust Controllers for Uncertain Linear Multivariable Systems", *Automatica*, Vol. 22, Jan. 1986, pp. 85 - 94.

[40] Z. Nehari, "On Bounded Bilinear Forms", *Ann. of Math* (2), 65, 1957, pp. 153 - 162.

[41] D.F. Enns, "Model Reduction for Control System Design", Ph.D. Thesis, Stanford University, Stanford, CA, 1984.

[42] R. Hooke and T.A. Jeeves, "'Direct Search' Solution of Numerical and Statistical Problems", *Journal of Ass. Comput. Mach.*, Vol. 8, 1961, pp. 212 - 229.

[43] R. Bronson, "A Modified Pattern Search", *IEEE Trans. Auto. Control*, Vol. AC-25, April 1980, pp. 306 - 307.

[44] S.P. Boyd, V. Balakrishnan, C.H. Barratt, N.M. Khraishi, X.M. Li, D.G. Meyer, and S.A. Norman, "A New CAD Method and Associated Architectures for Linear Controllers", *Proc. American Control Conference*, Minn., MN, 1987, pp. 611 - 616.

[45] G. Strang, *Linear Algebra and its Applications*, New York: Academic Press, 1980.

[46] M. Vidyasagar, *Control System Synthesis: A Factorization Approach*, Cambridge, MA: MIT Press, 1985.

[47] C.R. Johnson, A.S. Foss, G.F. Franklin, R.V. Monopoli, and G. Stein, "Toward Development of a Practical Benchmark Example for Adaptive Control: A Panel Discussion", *Proc. IEEE Conf. on Decision and Control*, San Diego, CA, 1981, pp. 751 - 754.

[48] G. Stein, "Big Bad κ[G]", Workshop on Robust Control, *American Control Conference*, Minn., MN, 1987.